universität wien

MASTERARBEIT / MASTER'S THESIS

Titel der Masterarbeit / Title of the Master's Thesis

„Cloud Radiative Effects of High-Level Clouds and their Impact on Climate“

verfasst von / submitted by

Kerstin Haslehner BSc

angestrebter akademischer Grad / in partial fulfilment of the requirements for the degree of

Master of Science (MSc)

Wien, 2023 / Vienna 2023

Studienkennzahl lt. Studienblatt / degree programme code as it appears on the student record sheet:	UA 066 614
Studienrichtung lt. Studienblatt / degree programme as it appears on the student record sheet:	Masterstudium Meteorologie
Betreut von / Supervisor:	Univ.-Prof. Dr. Aiko Voigt
Mitbetreut von / Co-Supervisor:	Dr. Blaž Gasparini, MSc ETH

Abstract

In this thesis, I study the interactions between radiation and high-level clouds, which I define as clouds with a cloud top at temperatures colder than -35°C, using climate simulations with the model ICON-ESM. The thesis consists of two parts: First, I investigate two different ways to diagnose high-level clouds and two different methods to compute the cloud radiative effects and cloud radiative heating of high-level clouds. Second, I study the impact of the radiative interactions of high-level clouds on present-day atmospheric circulation and precipitation.

A possible way to diagnose high-level clouds from simulation data is to define all clouds colder than a temperature threshold as high-level clouds. I call this way of diagnosing high-level clouds the "cirrus diagnostic". I study the cloud radiative effects and cloud radiative heating rates of high-level clouds using the "cirrus diagnostic", which has not been done in much detail so far. The temperature threshold that I use in this diagnostic is -35°C. Interestingly, I found that the use of the "cirrus diagnostic" causes a strong artificial cloud radiative heating of high-level clouds at the temperature threshold. This strong heating arises due to individual clouds with a cloud top at temperatures colder than the threshold and a cloud base at temperatures warmer than the threshold being separated by the diagnostic into a high-level cloud and a non-high-level cloud, thereby creating an artificial cloud base of the high-level cloud at the temperature threshold. To avoid the artificial heating, I also study a second diagnostic, the "cirrus + warm base diagnostic", which has never been investigated so far. This diagnostic always considers the entire cloud as a high-level cloud, if at least the cloud top is at temperatures colder than -35°C. Therefore, there is no artificial heating at the temperature threshold level when using this diagnostic. Furthermore, I investigate two methods to calculate the cloud radiative effects and the cloud radiative heating of high-level clouds, respectively. In the first method, I compute the cloud radiative effects and heating rates with respect to an all-sky atmosphere, and in the second method with respect to a clear-sky atmosphere. In general, the two methods differ and the radiative effects or heating rates are the same only in an atmospheric column where no clouds or only high-level clouds are present. The use of the second method results in shortwave and longwave effects of greater magnitude than the first method, because non-high-level clouds partially mask the effects of the high-level clouds.

Previous work has speculated that the radiative heating of high-level clouds plays a significant role in shaping the climate, however this has not been explicitly studied so far. To investigate the impact of the radiative heating of high-level clouds on the present-day atmospheric circulation and precipitation, I compare simulations with and without radiatively active high-level clouds. My results show that the radiative interactions of high-level clouds heat the tropical upper troposphere, which increases specific humidity in the tropics and strengthens the eddy-driven jet stream. There are no statistically significant cloud radiative impacts of the high-level clouds on the Hadley cell strength and the position of the Inter-Tropical-Convergence-Zone found in my simulations. However, I show that the radiative interactions of high-level clouds have the largest contribution of all clouds to the decrease in tropical mean precipitation. Overall, my results highlight and confirm the importance of the radiative interactions of high-level clouds for the climate. Although the radiative heating of high-level clouds differs considerably between "cirrus diagnostic" and the "cirrus + warm base diagnostic" around the temperature threshold level, the impacts on the circulation and precipitation between the two diagnostics vary mostly only in magnitude.

Zusammenfassung

In dieser Arbeit untersuche ich die Wechselwirkungen zwischen Strahlung und hohen Wolken, die ich als Wolken mit einer Wolkenobergrenze bei einer Temperatur unter -35°C definiere, anhand von Klimasimulationen mit dem Modell ICON-ESM. Die Arbeit enthält zwei Teile: Erstens analysiere ich zwei verschiedene Arten, hohe Wolken zu diagnostizieren, und zwei verschiedene Methoden, die Wolken-Strahlungseffekte und Wolken-Strahlungsheizraten zu berechnen. Zweitens untersuche ich den Strahlungseinfluss hoher Wolken auf die atmosphärische Zirkulation und den Niederschlag.

Eine Möglichkeit, hohe Wolken aus den Simulationsdaten zu bestimmen, besteht darin, alle Wolken als hohe Wolken zu definieren, deren Temperatur unter einem bestimmten Schwellenwert liegt. Diese Art, hohe Wolken zu diagnostizieren, bezeichne ich als die „Cirrus-Diagnostik“. In dieser Arbeit analysiere ich die Wolken-Strahlungseffekte und die Wolken-Strahlungsheizraten von hohen Wolken unter Verwendung der „Cirrus-Diagnostik“, was bisher noch nicht sehr detailliert gemacht wurde. Ich verwende dabei eine Schwellenwert-Temperatur von -35°C. Interessanterweise führt die Verwendung der „Cirrus-Diagnostik“ zu einer starken künstlichen Strahlungserwärmung der Wolken an der Schwellenwert-Temperatur. Diese starke Strahlungserwärmung resultiert daraus, dass bei diesem Ansatz einzelne Wolken, deren Obergrenze bei einer Temperatur kälter als der Schwellenwert liegt und deren Basis bei einer Temperatur wärmer als der Schwellenwert liegt, in eine hohe Wolke und eine nicht-hohe Wolke auftrennt, wodurch eine künstliche Cirrus-Wolkenbasis bei der Schwellenwert-Temperatur entsteht. Um die künstliche Erwärmung zu vermeiden, untersuche ich auch eine zweite Diagnose-Methode, die „Cirrus + warme Basis- Diagnostik“, die bisher noch nie untersucht wurde. Diese Diagnostik berücksichtigt immer die gesamte hohe Wolke, sofern zumindest die Wolkenobergrenze bei einer Temperatur unter -35°C liegt. Aus diesem Grund tritt keine künstliche Erwärmung an der Schwellenwert-Temperatur auf. Darüber hinaus untersuche ich jeweils zwei verschiedene Methoden, die Wolken-Strahlungseffekte und die Wolken-Strahlungsheizraten zu berechnen. In der ersten Methode ermittle ich die Wolken-Strahlungseffekte/-heizraten in Bezug auf eine Atmosphäre mit strahlungsaktiven Wolken und in der zweiten Methode in Bezug auf eine wolkenlose Atmosphäre. Im Allgemeinen unterscheiden sich die Methoden deutlich und die Wolken-Strahlungseffekte/-heizraten sind nur gleich in einer atmosphärischen Säule, in der keine Wolken oder nur hohe Wolken vorhanden sind. Die Verwendung der zweiten Methode führt zu absolut größeren kurzwelligen und langwelligen Effekten als die erste Methode, da die nicht-hohen-Wolken teilweise die Effekte der hohen Wolken maskieren.

Frühere Arbeiten haben vermutet, dass die Strahlungsheizung hoher Wolken, eine wichtige Rolle für die Ausprägung des Klimas spielt, aber dies wurde bisher noch nicht explizit untersucht. Um den Einfluss der Strahlungsheizung hoher Wolken auf die gegenwärtige atmosphärische Zirkulation und den Niederschlag zu ermitteln, vergleiche ich Simulationen mit und ohne strahlungsaktive hohe Wolken. Meine Ergebnisse zeigen, dass die Strahlungsinteraktionen der hohen Wolken die obere Troposphäre in den Tropen erwärmen. Dies erhöht die spezifische Feuchte in den Tropen und verstärkt den polaren Jetstream. Es gibt keinen statistisch signifikanten Wolken-Strahlungseinfluss der hohen Wolken auf die Stärke der Hadley-Zelle und die Position der intertropischen Konvergenzzone in meinen Simulationen. Ich zeige jedoch, dass die Strahlungswechselwirkungen der hohen Wolken den größten Beitrag aller Wolken zur Reduktion des mittleren tropischen Niederschlags liefern. Meine Ergebnisse unterstreichen und bestätigen insgesamt die Wichtigkeit der Strahlungswechselwirkungen hoher Wolken für das Klima. Obwohl die Strahlungsheizung der Atmosphäre bei Verwendung der „Cirrus-Diagnostik“ und der „Cirrus + warme Basis- Diagnostik“ in der Höhe der Schwellenwert-Temperatur

beträchtliche Unterschiede aufweist, unterscheiden sich die Auswirkungen auf die Zirkulation und den Niederschlag zwischen den beiden Diagnose-Methoden meist nur in der Größenordnung.

Contents

Abstract . . . 2
Zusammenfassung . . . 2

1. Introduction **5**

2. Research questions **12**

3. Methodology **13**
3.1. Model and simulation setup . . . 13
3.2. Diagnosing liquid, mixed-phase and ice clouds . . . 14
3.3. Cloud radiative effects and cloud radiative heating rates of high-level clouds . . . 15
3.4. High-level cloud diagnostics . . . 16
3.5. Methods to study the total cloud radiative impacts and the cloud radiative impacts of high-level clouds . . . 19
3.6. Circulation metrics . . . 20
3.7. Atmospheric net radiative balance . . . 21

4. Hypotheses on the cloud radiative impacts of high-level clouds **22**

5. Results and Discussion **25**
5.1. Cloud distribution . . . 25
5.2. Comparison of the cloud radiative effects of high-level clouds . . . 30
5.3. Comparison of the cloud radiative heating rates of high-level clouds . . . 36
5.4. The impact of cloud-radiation coupling on climate . . . 44
5.4.1. Temperature impact . . . 44
5.4.2. Zonal wind impact . . . 48
5.4.3. Specific humidity impact . . . 52
5.4.4. Tropical precipitation impact . . . 52
5.4.5. ITCZ position and Hadley cell impact . . . 54

6. Conclusion **56**

7. Outlook **58**

A. Appendix **60**

Bibliography **60**

List of Tables **65**

List of Figures **65**

1. Introduction

The interactions of clouds with radiation have been shown to shape the Earth's climate in the present-day and under global warming (Ceppi et al., 2017; Voigt et al., 2021). Previous studies have speculated that the radiative heating of high-level clouds might dominate much of the total cloud radiative impacts on climate (Voigt et al., 2019). This thesis studies the interactions of cloud and radiation of high-level clouds and how they affect the atmospheric circulation and precipitation.

High-level clouds, like all other clouds, influence the Earth's energy budget through their radiative interactions. In this thesis, I define high-level clouds as all clouds that have a cloud top at temperatures colder than -35°C, because at these temperatures the cloud microphysics scheme of ICON-ESM, which is the model that I use for my simulations, only allows for ice crystals to exist (Lohmann and Roeckner, 1996). Clouds, independent from their altitude, cool the Earth by reflecting incoming solar radiation back to space, but simultaneously warm the planet by reducing outgoing longwave radiation. The concept of the cloud radiative effect (CRE) is used to study the influence of clouds on the top of atmosphere (TOA), the surface, and inside the atmosphere. The CRE is defined as the difference between all-sky radiative fluxes $F_{all-sky}$ and clear-sky radiative fluxes $F_{clear-sky}$ (Siebesma et al., 2020):

$$\text{CRE} = F_{all-sky} - F_{clear-sky}, \tag{1}$$

where downward fluxes are defined as positive. The unit of the CRE is W/m^2. Positive values represent a radiative heating effect, while negative values denote a radiative cooling effect. The total cloud radiative effect can be split up in a shortwave cloud radiative effect and a longwave cloud radiative effect. The CRE computed at the TOA allows to investigate how much clouds contribute to the energy budget of Earth, while the CRE computed at the surface shows the impact of clouds on the surface energy balance (Siebesma et al., 2020).
The net radiative effect of clouds depends on the cloud location and cloud composition (Matus and L'Ecuyer, 2017). Liquid and mixed-phase clouds usually have an overall cooling effect on the Earth. Ice clouds, which are mostly high-level clouds, have a net warming effect at the TOA (Figure 1), because they interact little with shortwave radiation, but are efficient at absorbing longwave radiation and re-emitting it at a lower cloud temperature, thereby reducing outgoing longwave radiation (Gasparini and Lohmann, 2016; Hong et al., 2016). At the surface the CRE of ice clouds cools the tropics and mid-latitudes, but warms the high-latitudes (Figure 2). The cooling effect is due to the scattering of solar radiation, which reduces the amount of shortwave radiation reaching the surface. The longwave warming effect dominates over the shortwave cooling effect in the high-latitudes since there is less solar insolation and there is not as much water vapor and/or lower clouds, which could absorb and re-emit the longwave radiation (Hong et al., 2016). Compared to other cloud types, the surface CRE of ice clouds is small.

The difference between the CRE at the TOA and at the surface (SFC) results in the atmospheric cloud radiative effect (ACRE):

$$\text{ACRE} = \text{CRE}_{\text{TOA}} - \text{CRE}_{\text{SFC}}. \tag{2}$$

ACRE represents the amount of energy gained or lost within an atmospheric column due to the presence of a cloud. Figure 3 shows that ice clouds, which are mostly high-level clouds, contribute the

most to the total ACRE compared to all other cloud types. Especially in the tropics, high-level clouds heat the atmosphere considerably (Hong et al., 2016).

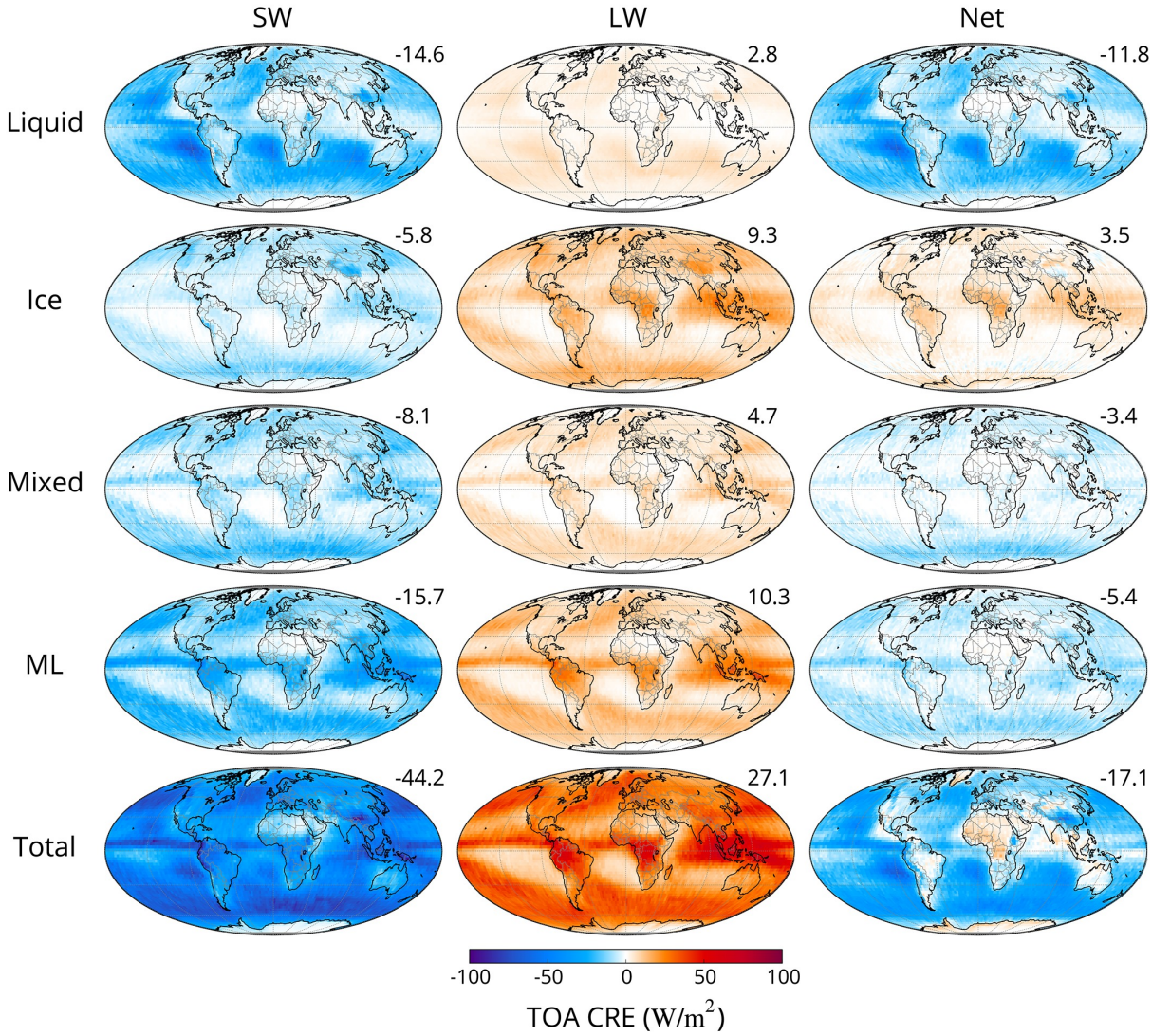

Figure 1: The TOA CRE of liquid clouds, ice clouds, mixed-phase clouds, multi-layer (ML) clouds (i.e., clouds containing separate ice and liquid cloud layers) and all clouds. The Figure is taken from Matus and L'Ecuyer (2017). The TOA CRE was derived from CloudSat and CALIPSO satellite retrievals.

Within an atmospheric column, clouds produce vertically varying heating and cooling. They have a net warming effect at their bases and a net cooling effect at their tops (Mayer, 2018). The cloud radiative heating or cooling at individual levels can be studied via the cloud radiative heating rate $\frac{\partial T}{\partial t}\Big|_{cloud}$, which is computed as (Siebesma et al., 2020):

$$\frac{\partial T}{\partial t}\Big|_{cloud} = -\frac{1}{\rho c_p}\frac{\partial (F_{all-sky} - F_{clear-sky})}{\partial z} = -\frac{1}{\rho c_p}\frac{\partial F_{cloud}}{\partial z}. \tag{3}$$

The cloud radiative heating rate is usually given in units of K/day. It affects the temperatures in the atmosphere and thus the atmospheric circulation and precipitation.

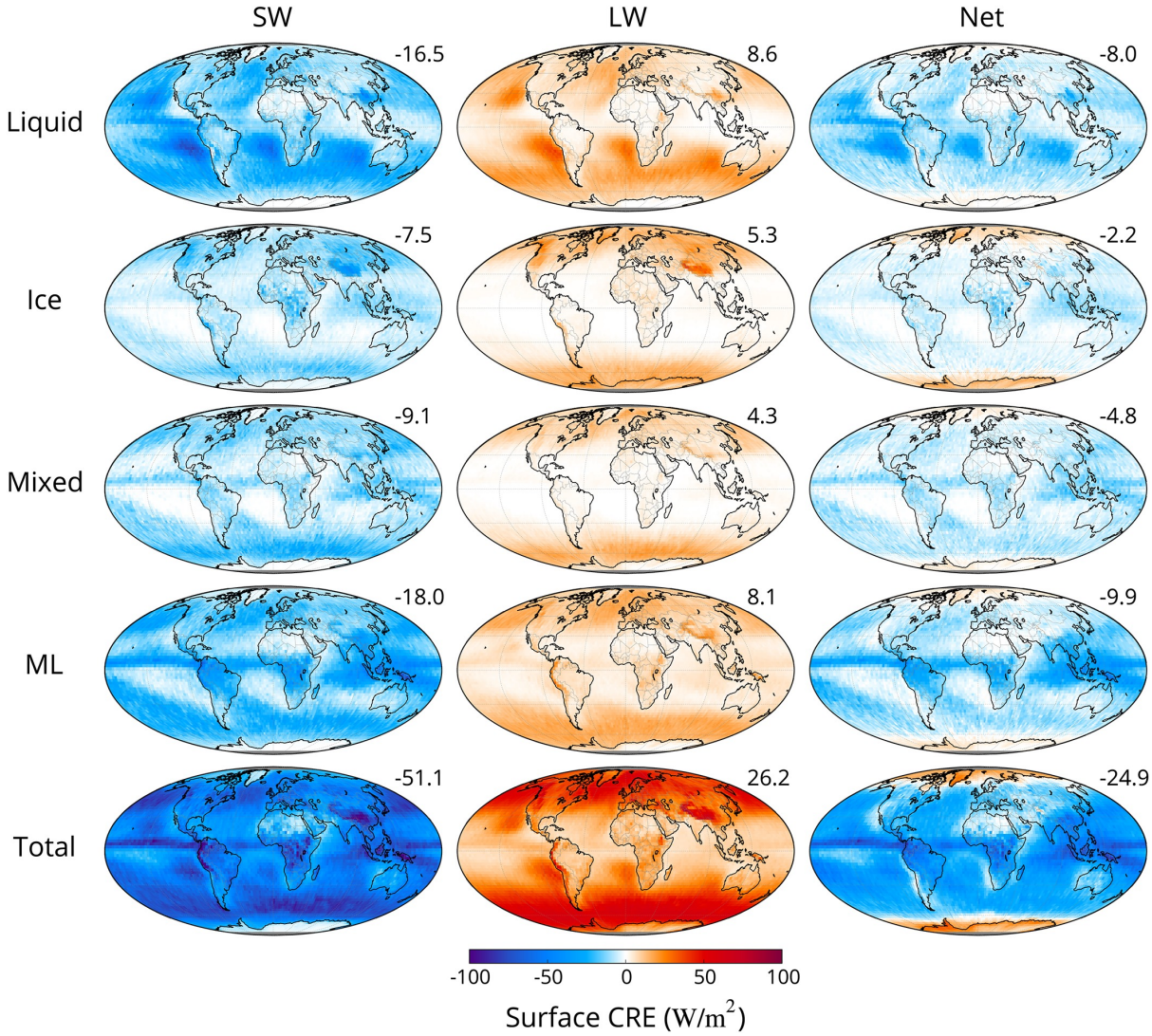

Figure 2: The surface CRE of liquid clouds, ice clouds, mixed-phase clouds, multi-layer (ML) clouds (i.e., clouds containing separate ice and liquid cloud layers) and all clouds. The Figure is taken from Matus and L'Ecuyer (2017). The surface CRE was derived from CloudSat and CALIPSO satellite retrievals.

The present-day cloud radiative impact in climate models can be studied by comparing a simulation with active cloud radiative heating ("clouds on") to a simulation without cloud radiative heating ("clouds off"). This technique is known as the Clouds On-Off Klimate Model Intercomparison Experiment (COOKIE) method (Stevens et al., 2012). Previous studies have suggested that much of the cloud radiative impact on the atmospheric circulation and precipitation found with the COOKIE approach is related to the radiative interactions of high-level clouds. The following part of this chapter briefly reviews the cloud radiative impacts and the proposed mechanisms by which the radiative interactions of high-level clouds influence the present-day climate and the climate under global warming.

Reduction of tropical mean precipitation

Li et al. (2015), Harrop and Hartmann (2016) and Albern et al. (2018) proposed that in the tropics the upper-tropospheric heating of high-level clouds (see Figure 4(a)) reduces tropical mean precipitation. Li et al. (2015) and Albern et al. (2018) argued that, according to the atmospheric energy budget, the radiative cooling of the atmosphere is primarily balanced by condensational heating. Therefore, in an

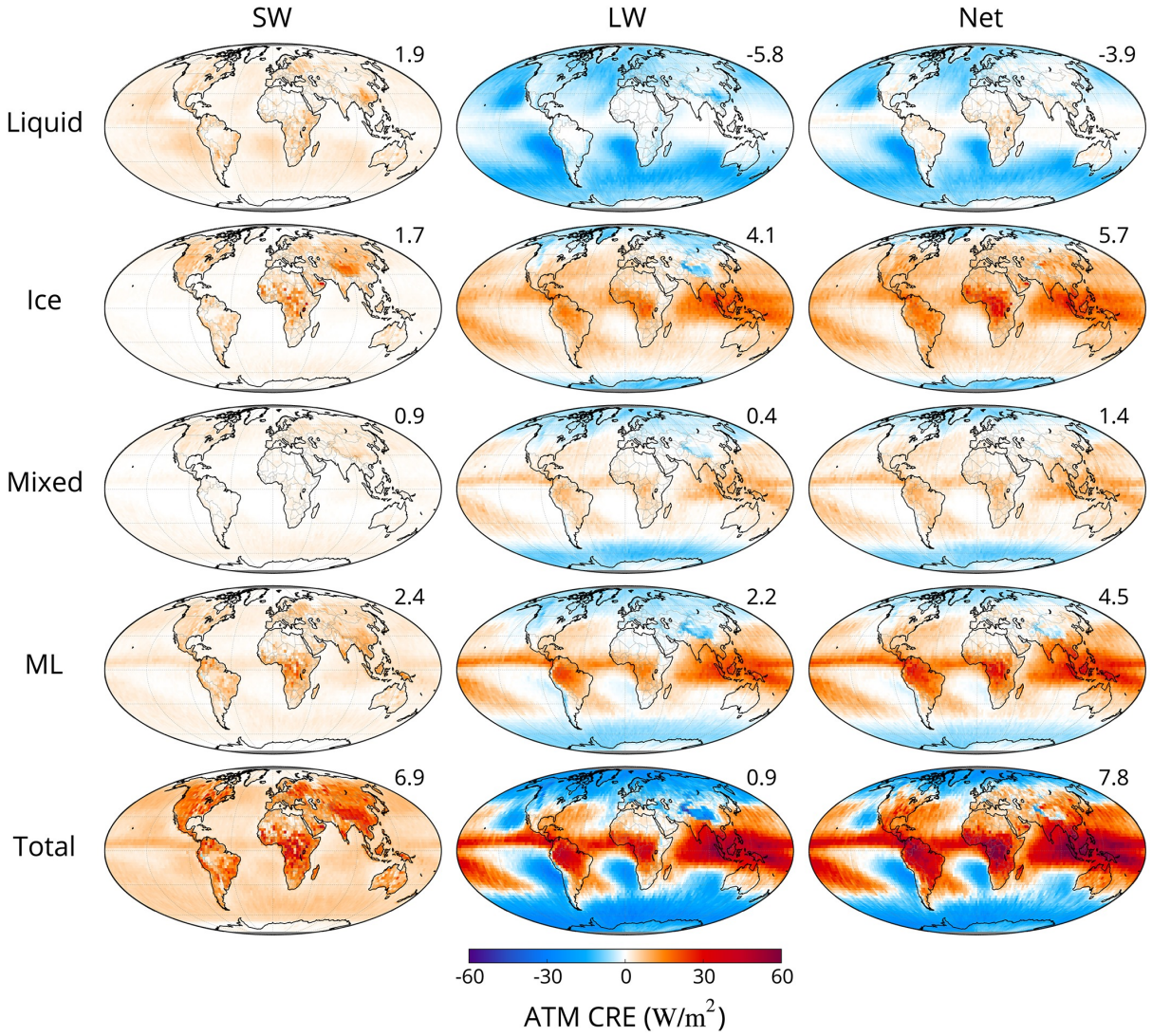

Figure 3: The ACRE of liquid clouds, ice clouds, mixed-phase clouds, multi-layer (ML) clouds (i.e., clouds containing separate ice and liquid cloud layers) and all clouds. The Figure is taken from Matus and L'Ecuyer (2017). The ACRE was derived from CloudSat and CALIPSO satellite retrievals.

atmosphere with radiatively active cirrus clouds, less condensational heating is necessary to balance the radiative cooling. Less condensational heating causes a decrease in precipitation.

Narrowing of the ITCZ width

Albern et al. (2018), Watt-Meyer and Frierson (2017) and Harrop and Hartmann (2016) suggested that the interactions of high-level clouds contribute significantly to a narrowing of the Inter-Tropical Convergence Zone (ITCZ), which is a zonal band of strong participation near the Equator where surface winds converge (Harrop and Hartmann, 2016). I follow the argument of Albern et al. (2018), who used an idealized two box model to explain the impact on the area of ascent. The two box model consists of an equatorial box with ascent and deep convection, and a subtropical box with descent and shallow convection. Assuming that precipitation is generated only by ascending motion in the equatorial box, tropical mean precipitation is a function of the ascent strength and the area of ascent. Net radiative heating strengthens the ascent, while static stability weakens it. This means that the radiative heating caused by high-level clouds increases the ascent strength in the "clouds on" simulation as long as static stability is not increased relative to the "clouds off" simulation. However, none of the

models in Albern et al. (2018) showed a weakening of the ascent strength. If the ascent increases and the precipitation decreases with active cloud radiative interactions of high-level clouds, then the area of ascent has to decrease, since tropical mean precipitation is assumed to be a function of the ascent strength and the area of ascending motion. This means that the ITCZ narrows.
Dixit et al. (2018) explicitly studied the cloud radiative impact of high-level clouds on the width of the ITCZ and showed that the lower-tropospheric heating caused by the tropical high-level clouds has the largest impact on the ITCZ narrowing. This is contradicting Albern et al. (2018), as they hypothesized that the upper-tropospheric heating of the high-level clouds causes the narrowing of the ITCZ. However, both Dixit et al. (2018) and Albern et al. (2018) highlight the role of high-level clouds for the narrowing of the ITCZ.

Increase in the strength of the Hadley cell
Harrop and Hartmann (2016), Watt-Meyer and Frierson (2017) and Albern et al. (2018) proposed that high-level clouds contribute to an increase in the strength of the Hadley cell, which is a thermally direct atmospheric circulation in the tropics (Hantel and Haimberger, 2016). Harrop and Hartmann (2016) and Watt-Meyer and Frierson (2017) argue that the heating of the upper troposphere by high-level clouds causes a larger meridional temperature gradient in their "clouds on" simulation compared to their "clouds off" simulation, which strengthens the Hadley cell and causes it to export more energy toward the poles.

Increase of strength of the eddy-driven jet
The interactions of high-level clouds with radiation appear to be related to a strengthening of the eddy-driven jet stream (Li et al., 2015) (Figure 4). The eddy-driven jet is a band of strong westerly winds in the mid-latitudes. It is described by the thermal wind relation, which relates the change in wind speed with height to the meridional temperature gradient. In the extratropics, high-level clouds contribute to an increase in the meridional temperature gradient (Li et al., 2015), which means that the eddy-driven jet strengthens, according to the thermal wind relation.

Influences on the position of the eddy-driven jet
Watt-Meyer and Frierson (2017) argued that the tropical ACRE, which is dominated by high-level clouds, increases the strength of the Hadley cell and thus the subtropical jet stream. A stronger subtropical jet is in turn related to an equatorward shift of the eddy-driven jet. However, this equatorward shift of the eddy-driven jet is counteracted by the extratropical clouds, which tend to increase the meridional temperature gradient on the poleward side of the eddy-driven jet, thereby shifting the jet toward the poles (Watt-Meyer and Frierson, 2017). The individual impact of extratropical and tropical clouds on the jet stream is therefore known, however the overall impact of high-level clouds remains unclear.

The radiative interactions of high-level clouds are not only important for the present-day circulation, but also for circulation changes under global warming. The cloud radiative heating of high-level clouds is expected to change under global warming (Voigt et al., 2019), which would affect the overall response of the atmospheric circulation. The impact of cloud radiative changes on the circulation under global warming has already been studied for aquaplanets, e.g., Voigt and Shaw (2015) and Voigt and Shaw (2016), and Earth-like simulation setups, e.g., Albern et al. (2019) and Voigt et al. (2019). The COOKIE method inadequately determines the cloud radiative impact on the circulation changes, since making clouds transparent changes the control climate (Voigt and Albern, 2019). Instead the cloud radiative impact under global warming is best studied by the cloud locking method (Voigt and Albern, 2019). This method prescribes ("locks") clouds from one climate state to another and thereby

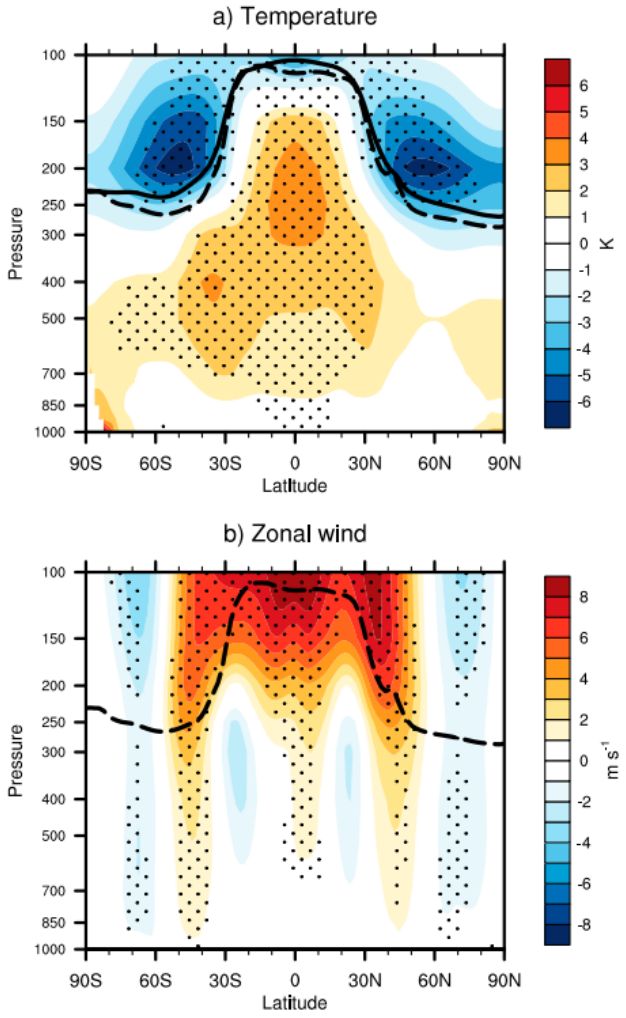

Figure 4: Cloud radiative impact on (a) temperature and (b) zonal wind, derived using the COOKIE method. The Figure is taken from Li et al. (2015). The solid line shows the tropopause height in the "clouds on" simulation and the dashed line shows the tropopause height in the "clouds off" simulation. These tropopause heights are derived from the tropopause air pressure output of the simulations. The stippling indicates where the cloud radiative impact is statistically significant at the 99% level. Note that the cloud radiative heating is largest in the upper troposphere, where the high-level clouds are located. The upper-tropospheric heating by clouds reduces the meridional temperature gradient and thus strengthens the eddy-driven jet.

breaks the coupling between ACRE and the circulation, which allows to study the cloud radiative impact. Studies using the cloud-locking technique have shown that cloud radiative changes contribute to a strengthening of the eddy-driven jet stream and a poleward jet shift under global warming (Voigt and Shaw, 2016; Voigt et al., 2019; Albern et al., 2020, 2021). Changes in high-level clouds are assumed to dominate the response of the jet (Voigt and Shaw, 2016; Voigt et al., 2019; Li et al., 2019; Albern et al., 2020, 2021). Li et al. (2019) and references therein argued that an increase in upper-tropospheric heating under global warming caused by high-level clouds increases the meridional gradient in the upper troposphere and static stability, both of which contribute to a poleward shift of the jet. Voigt and Shaw (2016) even showed directly that high-level clouds contribute the most to the poleward jet shift under global warming of all tropical or respectively mid-latitude cloud changes in an aquaplanet setup.

This literature review highlights that the radiative effects of high-level clouds are crucial in shaping the atmospheric circulation and precipitation in the present-day climate and under global warming. Despite their importance, the radiative heating of high-level clouds is currently not well represented in models, as the cloud radiative heating rates in the upper troposphere differ significantly between different models and between models and observations (Voigt et al., 2019). Reducing these model shortcomings could improve regional climate predictions. This highlights the importance of studying the cloud radiative heating of high-level clouds, which what I do in this thesis.

2. Research questions

The overall aim of my thesis is to improve the understanding of the cloud radiative impact of high-level clouds on the Earth's climate. To this end, I address the following two research questions:

1. **What is the best way to study the cloud radiative effects and the cloud radiative heating of high-level clouds using climate model simulations?**
   In this thesis, high-level clouds are diagnosed from model simulation data using a temperature threshold based approach. I show the disadvantage of this method and develop an alternative way to separate high-level clouds.
   The CRE and the cloud radiative heating of high-level clouds can be studied by using two different definitions respectively. Therefore, I compare two ways to diagnose the CRE of high-level clouds and two ways to study the cloud radiative heating of high-level clouds in this thesis.

2. **What is the cloud radiative impact of high-level clouds on the present-day atmospheric circulation and precipitation?**
   The cloud radiative effect of high-level clouds shapes the atmospheric circulation and precipitation in the present-day climate and under global warming. The impacts of high-level cloud changes on jet stream shifts under global warming (Voigt and Shaw, 2016) and on the present-day ITCZ width (Dixit et al., 2018) have already been explicitly studied using an aquaplanet setup. However, the cloud radiative impact of high-level clouds on present-day temperatures, zonal winds, specific humidity, the Hadley cell strength, ITCZ location and precipitation has never been explicitly investigated in a general circulation model before. Therefore, in this thesis, I study how high-level clouds affect present-day precipitation and the circulation using a general circulation model. Furthermore, I compare the cloud radiative impacts of high-level clouds with the total cloud radiative impacts.

3. Methodology

3.1 Model and simulation setup

I adress my research questions with the help of ICON-ESM (ICOsahedral Non-hydrostatic-Earth System Model) version 1.0 (Jungclaus et al., 2022), a recently developed climate model with biases that are comparable to other models participating in the Coupled Model Intercomparison Project (CMIP) (Jungclaus et al., 2022). ICON-ESM was developed by the Max Planck Institute for Meteorology in Hamburg and consists of a combination of the submodels ICON-A for the atmosphere, ICON-O for the ocean, and ICON-L for the land. The fluxes of energy, momentum, water, and carbon dioxide at the surface are coupled between the three component models. Furthermore, it includes the ocean biogeochemistry module named HAMOCC (HAmburg Ocean Carbon Cycle). Like other ICON models, ICON-ESM is based on unstructured, icosahedral grids (Jungclaus et al., 2022).
ICON-ESM enables to study the past, present and future climate of Earth. I perform model simulations with a horizontal grid resolution of R2B04, which is about 160 km, and 47 atmospheric levels. The model is coupled to the radiation scheme PSrad (Pincus and Stevens, 2013), the convective parameterization based on Tiedtke (1989), a 1-moment cloud microphysics scheme (Lohmann and Roeckner, 1996), and the cloud cover scheme by Sundqvist et al. (1989). The model time step is 15 minutes, except for the radiation scheme, which uses a time step of 90 minutes.

I run the model in a setup that is similar to the Atmospheric Model Intercomparison Project (AMIP) protocol. AMIP is a simulation protocol developed to assess the performance of atmospheric general circulation models (Gates, 1992). Models participating in this project simulate the evolution of climate using observed monthly averaged sea surface temperatures and sea ice concentrations from 1979 to the near present as boundary conditions (Gleckler, 2013). In contrast to the standard AMIP, I use monthly sea surface temperatures (SSTs) and sea ice concentrations that are averaged over 30 years (1979-2008). Aerosol optical properties, ozone and solar radiation are set to the respective monthly values between 1979-2009 from the CMIP6 dataset. Furthermore, greenhouse gas (CO_2, CH_4, N_2O, $CFC-11$, $CFC-12$) concentrations are prescribed to annual mean concentration values between 1979-2009.

I run a total of eight 31-year long simulations (1979-2009) with monthly averaged output files written every month. The first year (1979) is removed to avoid spin-up effects. One of these simulations is the control simulation, which I call the "clouds on" simulation, since all clouds are interacting with radiation. Four of the eight simulations are used to diagnose the cloud radiative effects and heating of high-level clouds, while the climate state stays the same as in the "clouds on" simulation. The remaining three are used to investigate the (high-level) cloud radiative impact on the climate; to this end the (high-level) cloud radiative effects are turned off and the climate is allowed to adjust to these changes. The simulation "diagnose cloud types" serves the purpose of evaluating the cloud fraction of different cloud types. It has instantaneous output with a frequency of 11 hours in order to have at least two outputs for each day with output files that are not always written at the same time for each location. Due to the large amount of data only 12 years (1979-1990) of data are used. Table 1 gives an overview of all simulations used for this thesis, including a short description, the number of years simulated and the averaging frequency.

Name	Description	Years of data considered	Averaging frequency
clouds on	Control simulation with all ACRE active.	30 years	monthly
diagnose cirrus all-sky	Simulation diagnosing the cloud radiative effects and heating of all clouds at temperatures colder than -35°C with respect to an all-sky atmosphere.	30 years	monthly
diagnose cirrus clear-sky	Simulation diagnosing the cloud radiative effects and heating of all clouds at temperatures colder than -35°C with respect to a clear-sky atmosphere.	30 years	monthly
diagnose cirrus + warm base all-sky	Simulation diagnosing the cloud radiative effects and heating of all clouds at temperatures colder than -35°C, including the cloud parts that extend to temperatures warmer than -35°C, with respect to an all-sky atmosphere.	30 years	monthly
diagnose cirrus + warm base clear-sky	Simulation diagnosing the cloud radiative effects and heating of all clouds at temperatures colder than -35°C, including the cloud parts that extend to temperatures warmer than -35°C, with respect to a clear-sky atmosphere.	30 years	monthly
clouds off	Simulation with ACRE of all clouds disabled.	30 years	monthly
cirrus off	Simulation with ACRE of all clouds at temperatures colder than -35°C disabled.	30 years	monthly
cirrus + warm base off	Simulation with ACRE of all clouds at temperatures colder than -35°C including the cloud parts that extend to warmer temperatures disabled.	30 years	monthly
diagnose cloud types	Simulation diagnosing the cloud fraction of different cloud types. ACRE of all clouds is active.	12 years	-

Table 1: Overview of all simulations used including their name, a short description, the simulated years and the output frequency.

3.2 Diagnosing liquid, mixed-phase and ice clouds

ICON-ESM simulates liquid, mixed-phase, and ice clouds. The locations of these cloud types can be diagnosed from the cloud liquid water *clw* and cloud ice water *ciw* content. For cloud-free regions,

both the *clw* and *ciw* are 0. For cloudy areas ($clw + ciw \neq 0$), I use the following liquid to ice water partitioning function P_{cloud} to diagnose the cloud type:

$$P_{cloud} = 1 - \frac{clw}{clw + ciw} \begin{cases} 1 \rightarrow \text{ice cloud} \\ 0 \rightarrow \text{liquid cloud} \\ else \rightarrow \text{mixed-phase cloud.} \end{cases} \tag{4}$$

This means that if at a location both cloud liquid water and cloud ice water are 0, there is no cloud present. Ice clouds have 0 cloud liquid water, while liquid clouds have 0 cloud ice content. All clouds containing both a liquid water content $\neq 0$ and an ice water content $\neq 0$ are mixed-phase clouds.

3.3 Cloud radiative effects and cloud radiative heating rates of high-level clouds

There are two different ways to study the CRE of high-level clouds (or any other cloud type). The first method diagnoses the high-level CRE (*HCRE*) by taking the difference between the all-sky radiative fluxes $F_{all-sky}$ and the radiative fluxes of all non-high-level clouds (nhlc) F_{nhlc}:

$$HCRE_{all-sky} = F_{all-sky} - F_{nhlc}. \tag{5}$$

F_{nhlc} is to this end calculated by disabling the radiative interactions of high-level clouds. However, the high-level clouds are still being simulated by the model. I refer to this method as $HCRE_{all-sky}$, because it is diagnosed by using an all-sky atmosphere as a reference.
The second method to diagnose the *HCRE* is to subtract the clear-sky radiative fluxes $F_{clear-sky}$ from the radiative fluxes of high-level clouds (hlc) F_{hlc}:

$$HCRE_{clear-sky} = F_{hlc} - F_{clear-sky}. \tag{6}$$

F_{hlc} is computed by making non-high-level clouds radiatively transparent. I refer to this second method as $HCRE_{clear-sky}$, because the reference is a clear-sky atmosphere. In order to diagnose $HCRE_{clear-sky}$, the radiative fluxes of all non-high-level-clouds are not considered, however the non-high-level clouds are still simulated by the model.

As for the *HCRE*, the cloud radiative heating rates $\frac{\partial T}{\partial t}_{cloud}$ of high-level clouds ($\partial_t T|_{hlc}$) can also be calculated in two different ways. The first method uses the differences of the all-sky radiative fluxes $F_{all-sky}$ and the radiative fluxes of all non-high-level clouds F_{nhlc} at different heights to compute the radiative heating rate of high-level clouds $\partial_t T|_{hlc,all-sky}$:

$$\partial_t T|_{hlc,all-sky} = \frac{\partial T}{\partial t}\Big|_{hlc,all-sky} = -\frac{g}{c_p}\frac{\partial (F_{all-sky} - F_{nhlc})}{\partial p}. \tag{7}$$

The second method uses the difference between the radiative fluxes of high-level clouds F_{hlc} and the clear-sky radiative fluxes $F_{clear-sky}$ at different heights to calculate $\partial_t T|_{hlc,clear-sky}$:

$$\partial_t T|_{hlc,clear-sky} = \frac{\partial T}{\partial t}\Big|_{hlc,clear-sky} = -\frac{g}{c_p}\frac{\partial (F_{hlc} - F_{clear-sky})}{\partial p}. \tag{8}$$

The $HCRE_{clear-sky}$ and $\partial_t T|_{hlc,clear-sky}$ are in contrast to $HCRE_{all-sky}$ and $\partial_t T|_{hlc,all-sky}$ independent of any other cloud types. Note that the $HCRE$ and $\partial_t T|_{hlc}$ studied by these two methods are generally not the same: $HCRE_{all-sky}$ and $\partial_t T|_{hlc,all-sky}$ compute the $HCRE$ by comparing an all-sky atmosphere to an atmosphere without radiatively active high-level clouds, while $HCRE_{clear-sky}$ and $\partial_t T|_{hlc,clear-sky}$ calculate the effect of high-level clouds in an atmosphere without any other clouds. These methods will produce the same radiative effects in an atmospheric column only if $F_{nhlc} = F_{clear-sky}$, i.e. only if high-level clouds and no other cloud types are present. I include a comparison and discussion of the two different $HCRE$ in the Section 5.2 and of the two different $\partial_t T|_{hlc}$ in Section 5.3.

3.4 High-level cloud diagnostics

To compute the $HCRE$ and $\partial_t T|_{hlc}$, I need a diagnostic that separates the cloud radiative fluxes of high-level clouds from all other cloud radiative fluxes. For this purpose I use a diagnostic based on a temperature threshold. To this end I define all clouds at temperatures colder than -35°C as cirrus clouds, because the cloud microphysics scheme of ICON-ESM does not allow any liquid water droplets to exist at temperatures colder than -35°C (Lohmann and Roeckner, 1996). This means that in my simulations only clouds composed of ice can exist at temperatures colder than -35°C, while at higher temperatures liquid water might still be present in clouds. In the real atmosphere, a small amount of super-cooled liquid water might still exist at temperatures between -35°C and -39°C, but in this temperature range the homogeneous formation of cirrus clouds becomes increasingly likely (Koop and Murray, 2016). I will refer to this diagnostic here as the "cirrus diagnostic". This approach to diagnose cirrus clouds was also used in Gasparini and Lohmann (2016) and Gasparini et al. (2020). Figure 5(a) visualizes the "cirrus diagnostic". When a cloud spans over temperatures both warmer and colder than the threshold the "cirrus diagnostic" considers only the cloud parts at temperatures colder than the threshold as high-level clouds. The warmer cloud parts are seen as non-high-level cloud by the diagnostic. I refer to this as "cutting through" individual clouds.

In an atmosphere with a radiatively active high-level cloud, the cloud top is heated in the shortwave by the absorption of the incoming shortwave radiation. In the longwave, there is a heating at the cloud base due to absorption and a cooling at the cloud tops caused by the emission of longwave radiation. For high-level clouds the longwave cooling at the cloud top is stronger than the shortwave heating, as shown in the vertical profiles of the cloud radiative heating rate of tropical high-level clouds in Dinh et al. (2022). A cloud located below a high-level cloud, as depicted in Figure 6(a), also has a longwave heating at the cloud base and a shortwave heating and longwave cooling at the cloud top. However, the lower cloud receives less shortwave radiation than the high-level cloud, since part of the incoming solar radiation has been absorbed by the high-level cloud. On the other hand, the high-level cloud increases the longwave radiation the lower cloud receives, since it re-emits the longwave radiation. Therefore, if cirrus clouds are not interacting with radiation, the radiative fluxes below them are more positive in the shortwave (Figure 6(b) and (d)) relative to the all-sky atmosphere (Figure 6(a)), because the clouds below the radiatively inactive cirrus clouds receive more incoming shortwave radiation. The longwave radiative fluxes are in this case more negative (Figure 6(c) and (e)) relative to the all-sky radiative fluxes at the top of the non-high-level clouds (which includes the high-level cloud parts at temperatures warmer than the threshold). This is because there is less down-

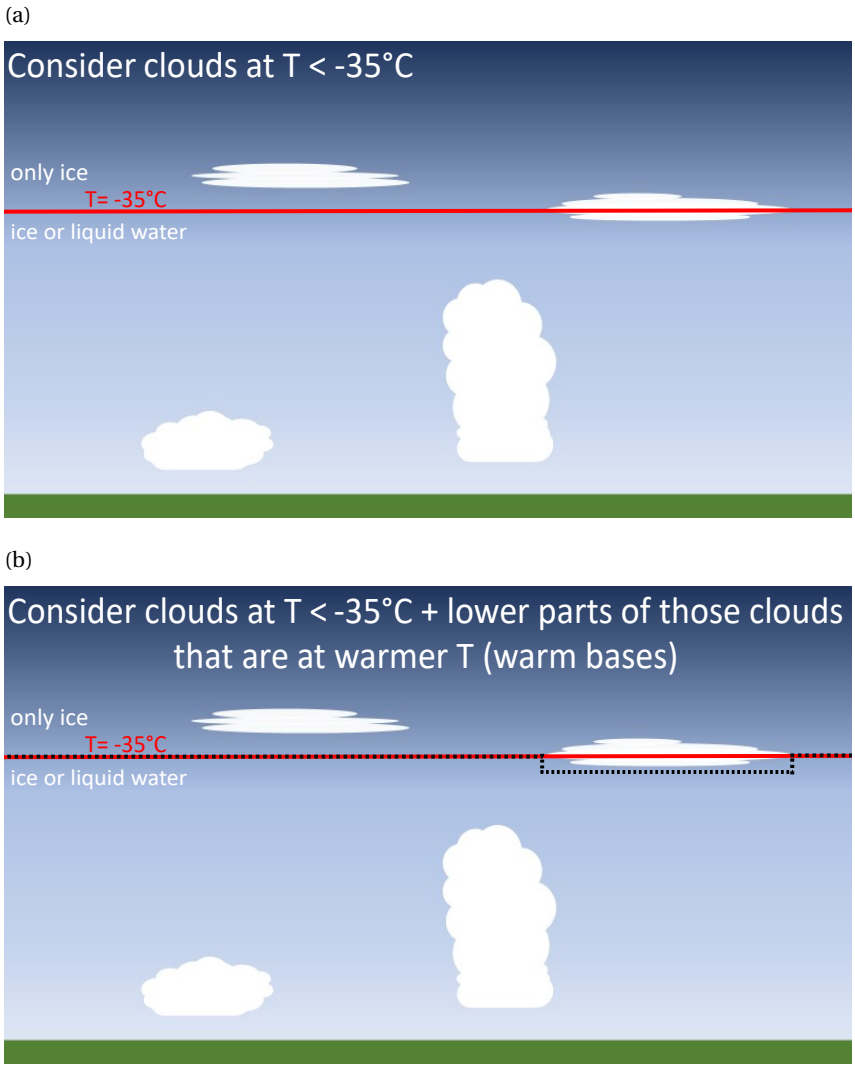

Figure 5: Depiction of the diagnostics used to separate high-level clouds from other clouds. The red line depicts the -35°C temperature, which serves as a temperature threshold. Panel (a) shows the "cirrus diagnostic", which considers all clouds at temperatures colder than -35°C as high-level clouds. Panel (b) depicts the "cirrus + warm base diagnostic", which diagnoses clouds above the stippled black line as high-level clouds. The stippled black line follows the -35°C isotherm but if a cloud is located at temperatures both colder and warmer than the threshold, it follows the outline of that cloud.

welling longwave radiation when cirrus clouds are not interacting with radiation. For the clouds and high-level cloud parts directly below the temperature threshold, the reduction of the received longwave radiation outweighs the increase in shortwave radiation, as they are at relatively high altitudes. Therefore, F_{nhlc} at the level directly below the temperature threshold is diagnosed to be more negative than $F_{all-sky}$ (Figure 6). To compute $HCRE_{all-sky}$ or $\partial_t T|_{hlc,all-sky}$, the difference between $F_{all-sky}$ and F_{nhlc} is taken (Equation 5 and Equation 7). Thus, a more negative F_{nhlc} at the temperature threshold causes a more positive $HCRE_{all-sky}$ or $\partial_t T|_{hlc,all-sky}$ at the same level. Depending on the optical depth of the clouds, how frequently high-level clouds are "cut through" and how often clouds are located directly below the temperature threshold, this heating can be quite strong. This heating at the threshold level is artificial, because it is mostly concentrated around the chosen temperature threshold and it is absent in the all-sky atmosphere.

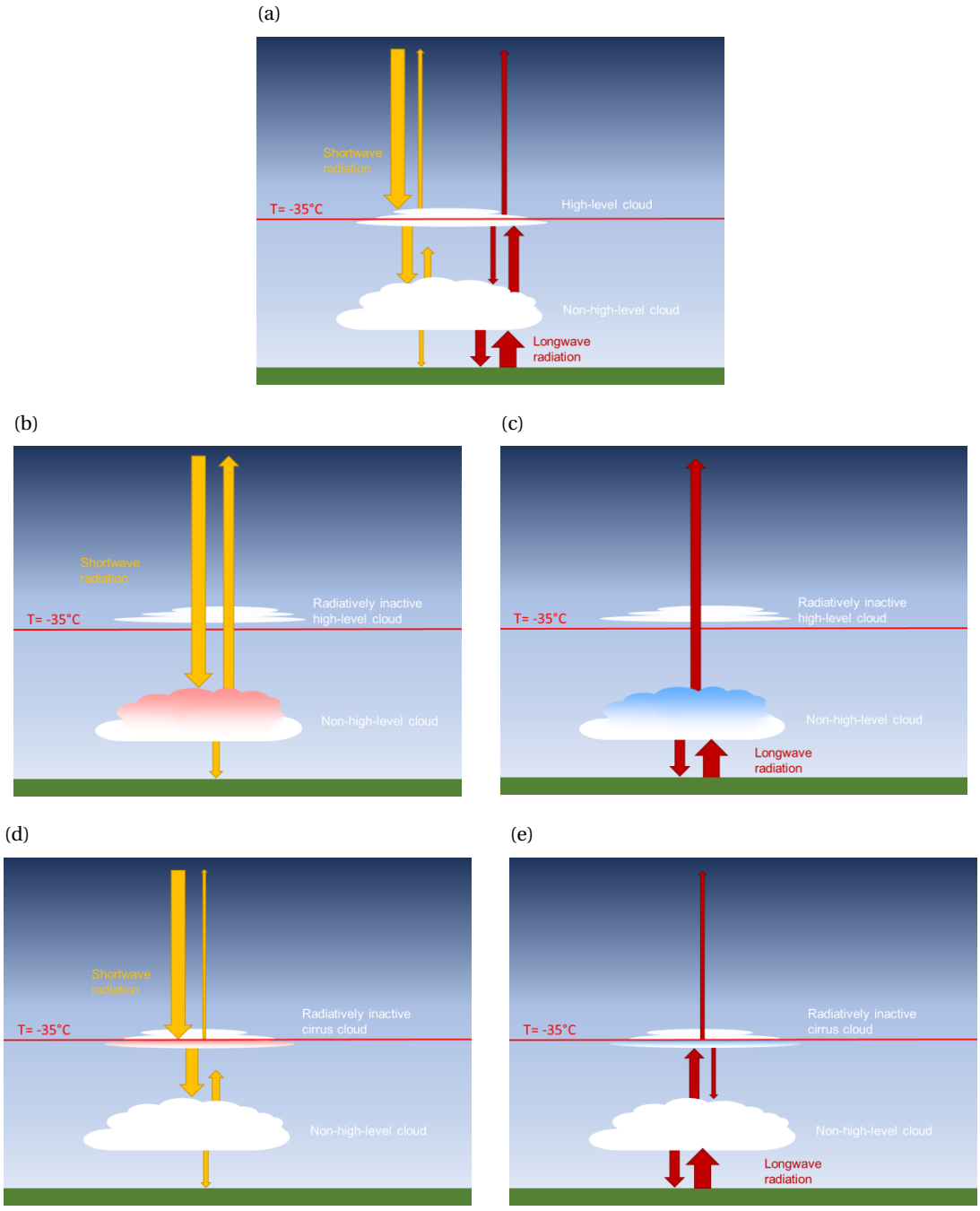

Figure 6: A depiction of the cloud radiation interactions in an atmosphere with radiatively active ACRE is shown in Panel (a), and in an atmosphere with radiatively transparent high-level clouds according to the "cirrus diagnostic" is shown in Panels (b), (c), (d) and (e). The red line shows the used temperature threshold of -35°C. Reflections from the Earth's surface are neglected. Panels (b) and (d) show the shortwave interactions in an atmosphere with inactive cirrus clouds and Panels (c) and (e) depict the longwave interactions. Panels (b) and (c) show the case for a high-level cloud that is located entirely at temperatures colder than the threshold, and a non-high-level cloud. Panels (d) and (e) visualize the case for a high-level cloud that spans over temperatures both colder and warmer than the threshold. The red shading on the clouds in Panels (b) and (d) indicates an increase of received shortwave radiation relative to Panel (a) caused by radiatively inactive cirrus, as more incoming solar radiation reaches the cloud (parts) as in case (a). The blue shading on the clouds in Panels (c) and (e) represents that there is less longwave radiation received relative to Panel (a) in the case of radiatively inactive cirrus clouds, because there is no re-emission of longwave radiation by the high-level clouds.

I use a second high-level cloud diagnostic that avoids the issue of "cutting through" individual clouds, thereby reducing the heating at the temperature threshold. This is achieved by including all clouds colder than -35°C and additionally, if parts of these clouds are at temperatures warmer than the threshold, those parts are included as well. I refer to this as "cirrus + warm base diagnostic". Figure 5(b) depicts this diagnostic. The high-level cloud "cirrus + warm base diagnostic" has never been studied before.

3.5 Methods to study the total cloud radiative impacts and the cloud radiative impacts of high-level clouds

I use the Clouds On-Off Klimate Model Intercomparison Experiment (COOKIE) technique (Stevens et al., 2012; Voigt and Albern, 2019) to study the overall cloud radiative impact on the present-day atmosphere. The COOKIE method compares a simulation with active ACRE, called a "clouds on" simulation, to a simulation in which clouds are not able to interact with radiation, the "clouds off" simulation. Note that in the "clouds off" simulation clouds are only transparent to the radiation scheme, but are still being simulated by the model and can, e.g., produce latent heating. I call the difference between the "clouds on" simulation and the "clouds off" simulation the COOKIE simulation set.

To study the impact of high-level clouds on the present-day atmosphere, I adapt the COOKIE method as follows: Instead of performing a "clouds off" simulation in which all cloud radiative interactions are disabled, I run a "cirrus off" simulation in which only all high-level clouds according to the "cirrus diagnostic" are made transparent to radiation. The "clouds on" simulation is then compared to this "cirrus off" simulation. I call this new method the Cirrus-COOKIE technique. The difference between the "clouds on" and the "cirrus off" simulation is referred to as the Cirrus-COOKIE simulation set.

Similarly, I use this COOKIE-type approach also with the "cirrus + warm base diagnostic". To this end I compare the "clouds on" simulation to a "cirrus + warm base off" simulation in which clouds colder than -35°C, including their warm bases, do not interact with radiation. I refer to this as the WB-Cirrus-COOKIE technique, where "WB" stands for "warm base". I call the difference between the "clouds on" and the "cirrus + warm base off" simulation the WB-Cirrus-COOKIE simulation set, which allows to study the impact of high-level clouds and their warm bases on the climate.

Name	Combination of simulations	Description
COOKIE	"clouds on" - "clouds off"	Studies the total cloud radiative impact
Cirrus-COOKIE	"clouds on" - "cirrus off"	Studies the cloud radiative impact of cirrus clouds
WB-Cirrus-COOKIE	"clouds on" - "cirrus + warm base off"	Studies the cloud radiative impact of cirrus clouds including their warm bases

Table 2: Overview of the COOKIE, Cirrus-COOKIE and WB-Cirrus-COOKIE simulation sets, including the combination of simulations used, and a short description.

The COOKIE, Cirrus-COOKIE and WB-Cirrus-COOKIE simulation sets always consist of a difference between two simulations. Table 2 summarizes which simulation combinations are used to study the (high-level) cloud impact on climate.

3.6 Circulation metrics

This section defines the circulation metrics used in this thesis to study the impact of high-level clouds on the atmospheric circulation. The circulation metrics examined in this thesis are the position of the eddy-driven jet stream, the strength of the eddy-driven jet stream, the Hadley cell strength, and the ITCZ latitude.

Position of the eddy-driven jet stream
Important features of the atmospheric circulation are the jet streams, which are bands of strong westerly winds. The highest wind speeds occur in the upper troposphere. There is a mid-latitude jet and a subtropical jet. The mid-latitude jet is also known as the eddy-driven jet or the polar jet. The position of the eddy-driven jet φ is determined as the latitude of the zonal wind maximum at 700 hPa. Following Barnes and Polvani (2013), I use a quadratic fit around the latitude of the zonal wind maximum. This is done to account for effects of the model grid.

Strength of the eddy-driven jet stream
I define the strength of the eddy-driven jet u_{jet} as the zonal wind speed at the jet position. The units are m/s.

Hadley cell strength
The Hadley cell or Hadley circulation involves rising air at the equatorial regions that moves poleward in the upper troposphere. The air then subsides between 20° and 40°N/S and moves equatorward, back to the region of ascent (Hantel and Haimberger, 2016). The Hadley cell strength HC is defined here for the Northern Hemisphere as the maximum of the mass stream function Ψ in between the Equator and 30°N, and 700 hPa to 200 hPa. For the Southern Hemisphere, the absolute value of the minimum of Ψ in between the Equator and 30°S, and 700 hPa to 200 hPa is used as HC. The formula for the mass stream function Ψ is (Hantel, 2013):

$$\Psi = \frac{2\pi\ a\ cos(\phi)}{g} \int_{p}^{p_s} v\ dp, \tag{9}$$

where a is the radius of the Earth, ϕ is the latitude, g is the acceleration of gravity, v is the zonal mean of the meridional wind, p is the pressure, and p_s is the surface pressure. The units of the mass stream function, and therefore of the Hadley cell strength, are kg/s.

ITCZ latitude
The zone where the surface winds of the Hadley cells in both hemispheres converge is called the ITCZ (Hantel and Haimberger, 2016). The ITCZ is associated with heavy precipitation, so its location is an important circulation metric for the tropics. The ITCZ latitude φ_{ITCZ} is determined as the latitudinal centroid of precipitation P between 20°N/S, following Harrop et al. (2018):

$$\varphi_{ITCZ} = \frac{\int_{20^\circ S}^{20^\circ N} \phi' cos(\phi') P\ d\phi'}{\int_{20^\circ S}^{20^\circ N} cos(\phi') P\ d\phi'}. \tag{10}$$

3.7 Atmospheric net radiative balance

The atmospheric net radiative balance ΔR_{ATM} compares how much energy the atmosphere receives with how much it loses. It is calculated as the difference between the radiative balance at the TOA ΔR_{TOA} and the radiative balance at the surface ΔR_{SFC}. ΔR_{TOA} is the difference between the incoming solar radiation (ISR_{TOA}) and the outgoing shortwave and longwave radiation (OSR_{TOA} and OLR_{TOA}) at the TOA and ΔR_{SFC} is the difference between the downwelling shortwave and longwave radiation (DSR_{SFC} and DLR_{SFC}) and upwelling shortwave and longwave radiation (USR_{SFC} and ULR_{SFC}) at the surface.

$$\begin{aligned} \Delta R_{ATM} &= \Delta R_{TOA} - \Delta R_{SFC} \\ &= ISR_{TOA} - (OSR_{TOA} + OLR_{TOA}) - (DSR_{SFC} + DLR_{SFC} - (USR_{SFC} + ULR_{SFC})). \end{aligned} \tag{11}$$

$\Delta R_{ATM} > 0$ represents a net gain of energy, while $\Delta R_{ATM} < 0$ implies a net loss of energy.

4. Hypotheses on the cloud radiative impacts of high-level clouds

In this section, I combine my understanding of the climate system, the CRE satellite retrievals of ice clouds, which I assume to be a good proxy for the CRE of high-level clouds, from Matus and L'Ecuyer (2017), and the literature reviewed in the Chapter 1 to create hypotheses on the expected changes in the Cirrus-COOKIE and WB-Cirrus-COOKIE simulation sets. In the following, I first present my hypotheses on the differences between the Cirrus-COOKIE and WB-Cirrus-COOKIE simulation sets. Then, I state my hypotheses on the impacts of high-level clouds on the climate in the tropics, mid-latitudes, and high-latitudes. Note that sea surface temperatures (SSTs) and sea ice cover do not change in the simulations because they are prescribed.

Differences in the impacts when using a diagnostic that includes cirrus and their warm bases

The main difference between the Cirrus-COOKIE and the WB-Cirrus-COOKIE simulation sets is that in WB-Cirrus-COOKIE a larger cloud fraction is made transparent to radiation in the "cirrus + warm base off" simulation than in the "cirrus off" simulation. Therefore, I expect the high-level cloud radiative impacts to differ in magnitude but not in sign between the two diagnostics, with WB-Cirrus-COOKIE having larger effects.

Impacts in the tropics

Temperature
High-level clouds heat the upper troposphere, as mentioned in Chapter 1, therefore I expect the upper-tropospheric temperatures to increase. In the tropics, the surface CRE for ice clouds is negative (Figure 2), because they reduce the incoming shortwave radiation. Therefore, ice clouds cool the surface. The ice clouds in the tropics are usually high-level clouds. This is why I expect a decrease in land surface temperatures in the Cirrus-COOKIE and WB-Cirrus-COOKIE simulation sets.

Precipitation
Based on the literature review in Chapter 1 I expect that high-level clouds contribute to a decrease in precipitation.

Specific humidity
I expect specific humidity to increase when high-level clouds interact with radiation based on an argument following the Clausius Clapeyron equation. According to this equation, a warmer atmosphere can hold more water vapor. Since the atmospheric CRE of high-level clouds is positive (Figure 3), the troposphere in the "clouds on" simulation should be warmer and therefore have a higher specific humidity.

ITCZ position
The ITCZ shifts to the warmer hemisphere over seasonal or longer time scales (Schneider et al., 2014). Matus and L'Ecuyer (2017) showed that the ACRE of ice clouds, which I assume to be mostly high-level

clouds, is more positive in the Northern Hemisphere. Therefore, I expect the ITCZ to shift northward in the Cirrus-COOKIE and WB-Cirrus-COOKIE simulation sets.

Hadley cell strength
I expect high-level clouds to strengthen the Hadley cell, since it is argued in the literature (see Chapter 1) that the heating in the upper troposphere causes a larger meridional temperature gradient in the "clouds on" simulation, which strengthens the Hadley cell and causes it to export more energy toward the poles.

Impacts in the mid-latitudes

Land surface temperature
In the mid-latitudes the surface net CRE of ice clouds is close to 0 (Figure 2), so I do not expect that high-level clouds change the land surface temperature in this region significantly.

Specific humidity
Since the ACRE of ice clouds is positive (Figure 3), I expect radiatively active high-level clouds to increase the atmospheric water vapor content and thus specific humidity in the mid-latitudes due to their warming of the atmosphere, similar to the tropics.

Eddy-driven jet stream
In most simulations in the literature, the mechanism of upper-tropospheric heating by high clouds causing a poleward jet shift dominates over the effect of Hadley cell strengthening causing an equatorward jet shift. Therefore, I expect the jet to shift poleward in the Cirrus-COOKIE and WB-Cirrus-COOKIE simulation sets.

Impacts in the high-latitudes

Land surface and sea ice temperature
High-level clouds warm the surface near the poles (Figure 2), because there are fewer other cloud types and less water vapor, which can interact with the re-emitted longwave radiation of the high-level clouds (Hong et al., 2016). Therefore, I expect an increase in land surface temperatures and sea ice temperatures in the Cirrus-COOKIE and the WB-Cirrus-COOKIE simulation sets. This warming at the poles would lead to a decrease in sea ice cover. However, I prescribe the mean climatological sea ice cover in the simulations, so the sea ice cover cannot change in my simulations.

Specific humidity
The ACRE of ice clouds in the polar regions is negative (Figure 3). Following the Clausius-Clapeyron equation, I therefore expect that high-level clouds reduce specific humidity in the high-latitude atmosphere. Close to the surface, I expect that specific humidity increases, since the surface is heated (Figure 2).

Summary of hypotheses

To summarize, I expect that the interactions of high-level clouds with radiation lead to

- increased upper-tropospheric temperatures in the tropics,

- decreased land surface temperatures in the tropics,
- decreased precipitation in the tropics,
- a northward shift of the ITCZ,
- an increase in the Hadley cell strength,
- a poleward shift of the eddy-driven jet stream,
- increased land surface and sea ice temperatures at the poles,
- increased specific humidity in the tropics and mid-latitudes and decreased in the high-latitudes, except close to the surface.

In the next section I test these hypotheses with my own simulation results.

5. Results and Discussion

In this chapter I present and discuss the results of my simulations. It is structured in the following way: In Section 5.1 I analyze the cloud (type) distributions in ICON-ESM. Then, in Section 5.2, I compare the $HCRE_{all-sky}$ and $HCRE_{clear-sky}$ using both the "cirrus diagnostic" and the "cirrus + warm base diagnostic". Section 5.3 assesses the differences between $\partial_t T|_{hlc,all-sky}$ and $\partial_t T|_{hlc,clear-sky}$ using again both high-level cloud diagnostics. Lastly, Section 5.4 presents and discusses the impact of (high-level) clouds on circulation and precipitation, and tests the hypotheses stated in Chapter 4.

5.1 Cloud distribution

Here I examine the mean cloud distribution of different cloud types simulated in ICON-ESM. To this end, I show the mean cloud fraction of liquid, mixed-phase, and ice clouds of the 12 year-long "diagnose cloud types" simulation. The cloud types are diagnosed using Equation 4. Later in this subsection I will also compare the cloud fraction of high-level clouds, diagnosed by the "cirrus diagnostic" and the "cirrus + warm base diagnostic" from the "diagnose cloud types" simulation.

Liquid clouds are simulated predominately in the lower troposphere of the mid-latitudes and at the ITCZ location (Figure 7(a)). No liquid clouds are simulated over Antarctica due to the low temperatures there. In principle, liquid clouds can be modeled at all temperatures warmer than -35°C in ICON-ESM. However, the liquid clouds in ICON-ESM are located well below the annual mean -35°C isotherm. The coldest liquid clouds are simulated over the high-latitudes of the Northern Hemisphere. Compared to the other cloud types, liquid clouds have a lower cloud fraction.
Mixed-phase clouds are frequently modeled over the high- and mid-latitudes (Figure 7(b)). A local peak in the mixed-phase cloud fraction is also present at the ITCZ location. In the subtropics the mixed-phase cloud fraction is minimized. Since mixed-phase clouds contain both water droplets and ice crystals, they can only be simulated at temperatures between 0°C and -35°C in ICON-ESM. That is why the mixed-phase clouds are concentrated in or close to the range of the 0°C annual mean isotherm to the -35°C annual mean isotherm. However, mixed-phase clouds are more frequent close to the annual mean 0° isotherm or close to the surface (if the temperatures close to the surface are colder than 0°C). The mixed-phase cloud fraction usually decreases with altitude.
The ice cloud fraction is highest in the upper troposphere (Figure 7(c)). They are frequently simulated also at temperatures warmer than the annual mean -35°C isotherm, but rarely at temperatures warmer than the annual mean 0°C isotherm, since ice clouds can only exist if temperatures are 0°C or lower. Ice clouds in my simulation dominate in the tropical and high-latitude upper troposphere, while in the subtropics there is a minimum in ice cloud fraction due to descending air motions. The peak of tropical ice clouds is related to the ascending air in the ITCZ. Over the high-latitudes of the Southern Hemisphere the ice cloud fraction extends well into the stratosphere. This is because ICON-ESM simulates polar stratospheric clouds there. These clouds are also considered in both high-level cloud diagnostics. However, these clouds are very thin and do not contribute much to the cloud radiative heating.

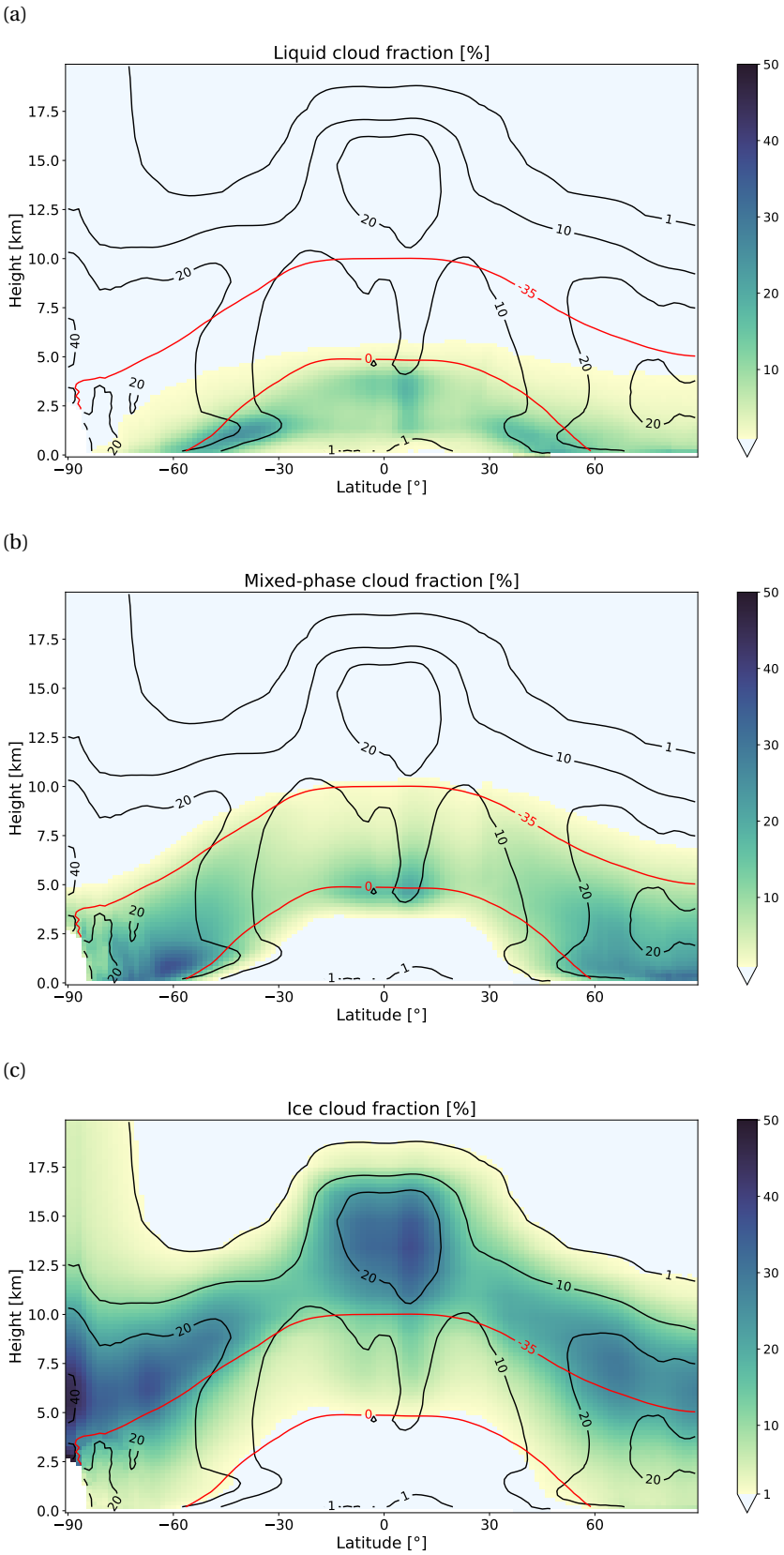

Figure 7: The zonally averaged cloud fraction of (a) liquid (all clouds with ice water content of 0%), (b) mixed-phase (all clouds containing both liquid water and ice), and (c) ice clouds (all clouds with liquid water content of 0%) averaged over 12 years is shown in colors. The black contour line depicts the total cloud fraction in % and the red contour lines show the -35°C and the 0°C isotherms. The light-blue color indicates where the cloud fraction is below 1%.

Figure 8 shows that liquid clouds dominate the lower troposphere over mid-latitudes and the tropics, while mixed-phase clouds are the most common cloud type in the lower troposphere over the high-latitudes. The highest altitudes, where mixed-phase clouds dominate, are at around 30°N/S. This is due to the descending air masses in these areas, which are unfavorable for ice cloud formation. Ice clouds dominate especially in the upper-troposphere.

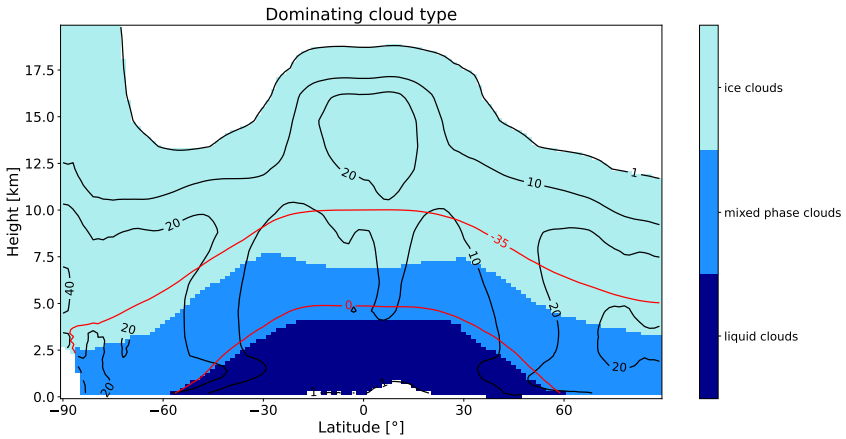

Figure 8: Zonal plot of the most dominant cloud type at a given location, i.e. the cloud type with the highest cloud fraction at each location. Black contour lines show the total cloud fraction and the red contour lines show the -35°C and the 0°C isotherms.

Figure 9 shows the vertical profiles of liquid, mixed-phase and ice clouds averaged over the tropics (30°N-30°S), in the mid-latitudes (30°-60°N/S), and the high-latitudes (60-90°N/S). In the tropics, the only cloud type that can be found close to the surface are liquid clouds, as the temperature of the lowest tropospheric levels is too high for mixed-phase and ice clouds to form. The liquid cloud fraction decreases to 0 at a height of about 8 km. The mixed-phase cloud fraction is greater than 0 from 2.5 km to about 11 km, with a peak at around 5 km. According to an evaluation of satellite retrievals of liquid water and ice water content by Huang et al. (2015), cloud ice is present in the tropics at altitudes higher than about 2.5 km and liquid water is present from a range of 0 to about 8 km. This means that according to the satellite retrievals mixed-phase clouds should only occur in the range of 2.5 to 8 km. Therefore, the lowest altitude at which mixed-phase clouds are simulated in ICON-ESM agrees well with the satellite retrievals, but the simulated mixed-phase clouds extend to too high altitudes. Ice clouds dominate in the tropics, as their cloud fraction is overall the largest, consistent with CloudSat-CALIPSO and CERES-MODIS satellite retrievals in Stanfield et al. (2014). The highest ice cloud fraction is located at around 14 km altitude, which agrees with the cirrus cloud cover derived from CALIPSO satellite retrievals, as shown in (Gasparini et al., 2018), and the total cloud cover derived from CloudSat/CALIPSO satellite retrievals shown in Voigt et al. (2021).
In the mid-latitudes, the highest liquid cloud fraction is found at about 1.5 km altitude. In contrast to the tropics, mixed-phase and ice clouds are also simulated close to the surface. The highest mixed-phase cloud fraction is located at about 4 km. The peak of ice cloud fraction is located at around 9 km. The liquid and mixed-phase clouds extend up to about same altitude as in the tropics, but the ice cloud fraction do not reach as high up compared to the tropics, because the tropopause is lower in the mid-latitudes.
The cloud type with the lowest cloud fraction in the high-latitudes is liquid clouds, as temperatures are lower in this region. This is also the case in the satellite retrievals of Matus and L'Ecuyer (2017). The highest liquid cloud fraction is simulated close to the surface. The peak of mixed-phase clouds is much closer to the surface than in the other regions, at around 1 km. Due to the lower temperatures

of the high-latitude troposphere the liquid cloud fraction decreases to 0 already at about 7 km altitude and the mixed-phase cloud fraction at around 9 km altitude. The ice cloud fraction does not reach 0 in the stratosphere, since the model simulates polar stratospheric clouds there. The highest ice cloud fraction is located at an altitude of about 6 km.

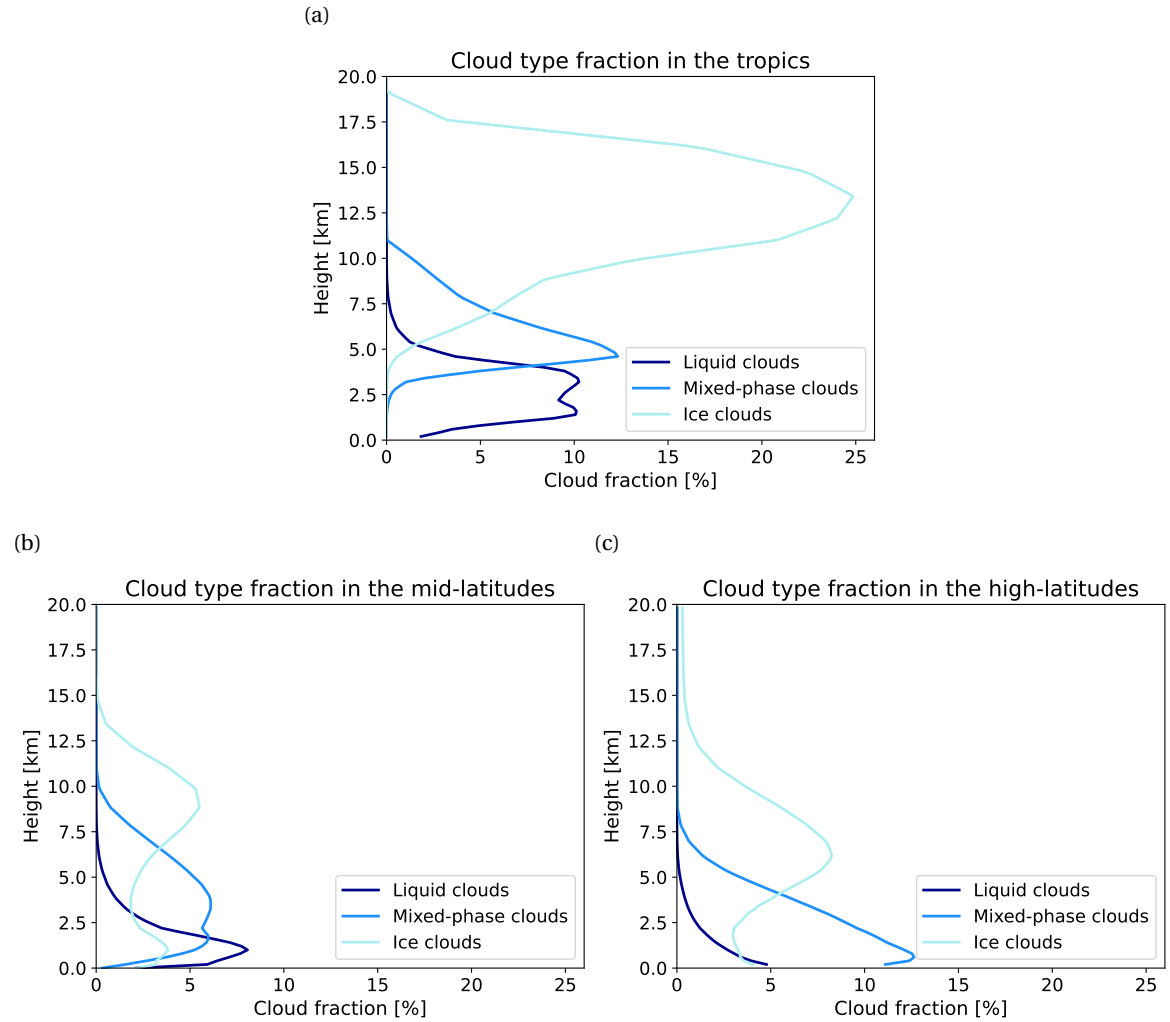

Figure 9: Vertical profiles of the cloud fraction of different cloud types averaged over the tropics, mid-latitudes, and high-latitudes.

In the following, I will compare the cloud fraction of high-level clouds, diagnosed by the "cirrus diagnostic" and the "cirrus + warm base diagnostic" from the "diagnose cloud types" simulation. Figure 10 shows the zonal high-level cloud fraction diagnosed by the "cirrus diagnostic" and the "cirrus + warm base diagnostic", which are defined in section 3.4. In both simulations, most high-level clouds are located in the tropics and in the high-latitudes, with a minimum in the subtropics. This is similar to the ice cloud fraction plot (Figure 7(c)), as all ice clouds colder than -35°C are included in both diagnostics. In the "cirrus diagnostic", some clouds are located below the -35°C isotherm. This is due to the fact that the plotted -35°C isotherm is the climatological mean. The "cirrus + warm base diagnostic" has a higher cloud fraction below the -35°C isotherm, because it considers the cloud parts at temperatures warmer than the -35°C threshold. Most warm bases are located in the tropics, especially at the ITCZ location, and in the mid-latitude regions.

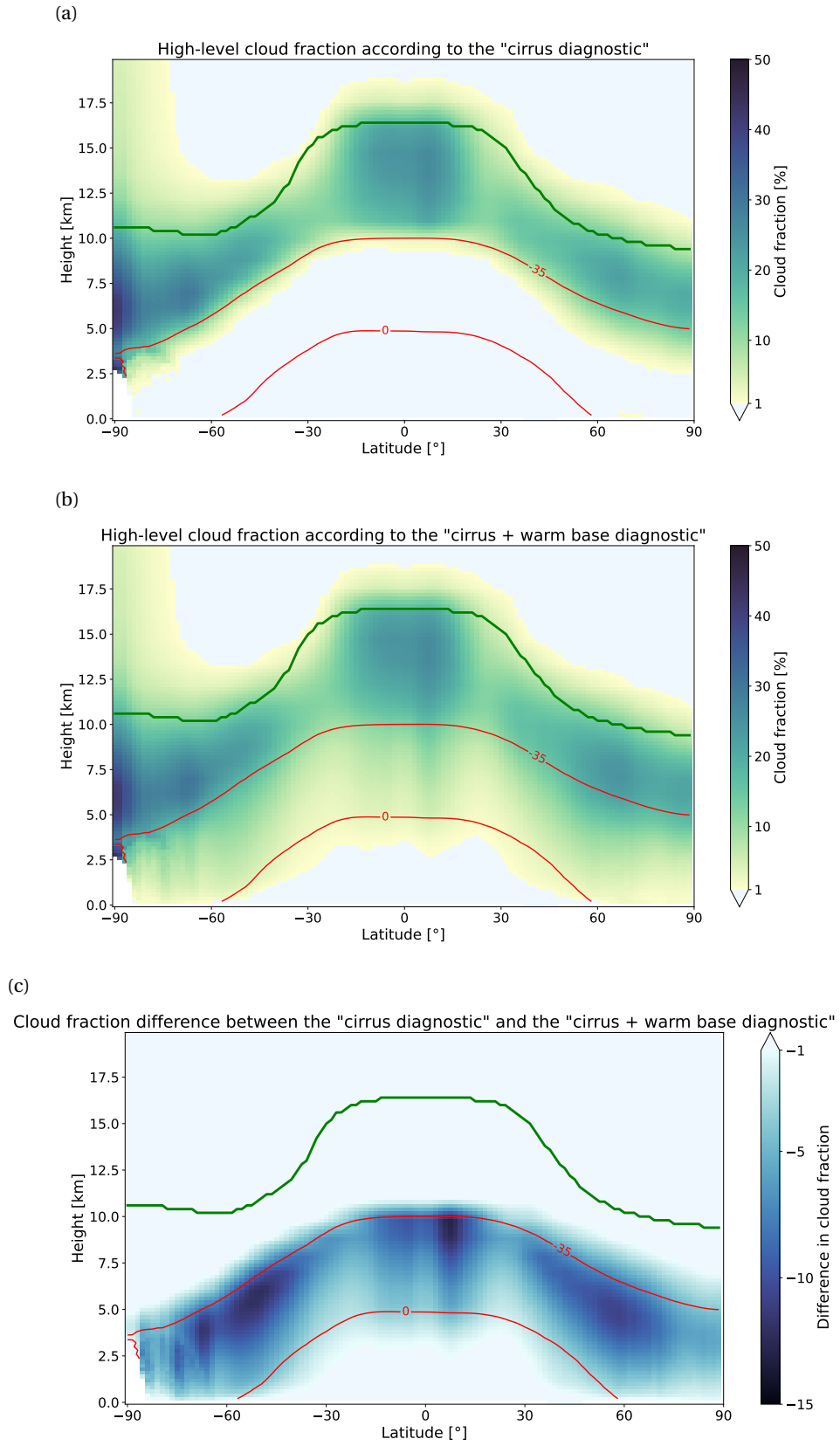

Figure 10: Zonal plot of high-level clouds diagnosed by the "cirrus diagnostic", "cirrus + warm base diagnostic" and the difference between the two diagnostics ("cirrus diagnostic" - "cirrus + warm base diagnostic"). Red contour lines show the mean -35°C and the 0°C isotherms. The green contour depicts the mean tropopause height, which is derived from the tropopause air pressure output of the simulation.

5.2 Comparison of the cloud radiative effects of high-level clouds

This section compares the mean CRE of high-level clouds according to the $HCRE$ definition of Equation 5 ($HCRE_{all-sky}$) and of Equation 6 ($HCRE_{clear-sky}$). I determine the $HCRE$ diagnostically from the "diagnose cirrus all-sky", "diagnose cirrus clear-sky", "diagnose cirrus + warm base all-sky" and "diagnose cirrus + warm base clear-sky" simulations (for a short description of the simulations see Table 1). First the $HCRE_{all-sky}$ and $HCRE_{clear-sky}$ are compared first using the "cirrus diagnostic" and then using the "cirrus + warm base diagnostic".

The TOA $HCRE_{all-sky}$ and $HCRE_{clear-sky}$ using "cirrus diagnostic" are shown in Figure 11. The TOA cools in the shortwave due to the scattering of the solar insolation. In the longwave, cirrus clouds cause a warming, which is particularly large in the tropics, where cirrus clouds can reside at colder temperatures and therefore reduce the outgoing longwave radiation more efficiently than in other regions. The net effect of high-level clouds is dominated by the longwave effect, therefore the overall radiative effect of cirrus clouds is a warming. The $HCRE_{all-sky}$ in my simulation is close to those in Gasparini and Lohmann (2016) and Gasparini et al. (2020). Furthermore, the results of the TOA CRE are qualitatively consistent with the satellite retrievals for ice clouds, which I assume to be predominantly high-level clouds, from Matus and L'Ecuyer (2017). The $HCRE_{all-sky}$ is smaller in magnitude than the $HCRE_{clear-sky}$. The shortwave effect is less negative in $HCRE_{all-sky}$, because when cirrus

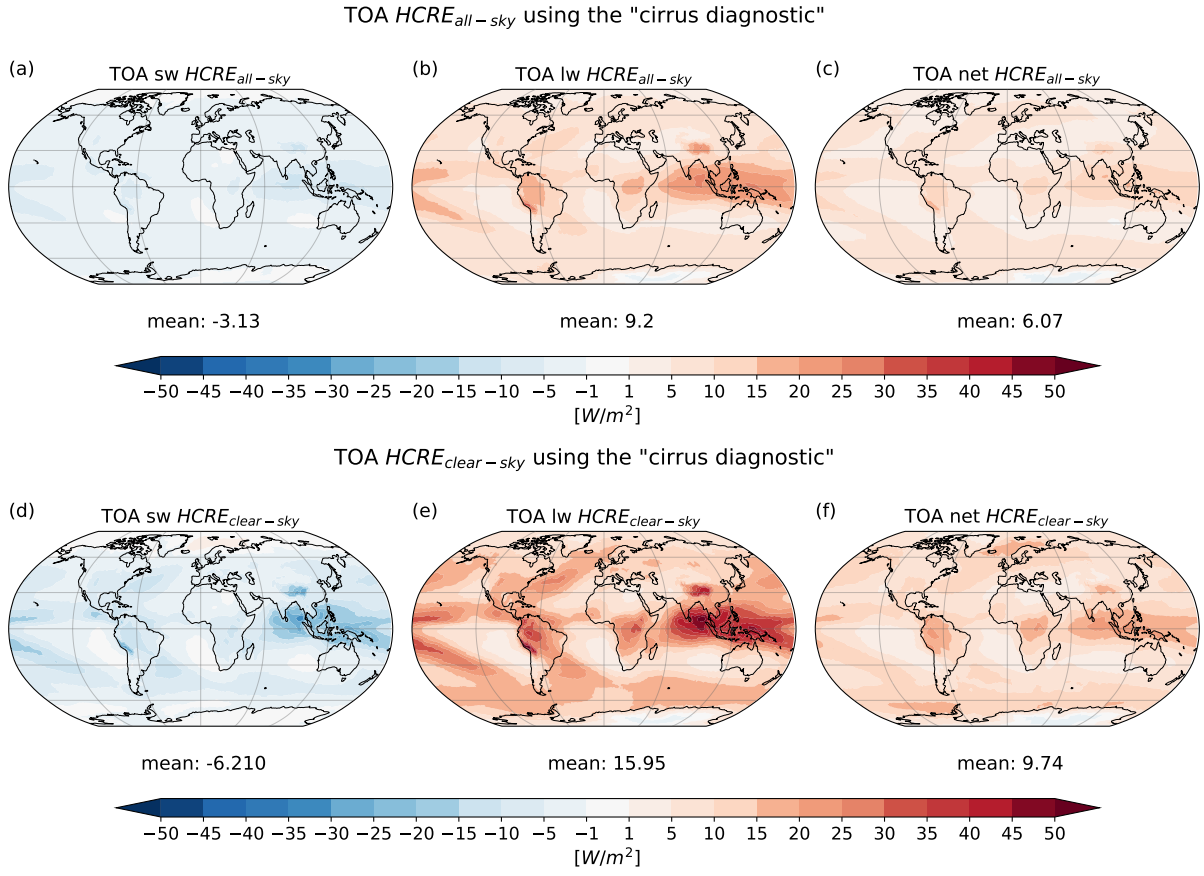

Figure 11: Shortwave (sw), longwave (lw) and net HCRE at the TOA according to the "cirrus diagnostic". The $HCRE_{all-sky}$ are shown in Panels (a), (b) and (c) and the $HCRE_{clear-sky}$ in Panels (d), (e) and (f).

clouds are radiatively inactive, the incoming shortwave radiation is partially absorbed and reflected back by non-cirrus clouds. If instead no clouds are radiatively active, more radiation will be absorbed and reflected back by the Earth's surface than in an all-sky atmosphere. However, the albedo of the surface is much lower than that of the non-cirrus clouds, so more energy is absorbed by the Earth system in a clear-sky atmosphere. This causes the more negative shortwave $HCRE_{clear-sky}$ at the TOA. The longwave effects of $HCRE_{clear-sky}$ are larger because the lower clouds cannot absorb and re-emit the longwave radiation emitted by the cirrus clouds.

Figure 12 depicts the surface mean shortwave, longwave and net $HCRE$ using the "cirrus diagnostic". The cirrus clouds cool the equatorial regions in the shortwave. This can be explained by their scattering of solar radiation, which reduces the amount of shortwave radiation reaching the surface. The surface longwave effect is a slight warming, which is maximal in Antarctica, Greenland and in the Himalayas, since there is not as much water vapor and/or lower clouds that could absorb and re-emit the longwave radiation. The net effect is dominated by the longwave effect at the high-latitudes and the shortwave effect in the tropics. The $HCRE_{clear-sky}$ is larger in magnitude than the $HCRE_{all-sky}$. In the shortwave this is due to more radiation being absorbed by the surface in a clear-sky atmosphere. The larger longwave effect in $HCRE_{clear-sky}$ is caused by the increased amount of longwave radiation, which is re-emitted by the high-level clouds, reaching the surface in an otherwise clear-sky

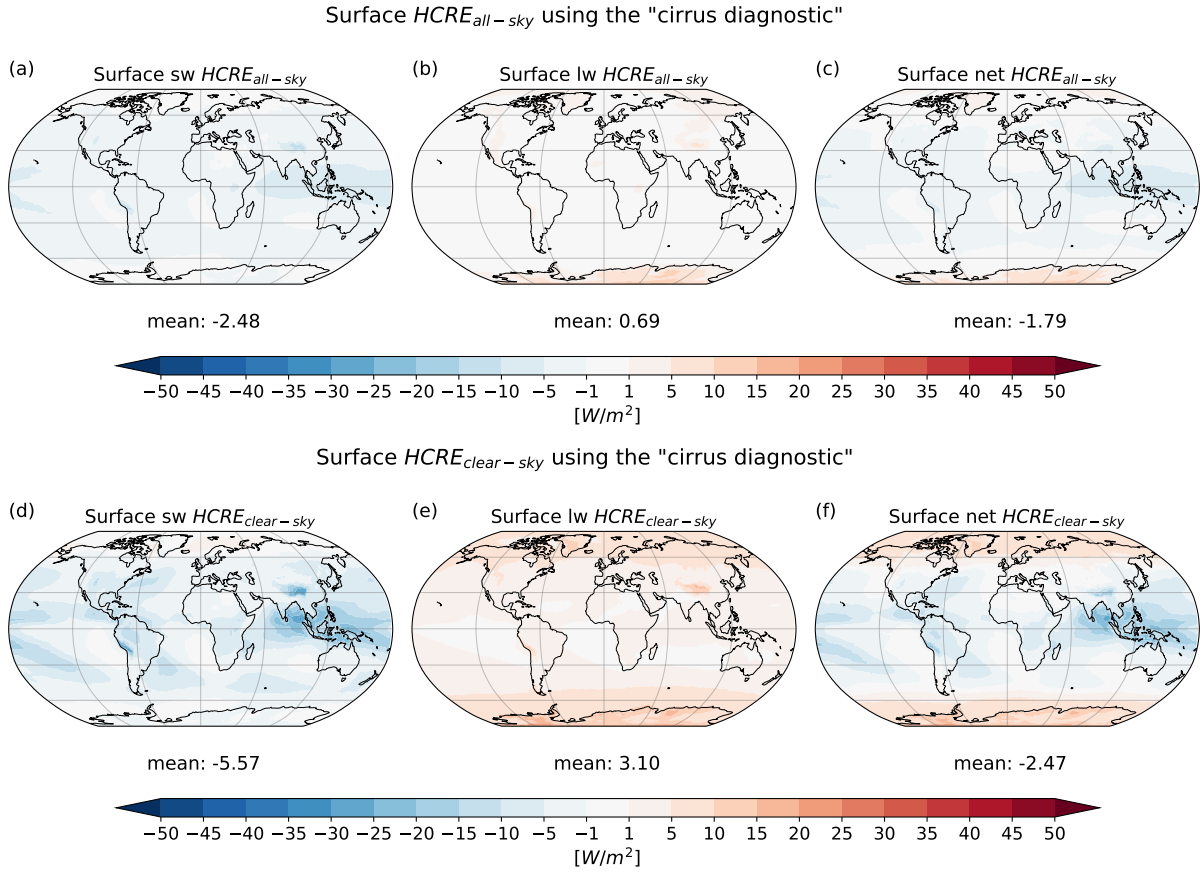

Figure 12: Shortwave (sw), longwave (lw) and net HCRE at the surface according to the "cirrus diagnostic". The $HCRE_{all-sky}$ is shown in Panels (a), (b) and (c) and the $HCRE_{clear-sky}$ in Panels (d), (e) and (f).

atmosphere. The overall patterns of the $HCRE_{all-sky}$ and the $HCRE_{clear-sky}$ are similar to those of the ice cloud satellite retrievals from Matus and L'Ecuyer (2017).

The difference between the TOA and surface radiative effects of cirrus clouds gives the ACRE of the cirrus clouds, which is shown in Figure 13. There are two effects that can lead to a shortwave heating of the atmosphere, shortwave absorption and enhanced absorption by the atmosphere above the cloud due to the scattering of solar radiation by the cirrus clouds. Clouds can also cause a shortwave cooling effect by reducing the shortwave absorption below the cloud (Hong et al., 2016). The latter effect dominates in ICON-ESM over most regions, while the satellite retrievals of Matus and L'Ecuyer (2017) mostly show an atmospheric shortwave warming.

Overall, the shortwave effect in the atmosphere is small, and the net CRE of cirrus clouds is dominated by the longwave effect. The longwave warming is particularly strong in the equatorial regions, where the temperature difference between the cloud top and the surface is the largest and the re-emission of longwave radiation occurs at much colder temperatures. Only over Antarctica there is a net cooling of the atmosphere due to the radiative heating of the surface. The patterns of the ICON-ESM simulation results are similar to the satellite retrievals in Matus and L'Ecuyer (2017), except for the shortwave. The shortwave $HCRE_{all-sky}$ and $HCRE_{clear-sky}$ are almost equal, indicating that the non-high-level clouds in an all-sky atmosphere do not significantly influence the shortwave effect of the cirrus clouds compared to an atmosphere with only cirrus clouds. The longwave effect and the

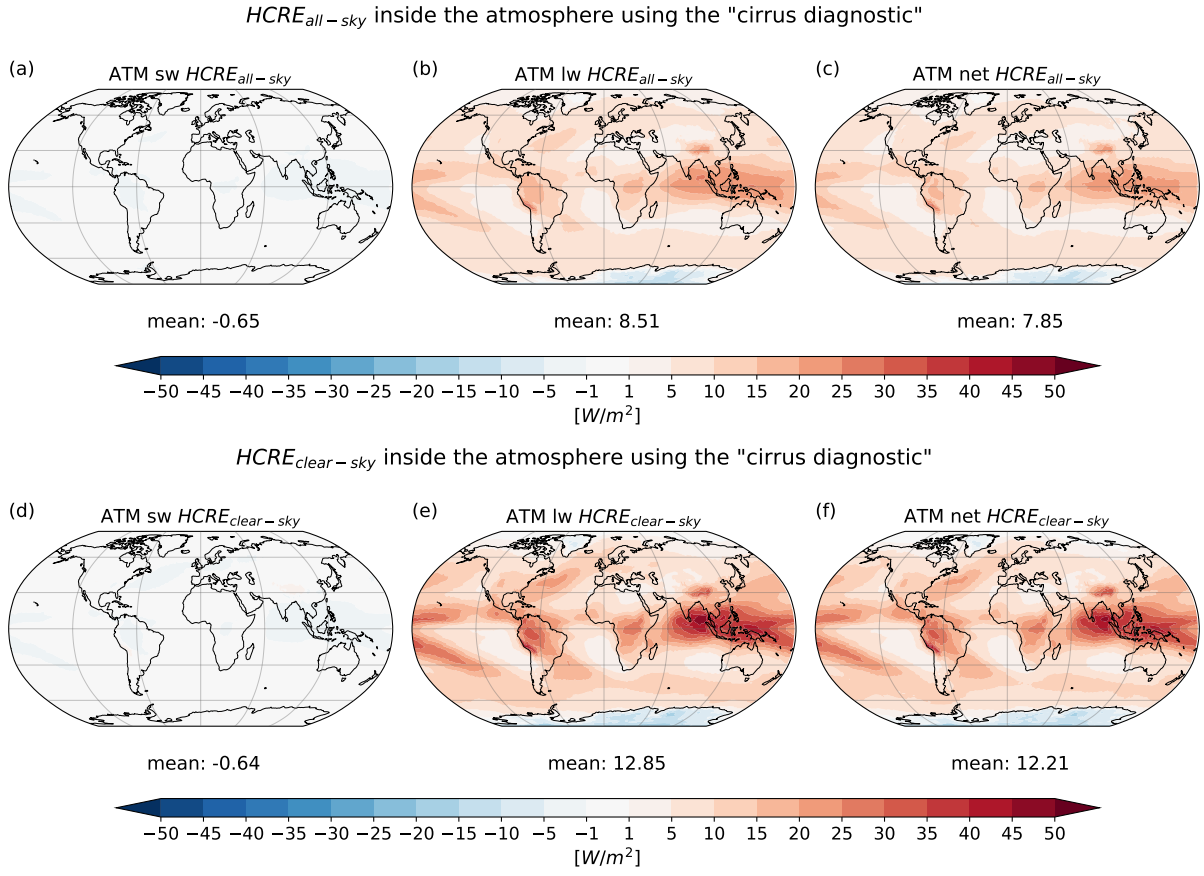

Figure 13: Shortwave (sw), longwave (lw) and net HCRE inside the atmosphere according to the "cirrus diagnostic". The $HCRE_{all-sky}$ is shown in Panels (a), (b) and (c) and the $HCRE_{clear-sky}$ in Panels (d), (e) and (f).

net effect are larger in $HCRE_{clear-sky}$ because more outgoing longwave radiation can be absorbed by high-level clouds when non-high-level clouds are radiatively inactive.

Next, I investigate the HCRE using the "cirrus + warm base diagnostic". The shortwave and longwave TOA $HCRE$ using the "cirrus + warm base diagnostic" (Figure 14) shows the same pattern as when using the "cirrus diagnostic" (Figure 15), but the magnitudes are larger, due to the larger cloud fraction considered by the "cirrus + warm base diagnostic". However, the net effect is smaller because the magnitude of the shortwave effect is more similar to that of the longwave effect, since the warm bases may contain liquid water and therefore reflect more shortwave radiation than the cirrus clouds alone. As for the "cirrus diagnostic", the $HCRE_{clear-sky}$ (Figure 14(d) and (e)) is larger in magnitude than the $HCRE_{all-sky}$ (Figure 14(a) and (b)). This is because non-high-level clouds cannot mask the effects of high-level clouds in $HCRE_{clear-sky}$.
While in the "cirrus diagnostic" all high-level clouds are ice clouds, the high-level clouds according to the "cirrus + warm base diagnostic" may include multi-layer clouds (i.e., clouds containing distinct layers of ice and liquid water), since the warm bases may contain liquid water. Nevertheless, the net $HCRE$ according to the "cirrus + warm base diagnostic" agrees well with the ice cloud radiative effect satellite retrievals of Matus and L'Ecuyer (2017) (Figure 1). This indicates that most high-level clouds in the "cirrus + warm base diagnostic" are ice clouds and not multi-layer clouds.

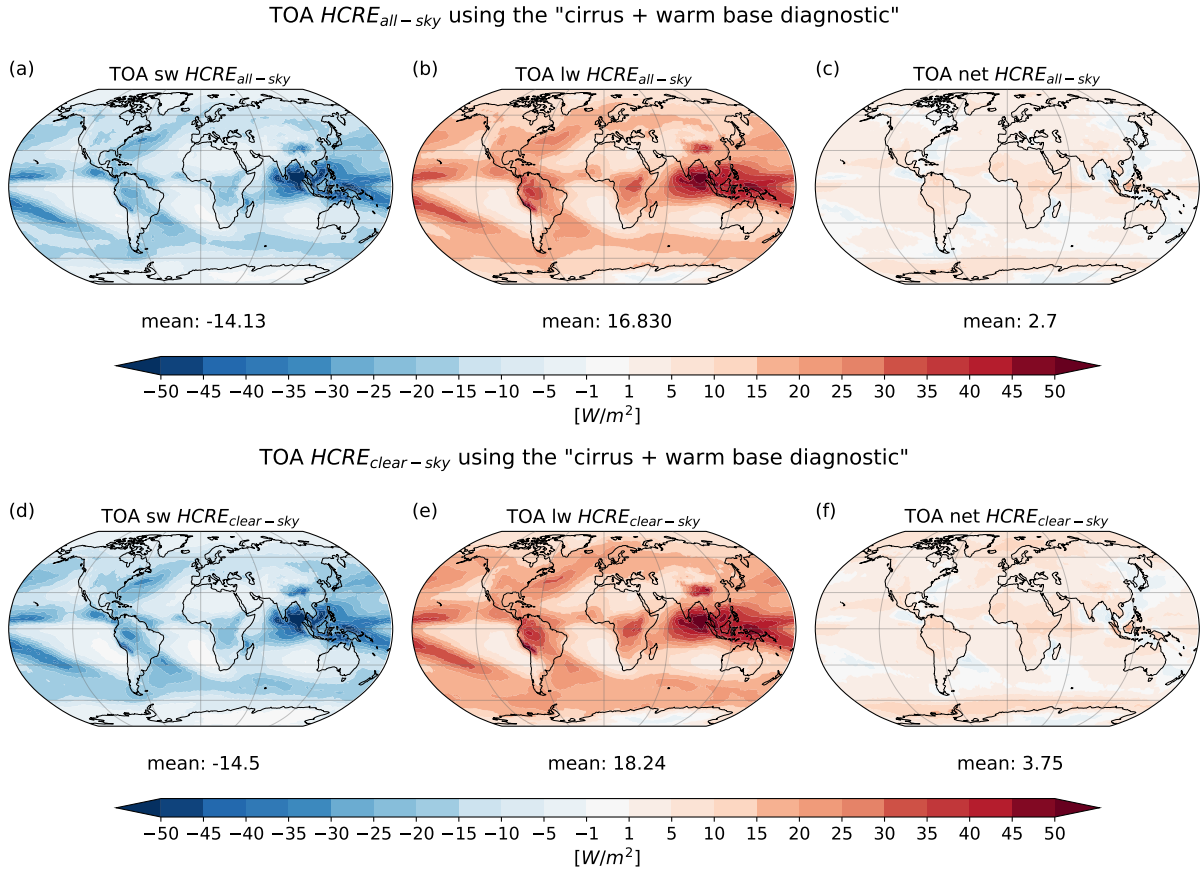

Figure 14: Shortwave (sw), longwave (lw) and net HCRE at the TOA according to the "cirrus + warm base diagnostic". The $HCRE_{all-sky}$ is shown in Panels (a), (b) and (c) and the $HCRE_{clear-sky}$ in Panels (d), (e) and (f).

As for the TOA $HCRE$, the surface $HCRE$ using the "cirrus + warm base diagnostic", shown in Figure 15, has a larger effect than when using the "cirrus diagnostic"(Figure 12), because the effects of the warm bases are considered in the "cirrus + warm base diagnostic". In particular, the shortwave cooling effect is more than doubled when the warm bases are taken into account. This shows that the warm bases reflect more shortwave radiation than their colder cloud tops. As in the "cirrus diagnostic", the shortwave and longwave surface $HCRE$ is larger in magnitude in $HCRE_{clear-sky}$ (Figure 15(d) and (e)) than in $HCRE_{all-sky}$ (Figure 15(a) and (b)). The net surface $HCRE_{clear-sky}$ is less negative, due to the more positive longwave effect. The surface shortwave $HCRE_{all-sky}$ and the surface longwave $HCRE_{all-sky}$ are more similar to those of $HCRE_{clear-sky}$ when using the "cirrus + warm base diagnostic", because there are less non-high-level clouds, since in contrast to the "cirrus diagnostic" the warm bases are not considered as non-high-level clouds. Fewer non-high-level clouds result in less masking of the effects of high-level clouds.
Compared to the satellite retrievals of surface CRE of ice clouds by Matus and L'Ecuyer (2017) (Figure 2) the longwave effect is of similar magnitude, while the shortwave effect is larger. This could be partly due to the fact that some multi-layer clouds are included in the "cirrus + warm base diagnostic", which cool the surface more than ice clouds.

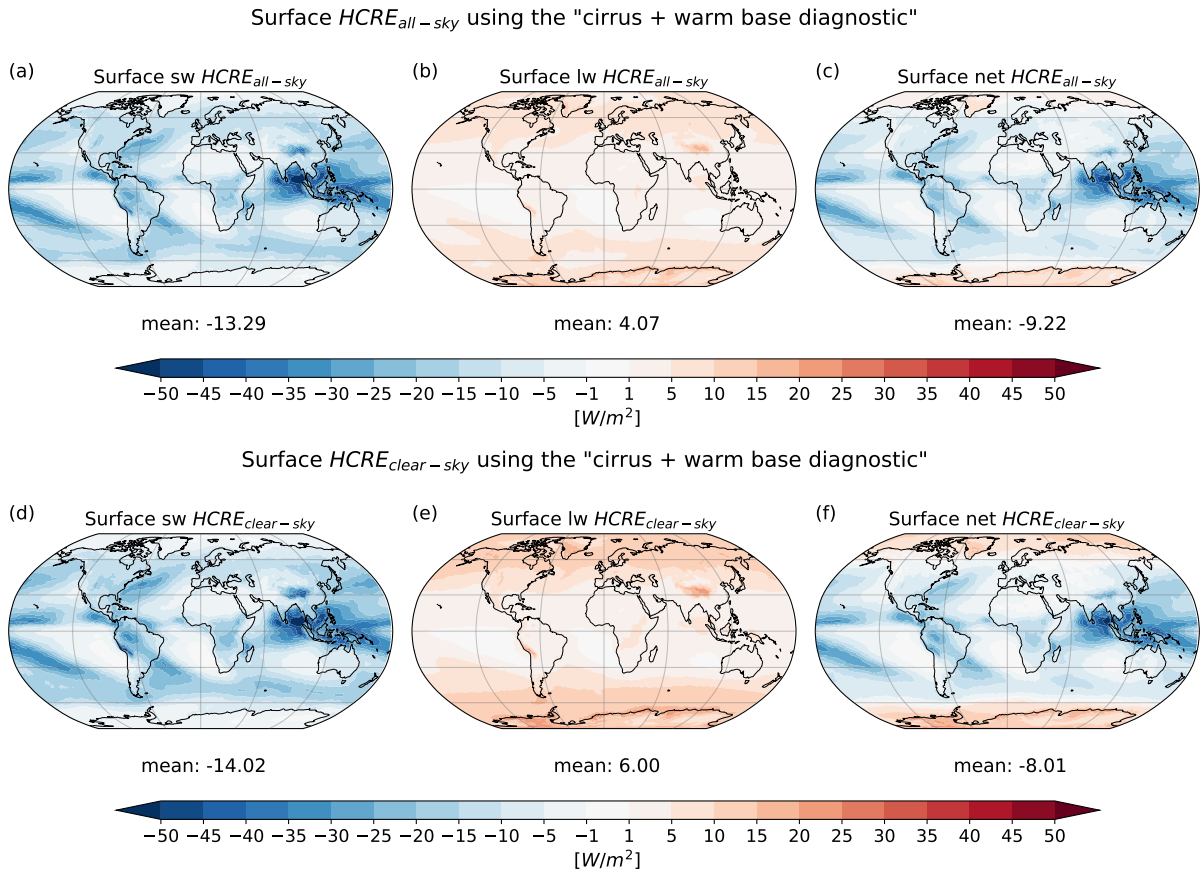

Figure 15: Shortwave (sw), longwave (lw) and net HCRE at the surface according to the "cirrus + warm base diagnostic". The $HCRE_{all-sky}$ is shown in Panels (a), (b) and (c) and the $HCRE_{clear-sky}$ in Panels (d), (e) and (f).

The shortwave effects inside the atmosphere using the "cirrus + warm base diagnostic" (Figure 16(a) and (d)) are similar in magnitude to those of the "cirrus diagnostic" (Figure 13(a) and (d)). The $HCRE_{clear-sky}$ is slightly less negative if the warm bases are considered, since more solar radiation is absorbed. However, the $HCRE_{all-sky}$ according to the "cirrus + warm base diagnostic" is more

negative than the $HCRE_{all-sky}$ according to the "cirrus diagnostic", although the additional shortwave heating effect of the warm bases is included. If only cirrus clouds are not radiatively active, the radiation received by the non-high-level clouds is not much different, because the cirrus clouds are typically optically thin and therefore do not interact much with the shortwave radiation. However, the warm bases of the cirrus clouds are likely to be optically thicker, which means they can influence the shortwave radiation more. This means that in an all-sky atmosphere a non-high-level cloud absorbs much less shortwave radiation than in an atmosphere with radiatively inactive cirrus clouds and their warm bases. The $HCRE_{all-sky}$ is more negative according to the "cirrus + warm base diagnostic" than according to the "cirrus diagnostic". This indicates that the cooling effect, caused by the non-high-level clouds receiving less solar radiation when the warm bases are active, seems to dominate over the heating effect of the warm bases absorbing more shortwave radiation.

The longwave and net effects in the atmosphere, according to both $HCRE_{clear-sky}$ and $HCRE_{all-sky}$, using the "cirrus + warm base diagnostic" (Figure 16), are slightly smaller than $HCRE_{clear-sky}$ using the "cirrus diagnostic" (Figure 13). The inclusion of the warm bases reduces $HCRE_{clear-sky}$ in the longwave, because the temperature difference between the surface and the cloud base is smaller. However, the longwave $HCRE_{all-sky}$ increases if the warm bases are included, because there are less non-high-level clouds compared to the "cirrus diagnostic", which can mask some effects of the high-level clouds. As for the TOA and the surface, the use of the "cirrus + warm base diagnostic" reduces the differences between the longwave $HCRE_{clear-sky}$ and $HCRE_{all-sky}$ in the atmosphere, with $HCRE_{all-sky}$ having slightly larger effects. Since the net effect inside the atmosphere is dom-

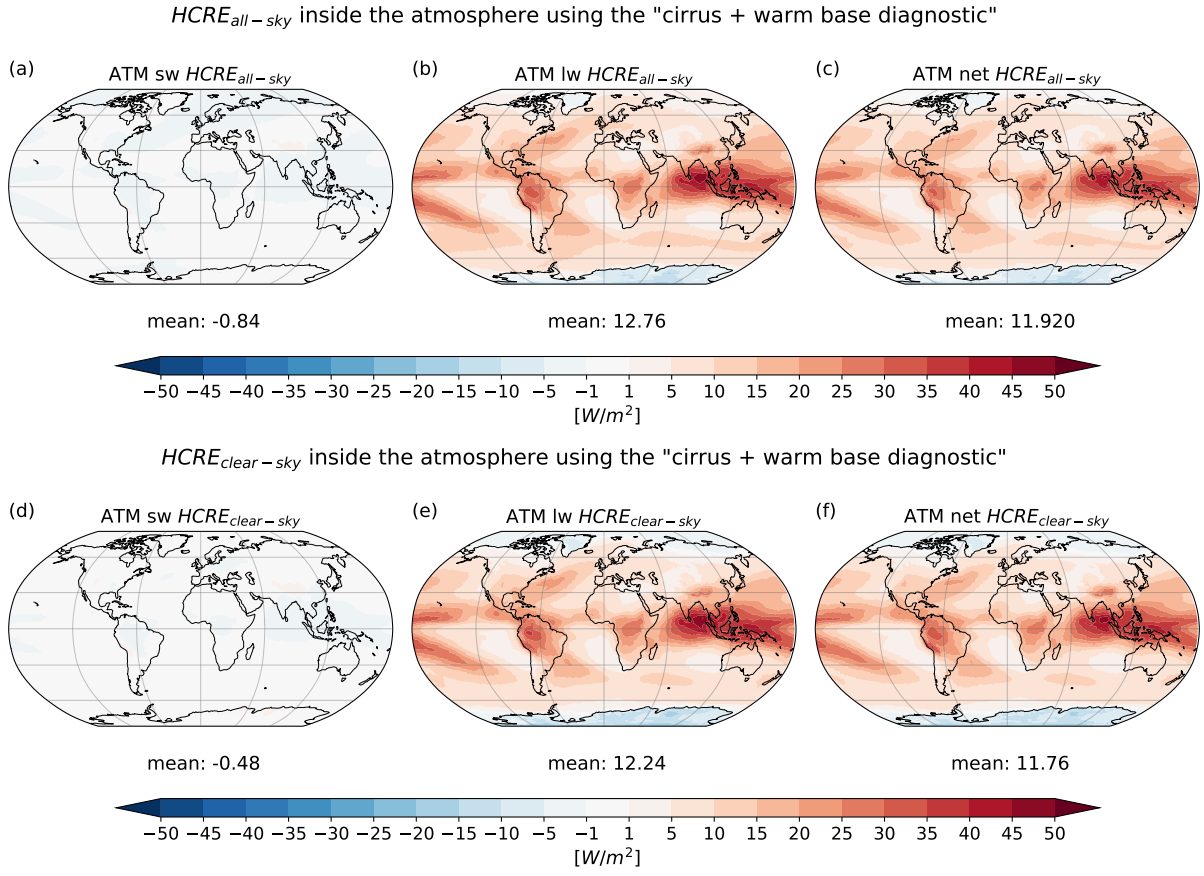

Figure 16: Shortwave (sw), longwave (lw) and net HCRE inside the atmosphere according to the "cirrus + warm base diagnostic". The $HCRE_{all-sky}$ is shown in Panels (a), (b) and (c) and the $HCRE_{clear-sky}$ in Panels (d), (e) and (f).

inated by the longwave effect, the net $HCRE_{clear-sky}$ and $HCRE_{all-sky}$ inside the atmosphere are also more similar when the warm bases are included as high-level clouds.
As for the net $HCRE$ in the atmosphere according to the "cirrus diagnostic", the net $HCRE$ in the atmosphere according to the "cirrus + warm base diagnostic" is larger in magnitude than the ACRE of ice clouds in the satellite retrievals from Matus and L'Ecuyer (2017) (Figure 3), but the patterns are qualitatively similar.

Overall, the simulation results of the $HCRE$ at the TOA, the surface and in the atmosphere shows physically meaningful patterns, for both high-level cloud diagnostics and for both methods of calculating the $HCRE$. At the TOA and at the surface, using the $HCRE_{clear-sky}$ results in shortwave and longwave effects of greater magnitude than using the $HCRE_{all-sky}$, because non-high-level clouds partially mask the effects of the high-level clouds. The "cirrus + warm base diagnostic" enhances the shortwave and longwave effects at the TOA and surface compared to the "cirrus diagnostic", since more high-level clouds are considered.

5.3 Comparison of the cloud radiative heating rates of high-level clouds

The mean radiative heating rates of high-level clouds according to the $\partial_t T|_{hlc}$ definition of Equation 7 ($\partial_t T|_{hlc,all-sky}$) and of Equation 8 ($\partial_t T|_{hlc,clear-sky}$) are compared in this section. First, the total cloud radiative heating is shown, then the two $\partial_t T|_{hlc}$ definitions are compared using the "cirrus diagnostic" and afterwards using the "cirrus + warm base diagnostic".

The shortwave warming effect in the total cloud heating rate, shown in Figure 17(a), is caused by the absorption of solar radiation by the clouds and by the enhanced molecular absorption above the cloud due to scattering by the clouds. In particular, clouds at temperatures colder than the mean -35°C isotherm contribute to this shortwave warming. Clouds below the mean 0°C isotherm reflect large amounts of solar radiation thereby reducing the absorption at their location and below. The longwave radiative cooling in the upper troposphere in Figure 17(b) is caused by the emission of

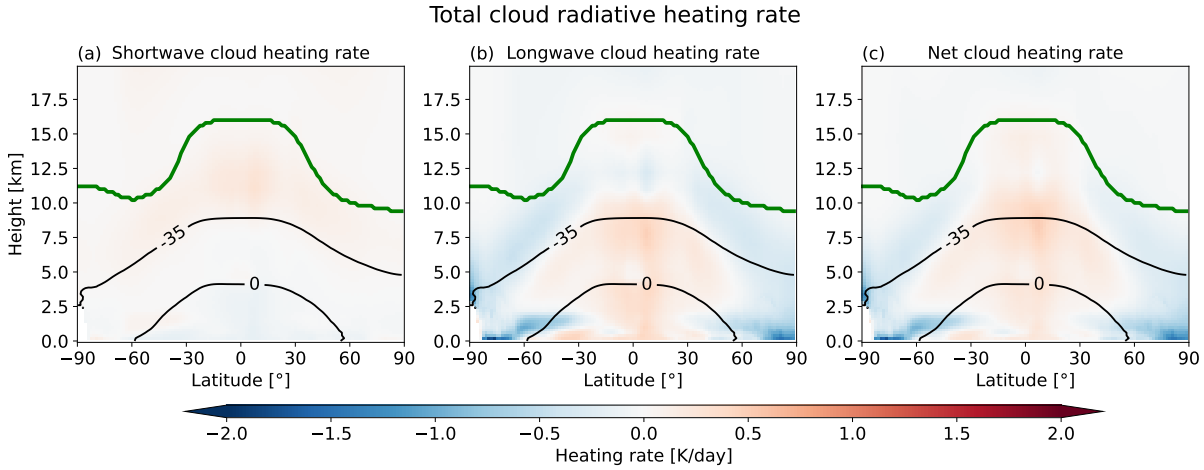

Figure 17: Shortwave, longwave and net cloud radiative heating rates. Black contour lines show the -35°C and the 0°C isotherms. The green contour depicts the mean tropopause height, which is derived from the tropopause air pressure output of the simulation.

radiation at the cloud tops and a radiative heating effect is caused by the longwave absorption at the cloud bases. The longwave heating rate of all clouds dominates the net heating rate of all clouds (Figure 17(c)), but the shortwave heating of clouds dominates in the tropical upper troposphere.

Panels (a) and (b) of Figure 18 show the all-sky radiative heating and the radiative heating in an atmosphere without any radiatively active cirrus clouds respectively. If cirrus clouds are not interacting with radiation, the clouds below to absorb more shortwave radiation, leading to a shortwave heating in these regions in the heating rate with only non-high-level clouds radiatively active, as shown in Figure 18(b). Since the heating rate with only non-high-level clouds radiatively active (Figure 18(b)) is then subtracted from the all-sky heating rate (Figure 18(a)), the heating below the high-level clouds then appears as a shortwave cooling in the radiative heating rate of high-level clouds (Figure 18(c)). For $\partial_t T|_{hlc,all-sky}$, the shortwave cooling below the tropical high-level clouds is therefore slightly larger than in $\partial_t T|_{hlc,clear-sky}$, which diagnoses the cloud radiative heating with a clear-sky atmo-

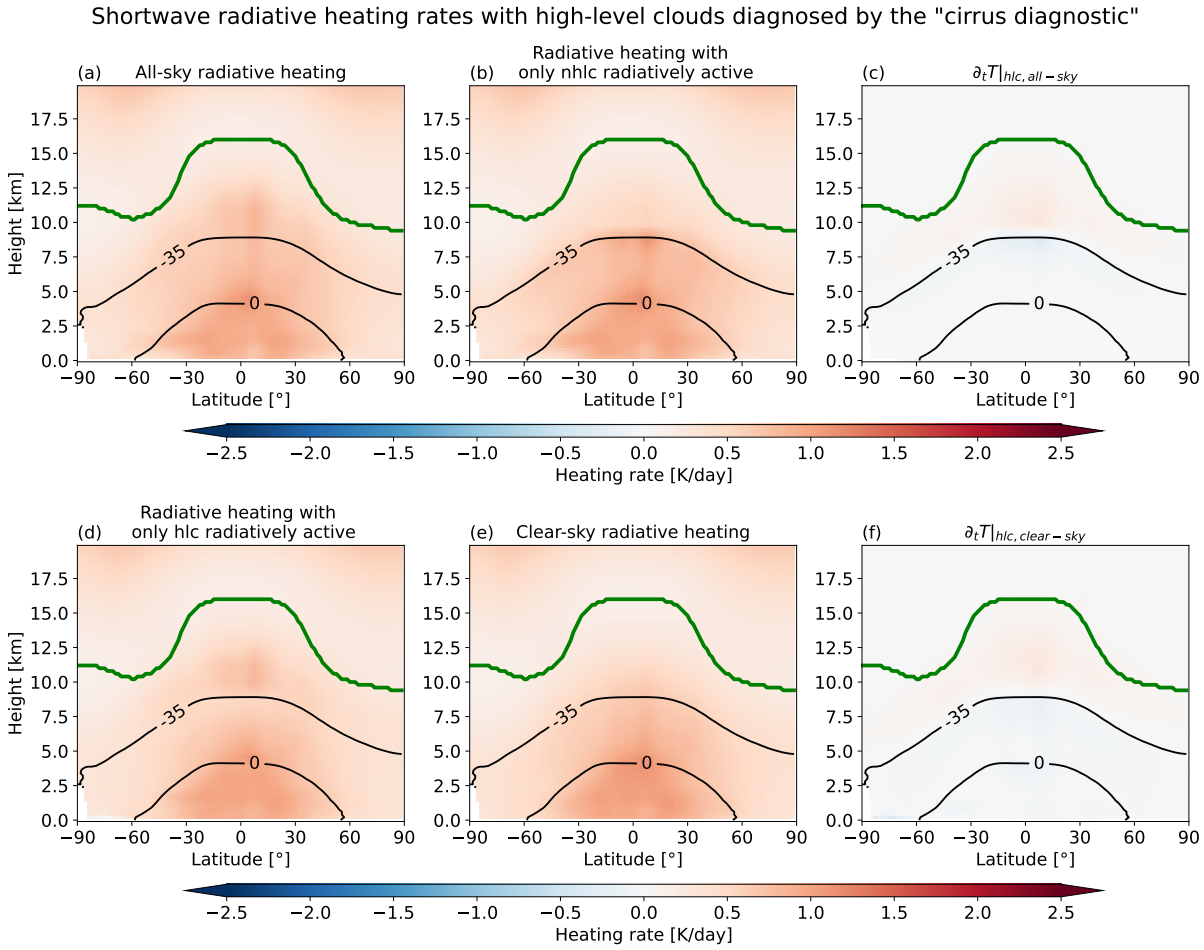

Figure 18: Shortwave radiative heating rates with high-level clouds diagnosed using the "cirrus diagnostic". Panel (a) shows the total cloud radiative heating rate, while Panel (b) depicts the radiative heating rate of an atmosphere without radiatively active high-level clouds. The difference between Panel (a) and (b) gives the cloud radiative heating rate of high-level clouds using $\partial_t T|_{hlc,all-sky}$, which is shown in Panel (c). Panel (d) depicts the radiative heating in an atmosphere with only high-level clouds radiatively active, while Panel (e) is the radiative heating of a clear-sky atmosphere. The difference between Panels (d) and (e) gives the cloud radiative heating rate of high-level clouds using $\partial_t T|_{hlc,all-sky}$ in Panel (f). Black contour lines show the -35°C and the 0°C isotherms. The green contour depicts the mean tropopause height, which is derived from the tropopause air pressure output of the simulation.

sphere as a reference. In $\partial_t T|_{hlc,clear-sky}$ (Figure 18(f)) no non-high-level clouds are radiatively active and therefore the radiative cooling below the high-level clouds is slightly weaker. The radiative cooling in $\partial_t T|_{hlc,clear-sky}$ is caused by the enhanced shortwave absorption in an atmosphere with only high-level clouds radiatively active (Figure 18(d)) compared to a clear-sky atmosphere (Figure 18(e)).

In an all-sky atmosphere, cirrus clouds absorb longwave radiation and re-emit it back to the lower levels. Figure 19(a) shows the longwave all-sky radiative heating. If the cirrus clouds are not interacting with radiation, they cannot absorb and re-emit longwave radiation back to the non-high-level clouds below them. Therefore, the tops of the non-high-level clouds directly below the radiatively inactive cirrus clouds receive less longwave radiation, causing a longwave cooling at the temperature threshold level, as shown in Figure 19(b). To diagnose the cirrus cloud radiative heating rate

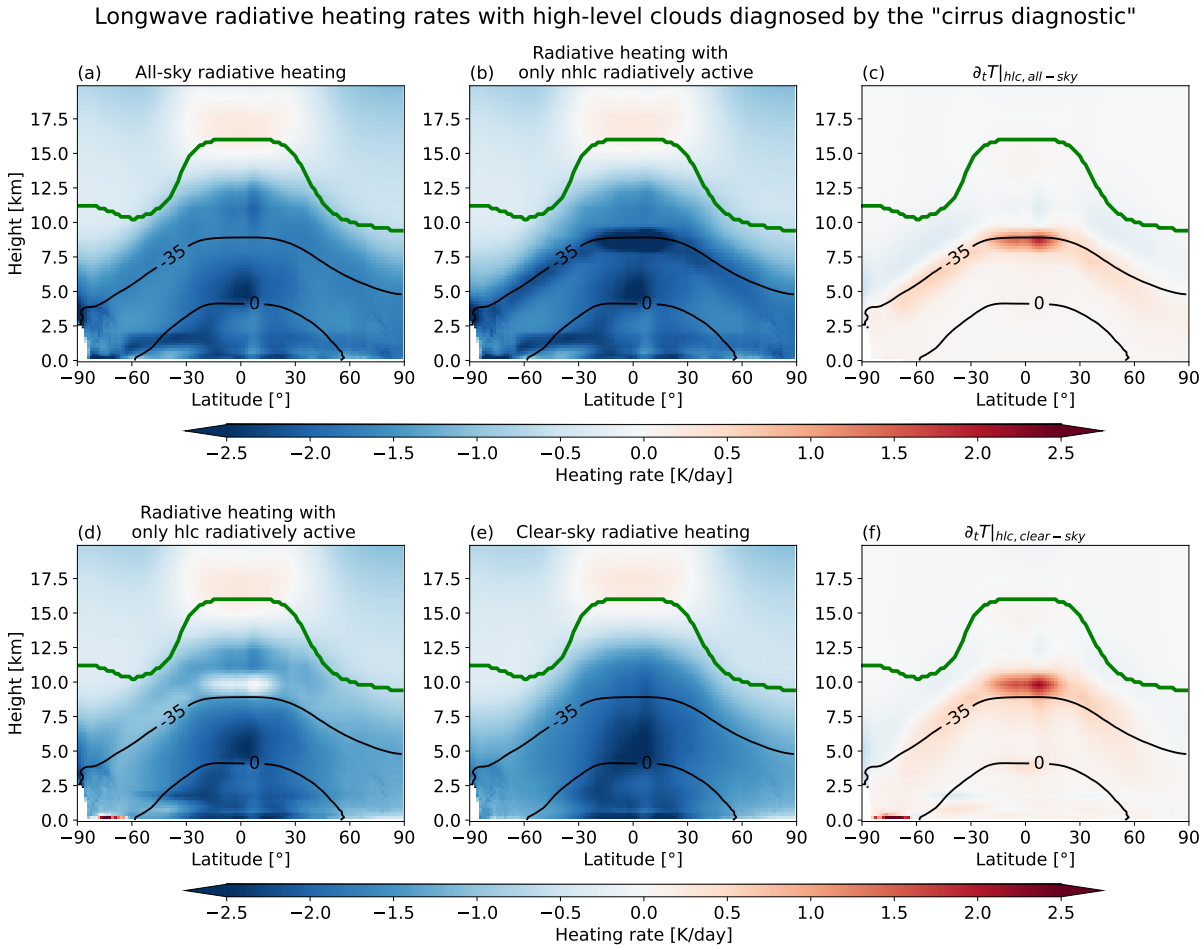

Figure 19: Longwave radiative heating rates with high-level clouds diagnosed using the "cirrus diagnostic". Panel (a) shows the total cloud radiative heating rate, while Panel (b) depicts the radiative heating rate of an atmosphere without radiatively active high-level clouds. The difference between Panel (a) and (b) gives the cloud radiative heating rate of high-level clouds using $\partial_t T|_{hlc,all-sky}$, which is shown in Panel (c). Panel (d) depicts the radiative heating in an atmosphere with only high-level clouds radiatively active, while Panel (e) is the radiative heating of a clear-sky atmosphere. The difference between Panels (d) and (e) gives the cloud radiative heating rate of high-level clouds using $\partial_t T|_{hlc,all-sky}$ in Panel (f). Black contour lines show the -35°C and the 0°C isotherms. The green contour depicts the mean tropopause height, which is derived from the tropopause air pressure output of the simulation.

according to the definition of $\partial_t T|_{hlc,all-sky}$ the difference between an all-sky atmosphere and an atmosphere without radiatively active high-level clouds is taken. The stronger longwave cooling at the tops of the non-high-level clouds below the cirrus clouds in an atmosphere without radiatively active cirrus clouds (Figure 19(b)) compared to the all-sky radiative heating (Figure 19(a)) results in the radiative heating at and slightly below the -35°C isotherm in $\partial_t T|_{hlc,all-sky}$, as shown in Figure 19(c). A longwave heating can also be caused by the absorption of radiation by cirrus clouds. However, Figure 10a shows that there are not many high-level clouds at the location of the largest longwave radiative heating. Therefore, the strongest longwave warming heating in $\partial_t T|_{hlc,all-sky}$ is not predominately caused by the cirrus clouds themselves, but by the non-high-level clouds, which include the warm bases. The longwave cooling in $\partial_t T|_{hlc,all-sky}$ is caused by the emission of longwave radiation at the cirrus cloud tops. In an atmosphere with only cirrus clouds radiatively interacting the absorption of longwave radiation at the cirrus cloud bases causes a stronger longwave heating rate (see Figure 19(d)) compared to a clear-sky atmosphere (see Figure 19(e)). This results in a longwave heating in $\partial_t T|_{hlc,clear-sky}$, which is shown in Figure 19(f). The longwave cooling is again caused by the emission of longwave radiation at the cirrus cloud tops.
In an atmosphere without any radiatively active non-high-level clouds (Figure 19(d)), there are areas above the -35°C temperature isotherm with a much weaker longwave cooling, caused by the absorption of longwave radiation at the cloud bases of the cirrus clouds. In the clear-sky atmosphere (Figure 19(e)), the radiative cooling in these regions is larger than in an atmosphere with only cirrus clouds radiatively active (Figure 19(d)). This results in the strong longwave heating in the upper troposphere shown in $\partial_t T|_{hlc,clear-sky}$ (Figure 19(f)). The longwave heating below the cirrus clouds is due to the high-level clouds scattering parts of the longwave radiation back toward the surface, which causes an enhanced absorption at the lower lying levels. There is also strong longwave heating close to the surface at the high-latitudes in the Southern Hemisphere in $\partial_t T|_{hlc,clear-sky}$, which is not present in $\partial_t T|_{hlc,all-sky}$. This is because in $\partial_t T|_{hlc,clear-sky}$ the longwave radiation re-emitted back toward the surface by high-level clouds cannot be absorbed by non-high-level clouds, since they are radiatively inactive. The longwave emission at the cloud tops of cirrus clouds leads to the longwave cooling, similarly to $\partial_t T|_{hlc,all-sky}$.

Figure 20 shows the sum of the shortwave and longwave radiative heating rates, where the longwave contribution dominates. However, in the tropical upper troposphere the shortwave cirrus cloud heating prevails over the longwave cooling at the cirrus cloud tops in both of the used diagnostics (Figure 20(c) and (f)). $\partial_t T|_{hlc,all-sky}$ has an overall weaker total heating than $\partial_t T|_{hlc,clear-sky}$ (see also Figure 13 (c) and (f)), due to non-high-level clouds partially masking the cloud radiative heating of high-level clouds. As for the longwave, the largest heating in both cloud radiative heating rates of high-level clouds is concentrated around the -35°C temperature isotherm, due to the artificial increase in the number of cloud bases that located at the temperature threshold by the "cirrus diagnostic". The net radiative heating around the -35°C isotherm is therefore much stronger than in the net radiative heating rate of all clouds in Figure 17(c). The strong heating in $\partial_t T|_{hlc,all-sky}$ is located lower in altitude than that of $\partial_t T|_{hlc,clear-sky}$, because in $\partial_t T|_{hlc,all-sky}$ the heating is mostly generated by the cloud tops of the non-cirrus clouds, while in $\partial_t T|_{hlc,clear-sky}$ it is caused by the heating at the cirrus cloud bases, which are located above the non-cirrus clouds.

In the following I compare the two $\partial_t T|_{hlc}$ using the "cirrus + warm base diagnostic". The shortwave $\partial_t T|_{hlc,all-sky}$ and $\partial_t T|_{hlc,clear-sky}$ in Panels (c) and (f) of Figure 21 are similar, except that the positive shortwave heating extends further below the -35°C isotherm in $\partial_t T|_{hlc,all-sky}$, while the heating is negative below the threshold temperature in $\partial_t T|_{hlc,clear-sky}$. The shortwave heating di-

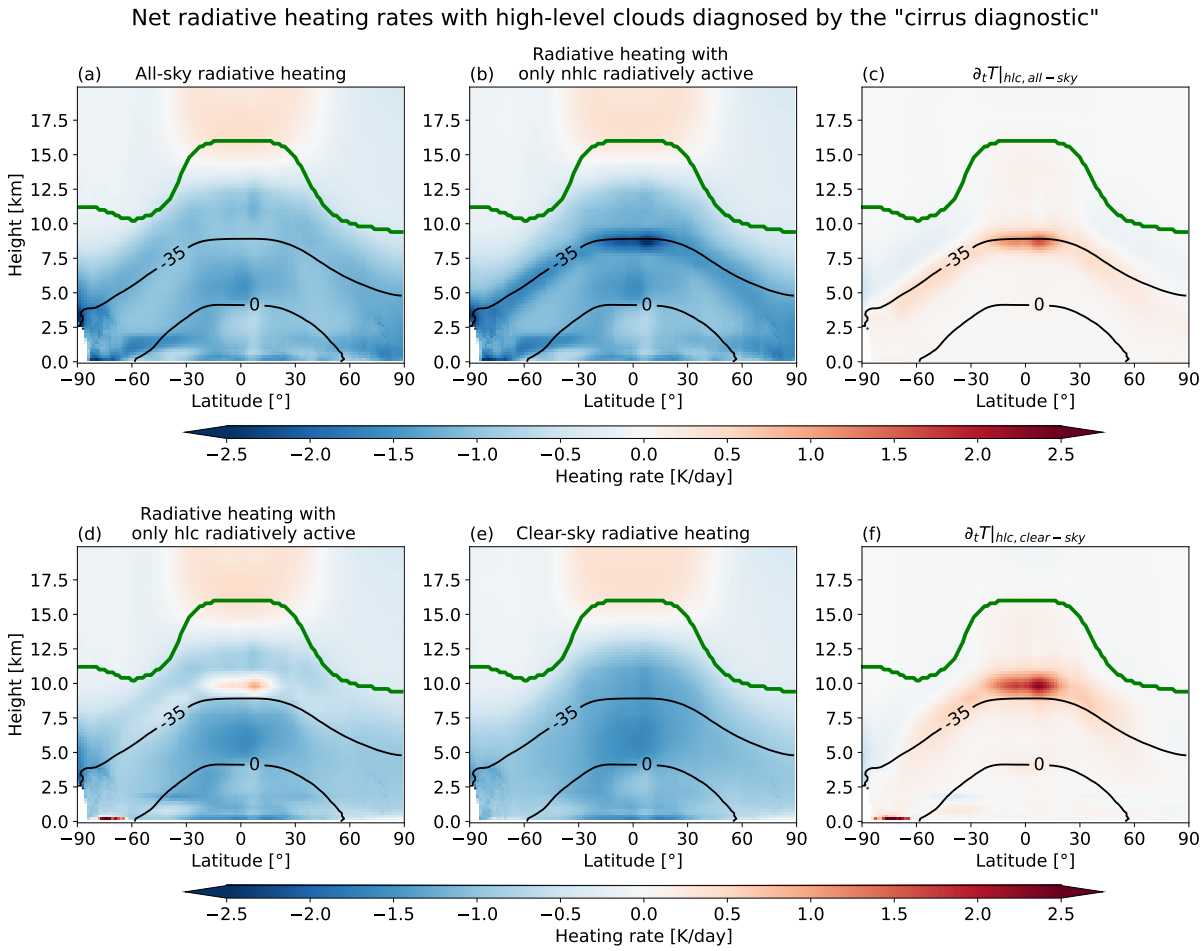

Figure 20: Net radiative heating rates with high-level clouds diagnosed using the "cirrus diagnostic". Panel (a) shows the total cloud radiative heating rate, while Panel (b) depicts the radiative heating rate of an atmosphere without radiatively active high-level clouds. The difference between Panel (a) and (b) gives the cloud radiative heating rate of high-level clouds using $\partial_t T|_{hlc,all-sky}$, which is shown in Panel (c). Panel (d) depicts the radiative heating in an atmosphere with only high-level clouds radiatively active, while Panel (e) is the radiative heating of a clear-sky atmosphere. The difference between Panels (d) and (e) gives the cloud radiative heating rate of high-level clouds using $\partial_t T|_{hlc,all-sky}$ in Panel (f). Black contour lines show the -35°C and the 0°C isotherms. The green contour depicts the mean tropopause height, which is derived from the tropopause air pressure output of the simulation.

rectly below the temperature threshold in $\partial_t T|_{hlc,all-sky}$, is due to high-level clouds absorbing the shortwave radiation scattered by the non-high-level clouds in an all-sky atmosphere.
The all-sky heating rate (Figure 21(a)) and the clear-sky heating rate (Figure 21(e)) are the same as those of the "cirrus diagnostic" (Figure 18(a) and (e)), because they are not affected by the choice of the high-level cloud diagnostic. The shortwave heating rates in an atmosphere with or without radiatively active high-level clouds according to the "cirrus + warm base diagnostic" (Figure 21(b) and (d)) are similar to those according to the "cirrus diagnostic" (Figure 18(b) and (d)). This causes the $\partial_t T|_{hlc,all-sky}$ and $\partial_t T|_{hlc,clear-sky}$ using the "cirrus + warm base diagnostic" (Figure 21(c) and (f)) to be similar to those using to the "cirrus diagnostic" (Figure 18(c) and (f)). This is not surprising since the $HCRE$ inside the atmosphere of both diagnostics differs only in the decimal places. However, in contrast to Panels (c) and (f) of Figure 18, the strongest shortwave cooling is not concentrated around the -35°C isotherm when the "cirrus + warm base diagnostic" is used. This is because the high-level cloud bases are then located at different altitudes, so the radiative cooling below a cloud is

more spread out over the troposphere (Figure 21(c) and (f)), whereas in the "cirrus diagnostic" high-level clouds with a cloud base at temperatures warmer than the threshold are seen by this diagnostic as having a cirrus cloud base at -35°C, thereby concentrating the shortwave cooling below that level (Figure 18(c) and (f)). Since the strong cooling directly below -35°C is not present in total cloud radiative heating (Figure 17(a)), the shortwave heating of the "cirrus + warm base diagnostic" resembles the total cloud radiative heating more than the "cirrus diagnostic".

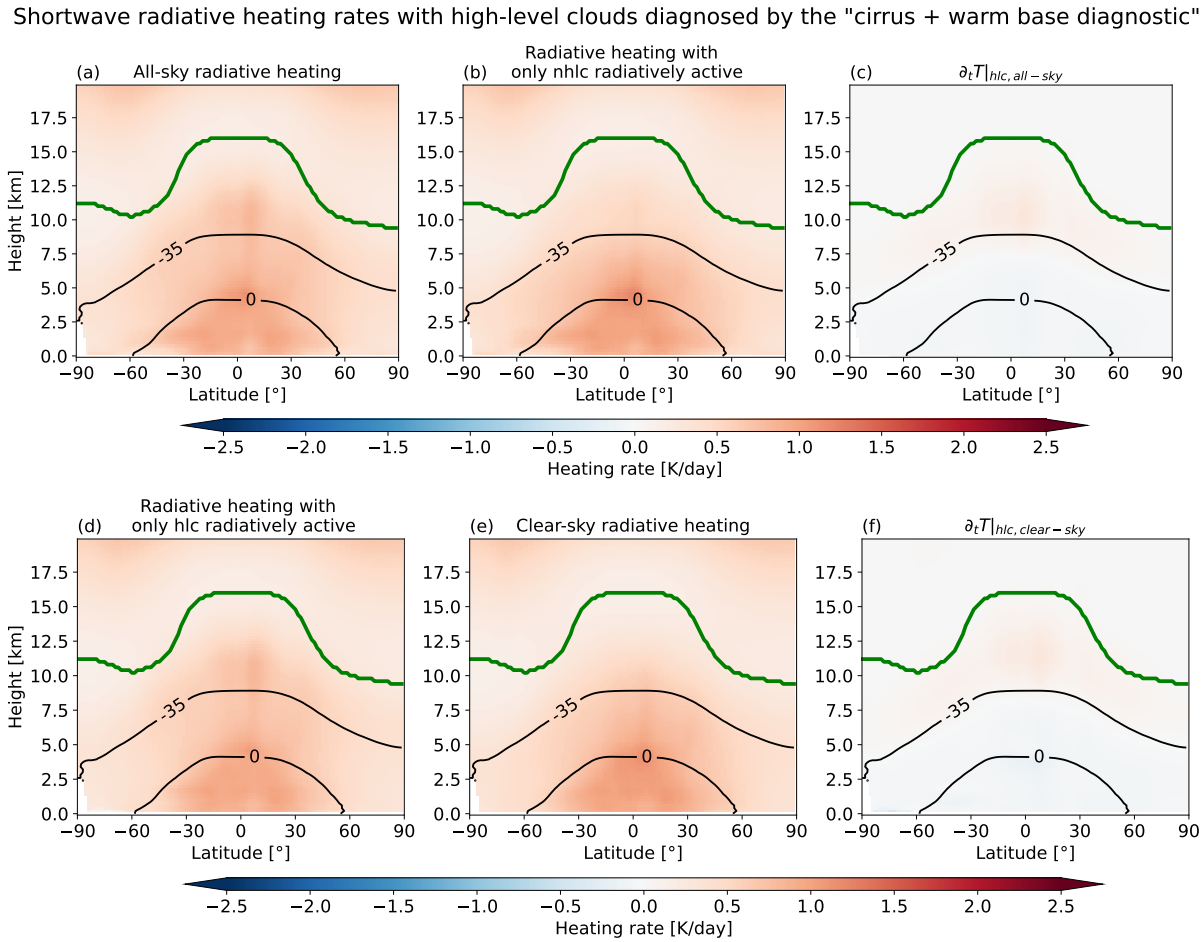

Figure 21: Shortwave radiative heating rates with high-level clouds diagnosed using the "cirrus + warm base diagnostic". Panel (a) shows the total cloud radiative heating rate, while Panel (b) depicts the radiative heating rate of an atmosphere without radiatively active high-level clouds. The difference between Panel (a) and (b) gives the cloud radiative heating rate of high-level clouds using $\partial_t T|_{hlc,all-sky}$, which is shown in Panel (c). Panel (d) depicts the radiative heating in an atmosphere with only high-level clouds radiatively active, while Panel (e) is the radiative heating of a clear-sky atmosphere. The difference between Panels (d) and (e) gives the cloud radiative heating rate of high-level clouds using $\partial_t T|_{hlc,all-sky}$ in Panel (f). Black contour lines show the -35°C and the 0°C isotherms. The green contour depicts the mean tropopause height, which is derived from the tropopause air pressure output of the simulation.

The tropical longwave heating above the -35°C isotherm is weaker in $\partial_t T|_{hlc,all-sky}$ (Figure 22(c)) than in $\partial_t T|_{hlc,clear-sky}$ and (Figure 22(f)), because non-high-level clouds reduce the amount of outgoing longwave radiation reaching the high-level clouds, thereby reducing their radiative heating. The radiative heating rates of $\partial_t T|_{hlc,clear-sky}$ are more similar to the total cloud heating (Figure 17(b)), since in $\partial_t T|_{hlc,clear-sky}$ there is more radiative heating in the tropical upper-troposphere.

The all-sky and clear-sky longwave heating rates in Panels (a) and (e) of Figure 22 are the same as those in Figure 19, as they are unaffected by the high-level cloud diagnostic. The longwave heating around the -35°C isotherm in both $\partial_t T|_{hlc,all-sky}$ and $\partial_t T|_{hlc,clear-sky}$ (Figure 22(c) and (f)) is much weaker than in the cloud radiative heating rate of high-level clouds when using the "cirrus diagnostic". For $\partial_t T|_{hlc,clear-sky}$ this is because the high-level cloud bases in the "cirrus + warm base diagnostic" are located at different altitudes, therefore the longwave absorption at the cloud bases in an atmosphere with only high-level clouds interacting with radiation is more spread out over different height levels (Figure 22(d)) than when using the "cirrus diagnostic" (Figure 19(d)). In $\partial_t T|_{hlc,all-sky}$ the longwave heating is not only caused by the absorption at the high-level cloud bases, but also partially by the radiative cooling at the non-high-level cloud tops below the high-level clouds in an atmosphere in which high-level clouds are radiatively inactive (Figure 22(b)). Due to weaker radiative cooling in the

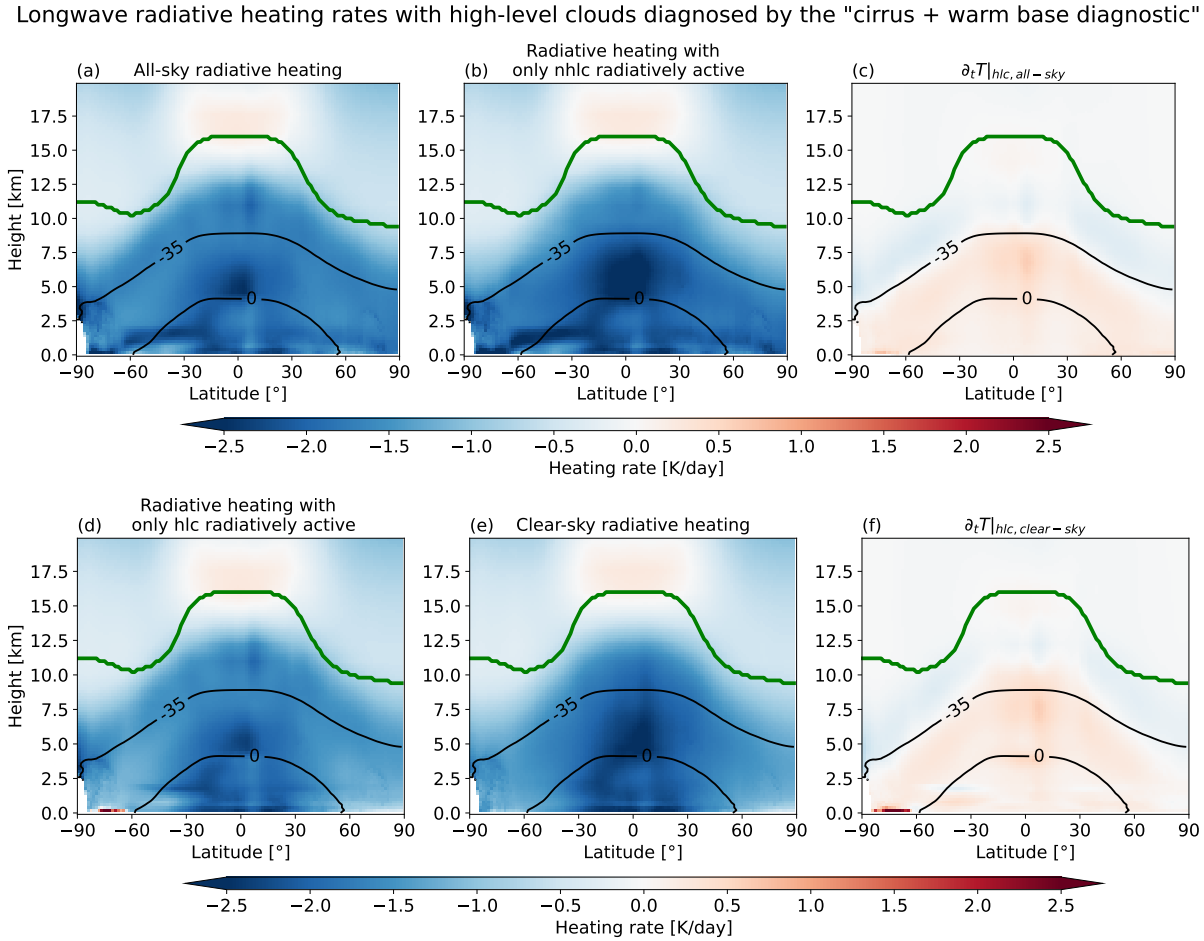

Figure 22: Longwave radiative heating rates with high-level clouds diagnosed using the "cirrus + warm base diagnostic". Panel (a) shows the total cloud radiative heating rate, while Panel (b) depicts the radiative heating rate of an atmosphere without radiatively active high-level clouds. The difference between Panel (a) and (b) gives the cloud radiative heating rate of high-level clouds using $\partial_t T|_{hlc,all-sky}$, which is shown in Panel (c). Panel (d) depicts the radiative heating in an atmosphere with only high-level clouds radiatively active, while Panel (e) is the radiative heating of a clear-sky atmosphere. The difference between Panels (d) and (e) gives the cloud radiative heating rate of high-level clouds using $\partial_t T|_{hlc,all-sky}$ in Panel (f). Black contour lines show the -35°C and the 0°C isotherms. The green contour depicts the mean tropopause height, which is derived from the tropopause air pressure output of the simulation.

all-sky atmosphere (Figure 22(a)) compared to that of an atmosphere with only non-high-level clouds radiatively active (Figure 22(b)), the non-high-level clouds cause a heating in $\partial_t T|_{hlc,all-sky}$. Since the cloud bases of the high-level clouds are located at various altitudes when using the "cirrus + warm base diagnostic", this longwave heating is more spread out over the mid and lower troposphere.

The longwave heating rates (Figure 22) again contribute the most to the net heating rates according to the "cirrus + warm base diagnostic" (Figure 23). As for the "cirrus diagnostic", in the tropical upper troposphere, the shortwave heating dominates in both $\partial_t T|_{hlc,all-sky}$ and $\partial_t T|_{hlc,clear-sky}$ (Figure 23(c) and (f)) over the longwave cooling. The net heating from both methods seems to be similar in strength. The largest difference is the strong heating close to the surface in the high-latitudes of the Southern Hemisphere.

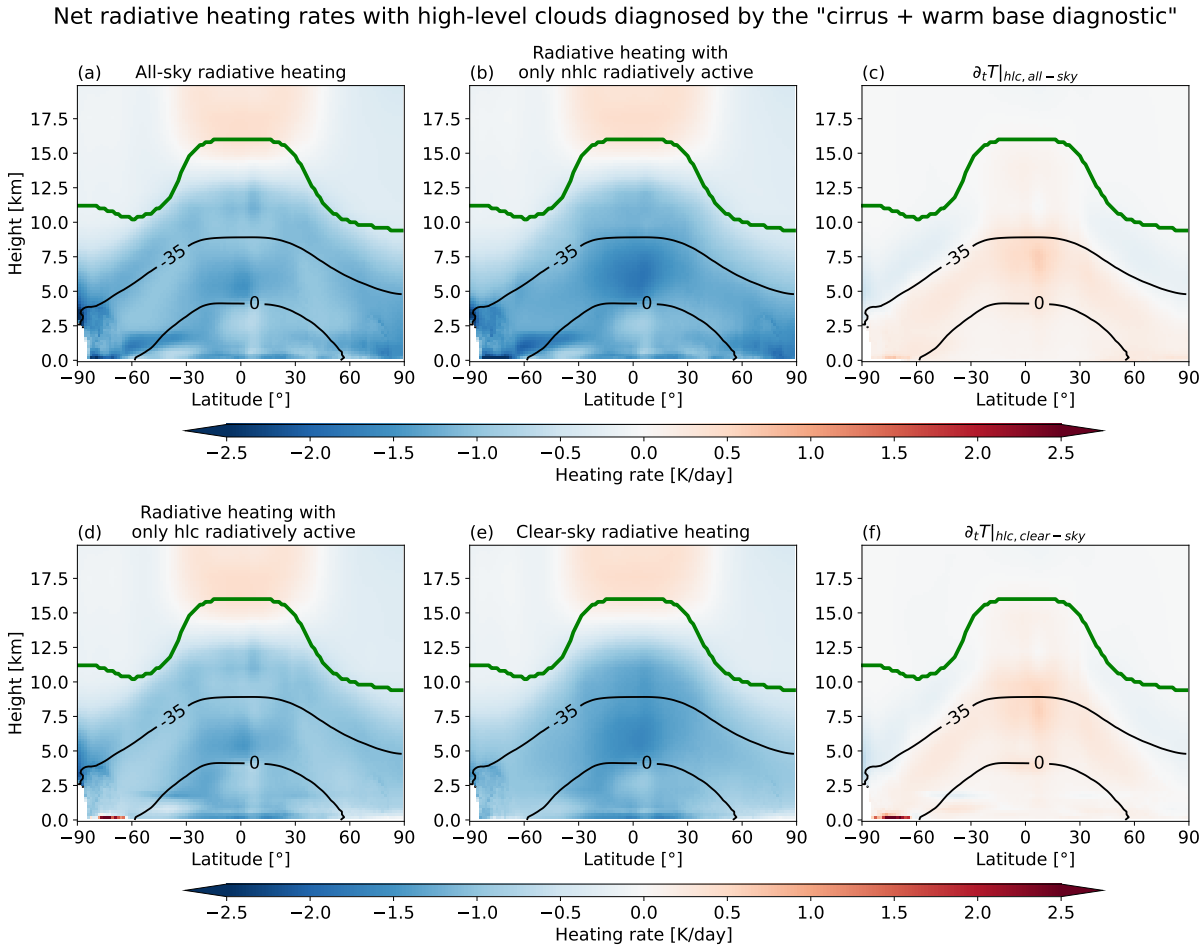

Figure 23: Net radiative heating rates with high-level clouds diagnosed using the "cirrus + warm base diagnostic". Panel (a) shows the total cloud radiative heating rate, while Panel (b) depicts the radiative heating rate of an atmosphere without radiatively active high-level clouds. The difference between Panel (a) and (b) gives the cloud radiative heating rate of high-level clouds using $\partial_t T|_{hlc,all-sky}$, which is shown in Panel (c). Panel (d) depicts the radiative heating in an atmosphere with only high-level clouds radiatively active, while Panel (e) is the radiative heating of a clear-sky atmosphere. The difference between Panels (d) and (e) gives the cloud radiative heating rate of high-level clouds using $\partial_t T|_{hlc,all-sky}$ in Panel (f). Black contour lines show the -35°C and the 0°C isotherms. The green contour depicts the mean tropopause height, which is derived from the tropopause air pressure output of the simulation.

The results shown in this section demonstrate that the cloud radiative heating rates using the two different methods to calculate $\partial_t T|_{hlc}$ are not the same. $\partial_t T|_{hlc,all-sky}$ is influenced the non-high-level clouds below, as their radiative interactions affect how much radiation a high-level cloud receives. The radiative heating rates according to the "cirrus diagnostic" differ considerably in strength near the temperature threshold level. Both $\partial_t T|_{hlc,all-sky}$ and $\partial_t T|_{hlc,clear-sky}$ include artificial heating rates when the high-level clouds are diagnosed with the "cirrus diagnostic", since the number of high-level cloud bases is artificially increased at the temperature threshold. For $\partial_t T|_{hlc,all-sky}$ the artificial heating is located slightly lower in altitude than for $\partial_t T|_{hlc,clear-sky}$, because the artificial heating in $\partial_t T|_{hlc,all-sky}$ is related to radiative interactions with non-high-level clouds, while in $\partial_t T|_{hlc,clear-sky}$ it is only caused by the heating at the artificial cirrus cloud base. Overall, the high-level cloud radiative heating using the "cirrus + warm base diagnostic" looks more realistic as it does not produce the strong artificial shortwave cooling and longwave heating at the temperature threshold.

5.4 The impact of cloud-radiation coupling on climate

In this section I present the total cloud radiative impact and the cloud radiative impact of high-level clouds on the atmospheric circulation and precipitation. For this purpose I use the Cirrus-COOKIE, the WB-Cirrus-COOKIE and the COOKIE simulation sets, i.e., I compare the "clouds on" simulation, which is the control simulation, with the "cirrus off", "cirrus + warm base off" and "clouds off" simulations, in which the climate is changed with respect to the control climate by making certain clouds transparent to radiation. The Cirrus-COOKIE simulation set is the difference between the "clouds on" and the "cirrus off" simulations, the WB-Cirrus-COOKIE simulation set is the difference between the "clouds on" and the "cirrus + warm base off" simulations and the COOKIE simulation set is difference between the "clouds on" and the "clouds off" simulations.

5.4.1 Temperature impact

The interactions of radiation and clouds have a heating or cooling effect on the atmosphere, which changes the atmospheric temperatures. Although the radiative heating patterns of the "cirrus diagnostic" and the "cirrus + warm base diagnostic" are distinct (Panels (c) and (f) of Figure 20 and of Figure 23), the tropospheric temperature impact (Figure 24) in Cirrus-COOKIE and the WB-Cirrus-COOKIE seems to differ mostly only in magnitude. The impact of the interaction of high-level clouds with radiation leads to a tropospheric warming effect, which is maximized in the upper troposphere. This is caused by absorption of longwave radiation at a higher temperature and re-emission at a colder temperature. The temperature impact is larger in the WB-Cirrus-COOKIE simulation set, because a larger fraction of clouds is disabled in the "cirrus + warm base off" simulation (Figure 10). The total cloud radiative impact, as shown in Figure 24(a), includes the heating of the upper troposphere, which is caused by the high-level clouds. An increase in tropospheric temperatures in the tropics was also present in all six COOKIE simulation sets of Harrop and Hartmann (2016). From about 50°N toward the North Pole, the troposphere is cooled in the COOKIE simulation set, except near the surface. The cooling is strongest in the lower levels, indicating that it is caused by low-level clouds. In the Southern Hemisphere clouds increase temperatures near the surface in the high-latitudes, while above the boundary layer there is mostly a temperature decrease. In contrast to the Cirrus-COOKIE and the WB-Cirrus-COOKIE simulation sets, the temperature in the uppermost parts of the high-lat-

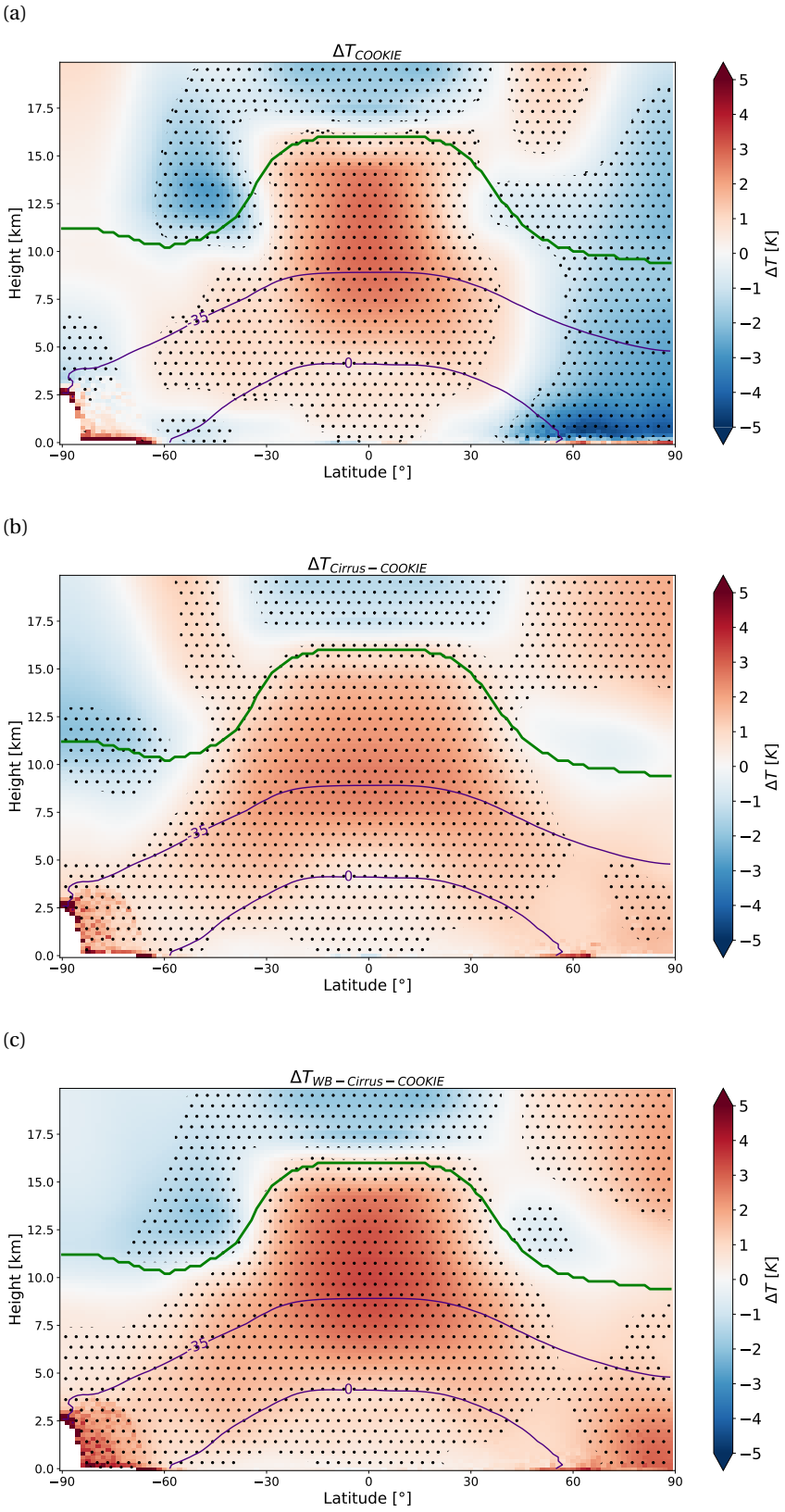

Figure 24: Temperature impact in the COOKIE (a), Cirrus-COOKIE (b), and WB-Cirrus-COOKIE (c) simulation sets. The stippling indicates where the temperature differences are statistically significant according to the Student's t-test with a significance level of 5%. Purple contour lines show the -35°C and the 0°C isotherms. The green contour depicts the mean tropopause height, which is derived from the tropopause air pressure output of the simulation.

itude troposphere are slightly increased in the COOKIE simulation set. Whereas in my COOKIE simulation set, clouds both increase and decrease temperatures in the atmosphere, in the COOKIE simulation set of Li et al. (2015), clouds only increase the tropospheric temperatures (see Panel (a) in Figure 4). The temperature impact in Li et al. (2015) is more similar to my Cirrus-COOKIE and WB-Cirrus-COOKIE simulation set, suggesting that in the simulations of Li et al. (2015) high-level clouds dominate the total cloud radiative impact on temperatures.

The tropical stratosphere is cooled in the COOKIE, Cirrus-COOKIE and WB-Cirrus-COOKIE simulation sets, as shown in Figure 24. This is related to the absorption of longwave radiation by the tropical high-level clouds, which traps the energy in the troposphere. In the extratropical stratosphere, however, the patterns of the stratospheric temperature impact differ between the COOKIE, Cirrus-COOKIE and WB-Cirrus-COOKIE simulation sets. These differences in the temperature impact might be caused by differences in the Brewer-Dobson circulation in the simulations. In the COOKIE simulation set of Harrop and Hartmann (2016), the stratosphere was cooled except over the high-latitudes, where it was warmed. In Li et al. (2015) stratospheric temperatures are lower with active ACRE (see Panel (a) in Figure 4). This is mostly in agreement with my COOKIE simulation set, except that at about 50°N the stratospheric temperatures increase statistically significant above 15 km.

The surface temperature impact for the COOKIE, Cirrus-COOKIE and the WB-Cirrus-COOKIE simulation sets are shown in Figure 25(a), (b), and (c). The sea surface temperature does not change in the simulations since it is prescribed, but the land and sea ice temperatures can change. In the COOKIE simulation set, surface temperatures increase over the poles, much of Africa, Brazil, Indonesia, and northeastern Australia. In the mid-latitudes, land surface temperatures are decreased by radiatively active clouds. This decrease is only present in the COOKIE simulation set and not in the Cirrus-COOKIE and the WB-Cirrus-COOKIE simulation sets, showing that the decrease in land surface temperature is not caused by cirrus clouds or their warm bases. Harrop and Hartmann (2016) stated that the surface temperatures in their COOKIE simulation set did "not show much change". However, in my COOKIE simulation set, the land surface and sea ice temperatures do change significantly. The Cirrus-COOKIE and the WB-Cirrus-COOKIE results show that radiatively active cirrus clouds warm the surface, especially over Antarctica and Greenland. The change in land surface and sea ice temperature at the poles follows, as expected, the CRE at the surface shown in Figure 12, which indicates a warming effect of high-level clouds at the poles. The overall land surface and sea ice temperature increase is again stronger in the WB-Cirrus-COOKIE simulation set. In contrast to the other two simulation sets, there is only little warming over Africa in the Cirrus-COOKIE simulation set. This indicates that the land surface temperature increase on much of this continent can be attributed to the warm bases.

The increase in tropical surface temperatures in all three simulation sets is surprising, since the surface CRE (Figure 2, Figure 12 (c) and (f), and Figure 15 (c) and (f)) indicates that (high-level) clouds are cooling the surface. A possible reason for the surface temperature increase could be that in the "clouds off", "cirrus off" and "cirrus + warm base off" simulations feedbacks and adjustments to the new climate state lead to a surface cooling compared to the "clouds on" simulation, meaning that the surface in the "clouds on" simulation is heated by radiatively active clouds. If this is the case there should be a surface heating in the COOKIE, Cirrus-COOKIE and WB-Cirrus-COOKIE simulation sets. To investigate this hypothesis, I compare the changes in the radiative energy fluxes over tropical land due to the active (high-level) clouds, diagnosed by the "clouds on", "diagnose cirrus all-sky" and

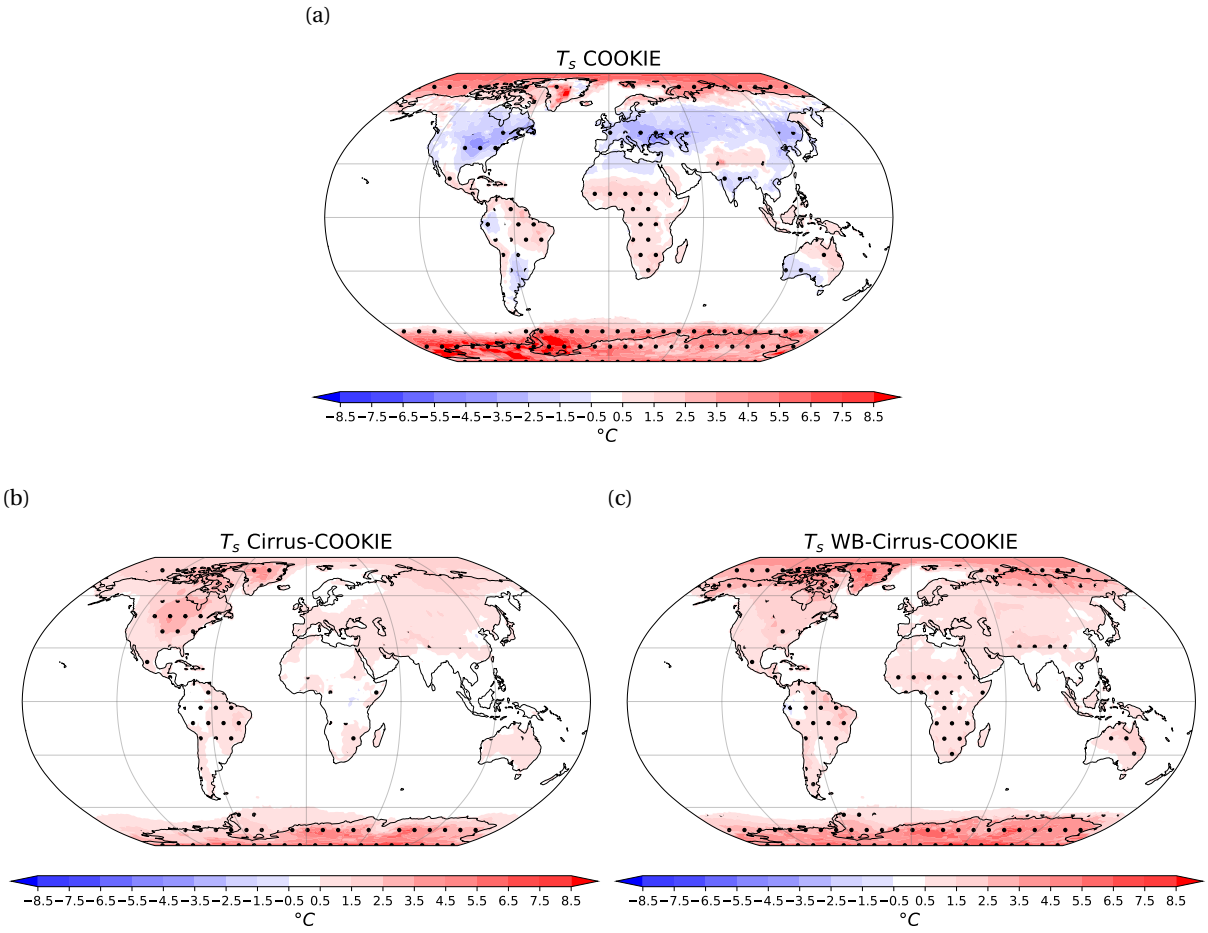

Figure 25: Land surface and sea ice temperature impact for the COOKIE (a), Cirrus-COOKIE (b) and the WB-Cirrus-COOKIE (c) simulation sets. The stippling indicates statistical significant differences according to the Student's t-test with a significance level of 5%.

"diagnose cirrus + warm base all-sky" simulations with the energy flux changes from the COOKIE, Cirrus-COOKIE, and WB-Cirrus-COOKIE simulation sets. A positive sum of the change in shortwave radiation at the tropical land surface ΔSW and the change in longwave radiation at the tropical land surface ΔLW means the tropical land surface is heated by (high-level) cloud radiative interactions, while a negative sum of the ΔSW and ΔLW indicates a cooling of the tropical land surface by (high-level) cloud radiative interactions. For all simulation sets, the changes in the shortwave, longwave, sensible heat flux, and the latent heat flux add up to approximately 0 (Figure 26), which means that the surface energy fluxes are balanced. In the Cirrus-COOKIE and the WB-Cirrus-COOKIE, the diagnosed energy flux changes (Figure 26 (c) and (e)) differ considerably from the changes when the climate state is allowed to adjust (Figure 26 (d) and (f)). However, the signs of the sums of ΔSW and ΔLW are consistent, so even in the COOKIE, Cirrus-COOKIE and WB-Cirrus-COOKIE simulation sets the surface is cooled by the presence of (high-level) clouds. Therefore, the cause of the surface temperature increase remains unknown and needs to be further investigated in the future.

Evaluation of the hypotheses

The increase in the upper-tropospheric temperatures is consistent with my hypothesis. High-level clouds also warm the surface at the poles, following the CRE at the surface (Figure 12), as expected. However, based on the surface CRE of high-level clouds in the tropics, I expected to see a cooling of the tropical surface, but the results range from no significant change in land surface temperature to

a weak increase. The reason for this remains unclear. The WB-Cirrus-COOKIE temperature response is larger in magnitude than the Cirrus-COOKIE results, consistent with my initial hypothesis.

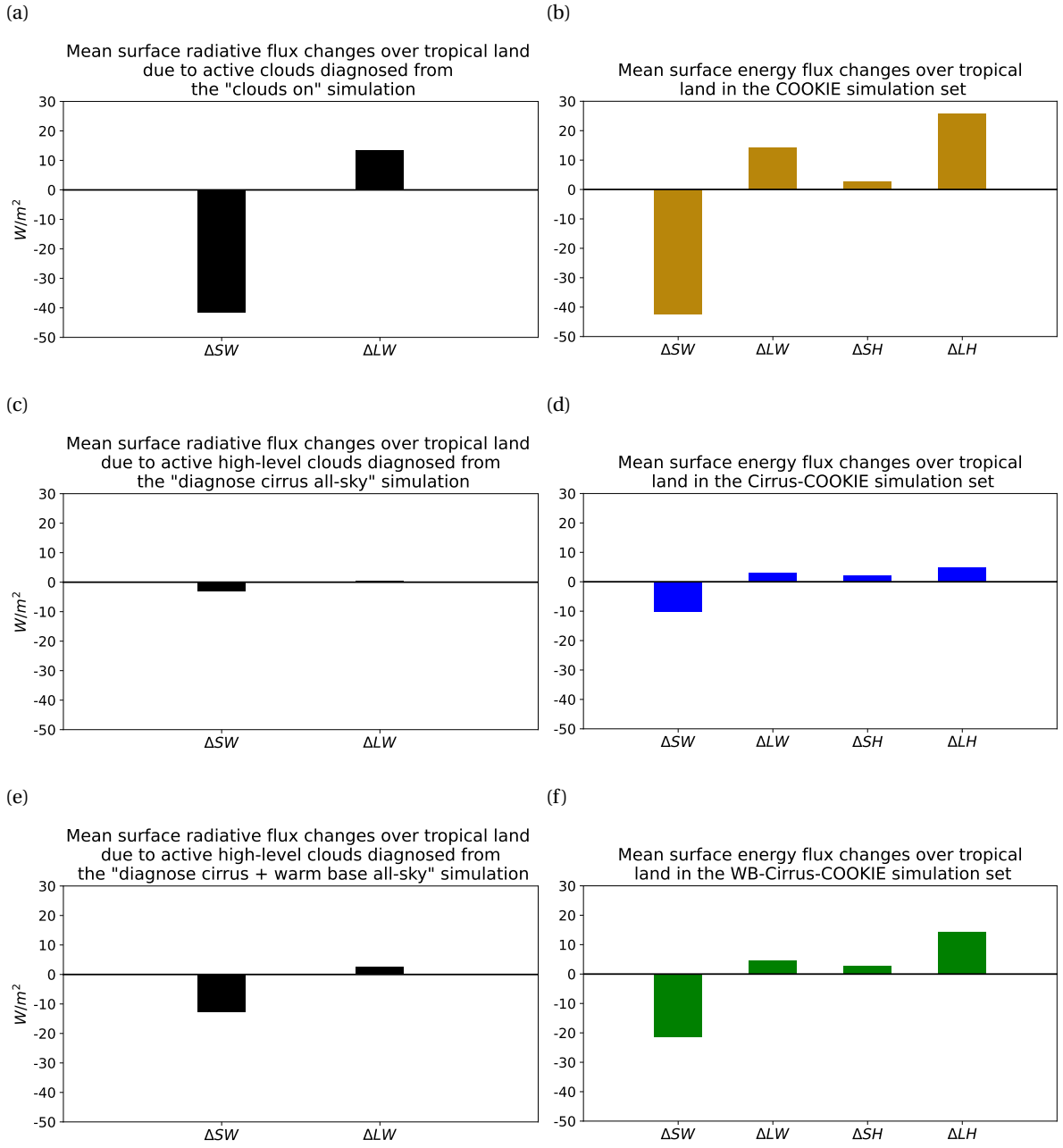

Figure 26: Radiative energy flux changes at the tropical land surface diagnosed from (a) the "clouds on", (b) the "diagnose cirrus all-sky" and (c) the "diagnose cirrus + warm base all-sky" simulations. Panels (b), (d) and (f) show the energy flux changes at the tropical land surface from the (b) COOKIE, (d) Cirrus-COOKIE and (f) the WB-Cirrus-COOKIE simulation sets.

5.4.2 Zonal wind impact

Changes in temperatures drive anomalies in the wind patterns, as shown in the contours of Figure 27. The largest zonal wind difference in the COOKIE and WB-Cirrus-COOKIE simulation set is an eastward wind anomaly in the tropical upper troposphere (Figure 27), similar to the COOKIE simulation

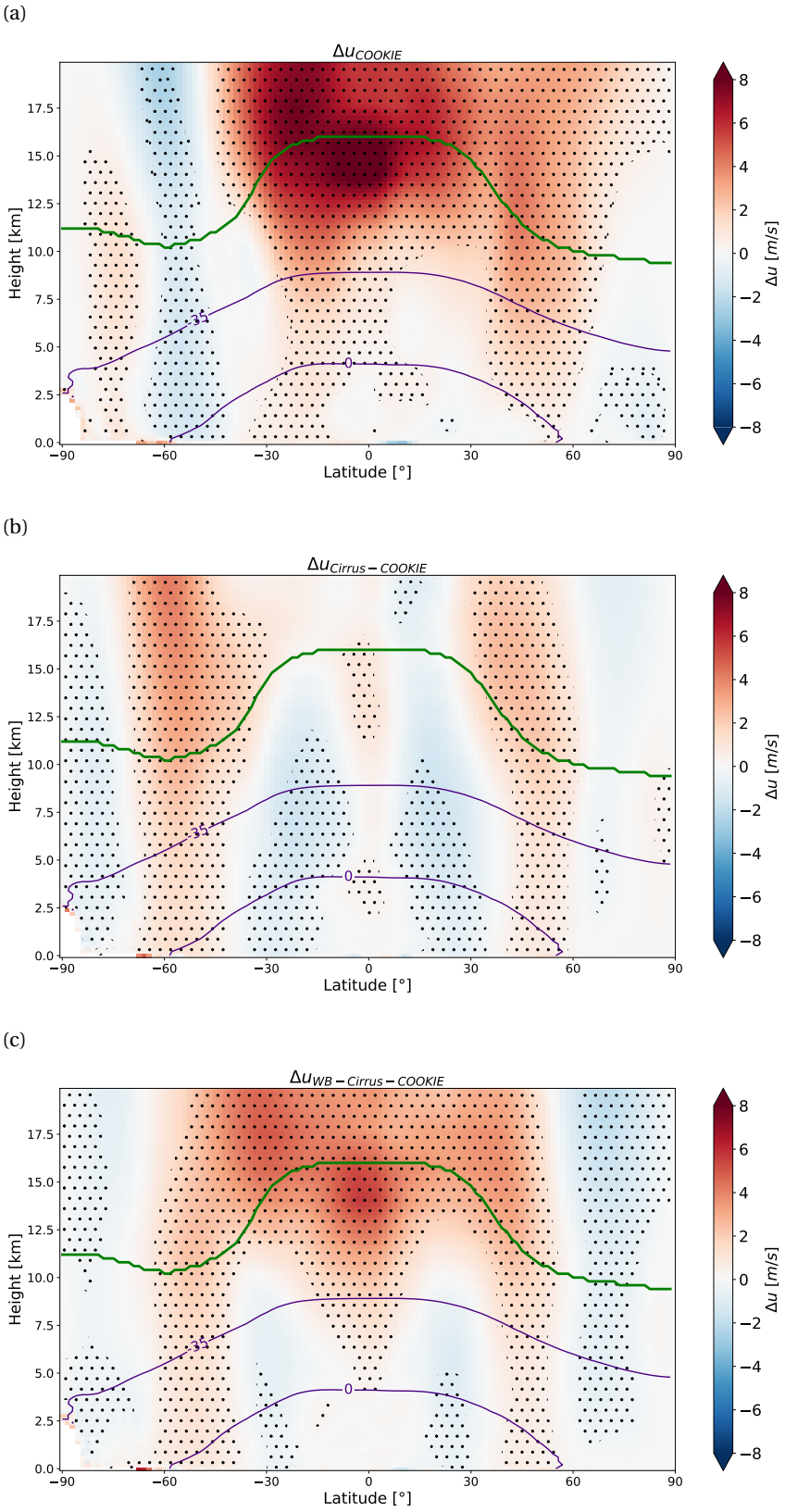

Figure 27: Zonal wind impact of the COOKIE, Cirrus-COOKIE and WB-Cirrus-COOKIE simulation sets. The stippling indicates where the wind differences are statistically significant according to the Student's t-test with a significance level of 5%. Purple contour lines show the -35°C and the 0°C isotherms. The green contour depicts the mean tropopause height in the "clouds on" simulation, which is derived from the tropopause air pressure output of the simulation.

set from Li et al. (2015) (see Panel (b) in Figure 4). They related this cloud influence to an increase in the amplitude of equatorial planetary waves, which are driven by zonally asymmetric temperature gradients in the tropics, which are in turn influenced by clouds. Interestingly, the upper-tropospheric zonal wind increase is much weaker in the Cirrus-COOKIE simulation set. This may be related to the fact that the upper-tropospheric temperature impact in the tropics is smaller than in the COOKIE and the WB-Cirrus-COOKIE simulation sets. The zonal wind also strengthens at around 50°N/S in the Cirrus-COOKIE (Figure 27(b)) and the WB-Cirrus-COOKIE simulation sets(Figure 27(c)). This could signal a poleward jet shift or a pure jet strengthening.

Figure 28 and Table 3 show that the eddy-driven jet strength increases in the Cirrus-COOKIE and the WB-Cirrus-COOKIE simulation sets. This demonstrates that high-level clouds contribute to a strengthening of the jet. The increase in the jet strength can be explained by the warming of the upper troposphere by high-level clouds, which increases the meridional temperature gradient and thus the jet stream via thermal wind balance. The non-high-level clouds have an even stronger, but opposite, impact on the jet in the Southern Hemisphere. In the Northern Hemisphere, however, the total cloud radiative impact is a jet strengthening, like the cloud radiative impact of high-level clouds. In Voigt et al. (2021), three out of five COOKIE simulation sets using different models also showed this impact of an increased jet strength in the Northern Hemisphere and a weakening of the jet in the Southern Hemisphere. The decrease in the jet strength in the Southern Hemisphere in the COOKIE simulation set could be related to the lower-tropospheric cooling between about 40°S to 60°S (Figure 24(a)), which decreases the lower-tropospheric temperature gradient.

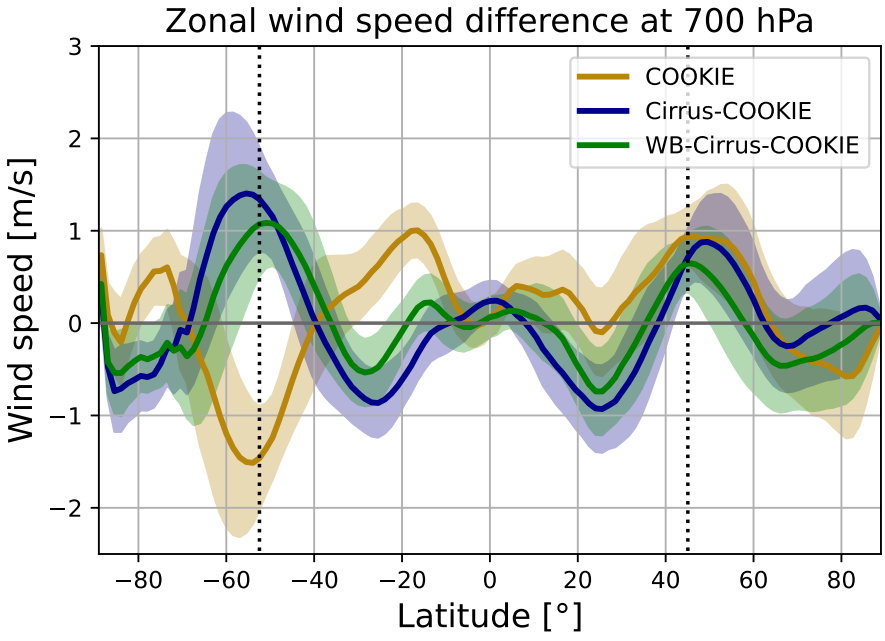

Figure 28: 700 hPa zonal wind differences in the COOKIE, Cirrus-COOKIE and WB-Cirrus-COOKIE simulation sets. The dotted vertical line shows the position of the eddy-driven jet in the "clouds on" simulation. The shading shows the range of one annual standard deviation of the "clouds on" simulation, which is computed via the yearly average, for which the monthly values are weighted according to their number of days.

	φ_{NH}	φ_{SH}	$u_{jet,NH}$	$u_{jet,SH}$
COOKIE	0.6	-0.0	**0.8**	**-1.3**
Cirrus-COOKIE	**2.0**	**0.8**	**0.7**	**1.3**
WB-Cirrus-COOKIE	0.7	0.0	**0.6**	**0.9**

Table 3: Jet position and jet strength changes in the COOKIE, Cirrus-COOKIE and WB-Cirrus-COOKIE simulation sets. The jet stream position change φ is given in °N or respectively °S. It is determined from the zonal wind changes at 700 hPa following Barnes and Polvani (2013). Positive values indicate a poleward shift of the jet position, negative values an equatorward shift. The jet strength change u_{jet} is the zonal wind impact at the jet position in m/s. The analysis script used in creating this table is an adaptation from the one used in Voigt et al. (2021). Statistically significant results according to a Student's t-test with a significance level of 5% are shown in bold.

The jet shift should not be diagnosed from Figure 28, since the largest difference between the zonal winds is not necessarily at the location of the maximum zonal winds in the "clouds off", "cirrus off" or "cirrus + warm base off" simulation. In Figure 29 shows the zonal wind speeds in the "clouds on", "clouds off", "cirrus off" and "cirrus + warm base off" simulation, but there is no clear shift of the jet in the "cloud off", "cirrus off" and "cirrus + warm bases off" simulation compared to the "clouds on " simulation. Table 3 shows that the eddy-driven jet does shift in the Northern Hemisphere of all three simulation sets and in the Southern Hemisphere of the Cirrus-COOKIE simulation set, but the shifts are only statistically significant for the Cirrus-COOKIE simulation set. The shifts in the Cirrus-COOKIE simulation set are poleward and larger in the Northern Hemisphere than in the Southern Hemisphere. This may be due to a stronger warming of the lower troposphere in the high-latitudes of the Southern Hemisphere (Figure 27(b)), which decreases the meridional temperature gradient near the surface, causing a weaker poleward jet shift. The fact that the jet shifts in the WB-Cirrus-COOKIE

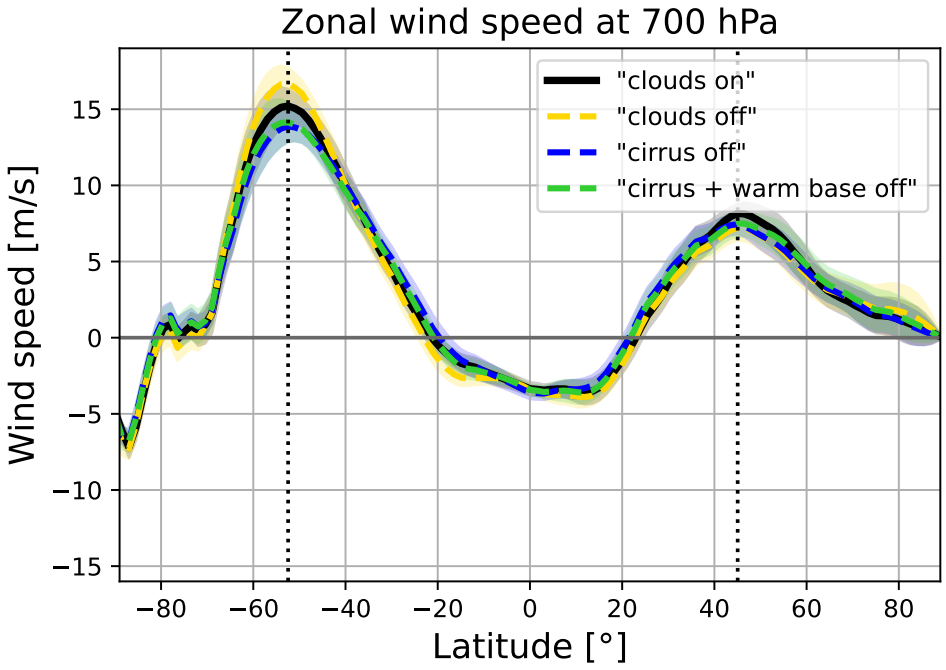

Figure 29: 700 hPa zonal wind in the "clouds on", "clouds off", "cirrus off" and "cirrus + warm base off" simulations. The dotted vertical line shows the position of the eddy-driven jet in the "clouds on" simulation. The shading shows the range of two annual standard deviations, which are computed via the yearly average, for which the monthly values are weighted according to their number of days.

are much weaker and not statistically significant indicates that the radiative interactions of the warm bases partially counteract the poleward shift of the eddy-driven jet caused by the cirrus clouds.

Evaluation of the hypotheses
Consistent with my hypothesis, high-level clouds strengthen the eddy-driven jet. I expected high-level clouds to contribute to a poleward shift of the eddy-driven jet, which is only the case in the Cirrus-COOKIE simulation set. In the WB-Cirrus-COOKIE simulation set, the jet location shifts equatorward in the Northern Hemisphere and remains unperturbed in the Southern Hemisphere. However, those changes are not statistically significant. The fact that the Cirrus-COOKIE and the WB-Cirrus-COOKIE responses differ in sign also contradicts my hypothesis that the high-level cloud radiative impacts of the Cirrus-COOKIE and the WB-Cirrus-COOKIE simulation sets differ only in magnitude.

5.4.3 Specific humidity impact

Atmospheric temperature changes are also the primary driver of changes in specific humidity. Figure 30 shows the change in specific humidity in the COOKIE, Cirrus-COOKIE and WB-Cirrus-COOKIE simulation sets divided by the specific humidity in the "clouds on" simulation, i.e. the relative change of the specific humidity. Radiatively active cirrus (and their warm bases) mostly increase the specific humidity. The largest relative increase in specific humidity for all COOKIE-type simulation sets is in the upper troposphere. This is due to the temperature increase caused by the high-level clouds, which increases the amount of water vapor that the tropical troposphere can store. The increase in specific humidity in the tropics appears to be a robust cloud radiative impact, as it agrees with all six COOKIE simulation sets of Harrop and Hartmann (2016). In the COOKIE simulation set, the specific humidity decreases considerably in the extratropics of the Northern Hemisphere, which is related to the temperature decrease of the extratropical troposphere in the Northern Hemisphere (Figure 24(a)).

Evaluation of the hypotheses
As expected, radiatively active high-level clouds increase the specific humidity in the tropics, since they warm the troposphere, allowing it to hold more moisture. In the high-latitudes, the specific humidity increases near the surface, as hypothesized. However, contradicting to hypothesis there are no statistically significant decreases in upper-tropospheric specific humidity over the high-latitudes. This might due to the upper-tropospheric temperature decreases over the high-latitudes being too weak or even absent in the Cirrus COOKIE and WB-Cirrus-COOKIE simulation sets, as shown in Figure 24 (b) and (c).

5.4.4 Tropical precipitation impact

The warming of the tropical upper-troposphere by high-level clouds should reduce the need for condensational heating to balance the radiative cooling of the atmosphere. A decrease in condensational heating implies a reduction in precipitation. Figure 31 and Table 4 show that tropical precipitation is decreased in the COOKIE, the Cirrus-COOKIE and the WB-Cirrus-COOKIE simulation sets. Overall, the decrease is greatest in the WB-Cirrus-COOKIE, indicating that the ACRE of cirrus clouds and their warm bases dominates the total cloud radiative impact. Therefore, high-level clouds play an important role for zonal mean precipitation. Due to the reduction of the tropical mean, global precipitation also decreases in all three simulation sets.

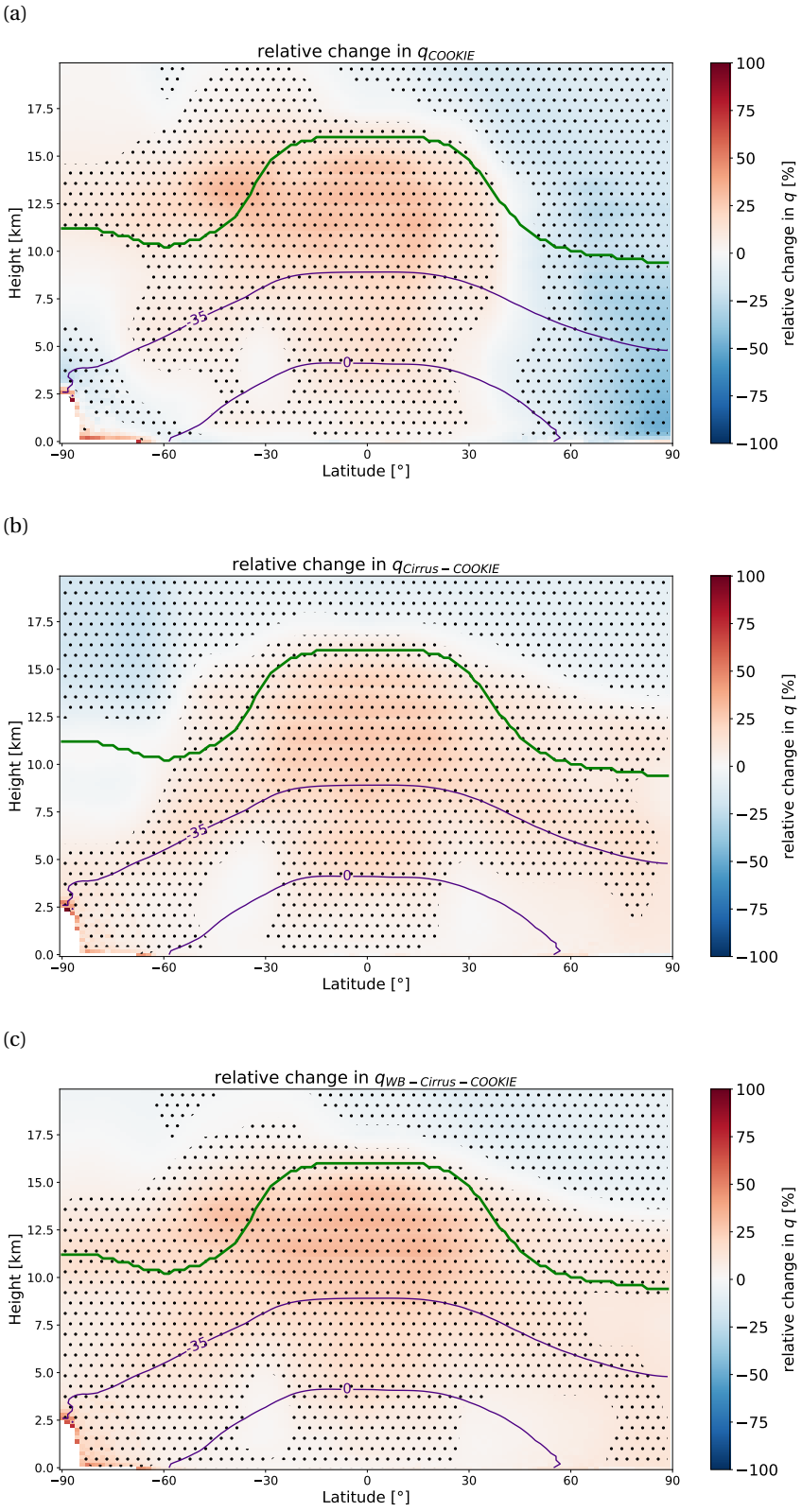

Figure 30: Zonal cross-section of the relative impact on specific humidity in the COOKIE, Cirrus-COOKIE and the WB-Cirrus-COOKIE simulation sets. The stippling indicates statistical significant differences according to the Student's t-test with a significance level of 5%. Purple contour lines show the -35°C and the 0°C isotherms. The green contour depicts the mean tropopause height, which is derived from the tropopause air pressure output of the simulation.

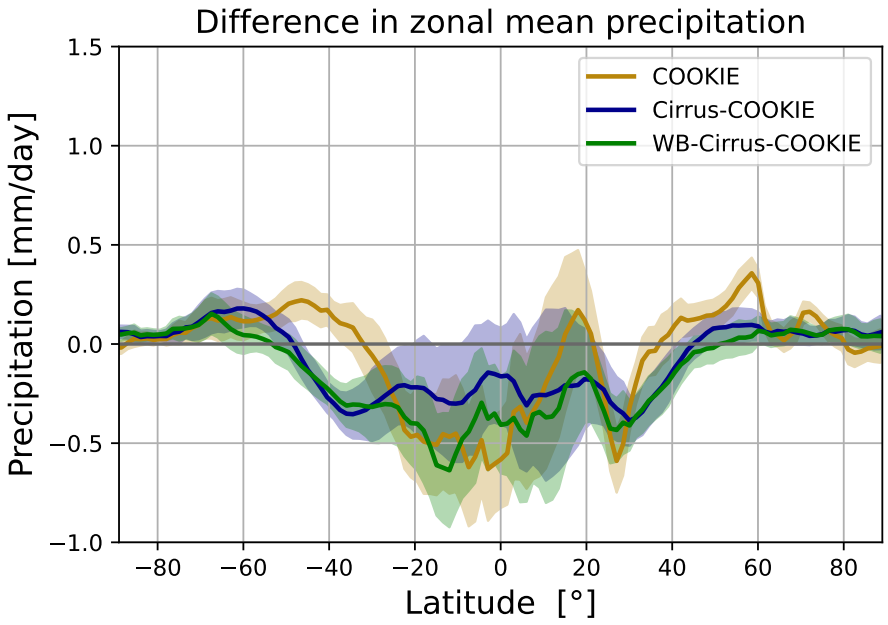

Figure 31: Zonal average precipitation difference in the COOKIE, Cirrus-COOKIE and WB-Cirrus-COOKIE simulation sets. The shading shows the range of one annual standard deviation of the "clouds on" simulation, which is computed via the yearly average, for which the monthly values are weighted according to their number of days.

	P_t	P_g
COOKIE	**-0.33**	**-0.12**
Cirrus-COOKIE	**-0.24**	**-0.15**
WB-Cirrus-COOKIE	**-0.38**	**-0.23**

Table 4: Changes of zonally averaged precipitation in the COOKIE, Cirrus-COOKIE and WB-Cirrus-COOKIE simulation sets. The change in tropical (t) and global (g) precipitation P is given in mm/day. Tropical refers here to latitudes between 30°N/S. Statistically significant results according to a Student's t-test with a significance level of 5% are shown in bold.

Evaluation of the hypotheses

My hypothesis that high-level clouds contribute to a decrease in tropical precipitation is confirmed by the simulation results. Moreover, the impacts of the WB-Cirrus-COOKIE simulation set on precipitation are larger in magnitude than those of the Cirrus-COOKIE simulation set, confirming my expectations.

5.4.5 ITCZ position and Hadley cell impact

The atmospheric heating has been shown to impact the ITCZ position (Voigt et al., 2021) and the strength of the Hadley cell circulation in COOKIE simulation sets (Harrop and Hartmann, 2016; Watt-Meyer and Frierson, 2017). Table 5 shows that the radiative interactions of high-level clouds do not cause a statistically significant ITCZ shift. The ITCZ shift is only statistically significant for the COOKIE simulation set. The reason why the COOKIE simulation set has the largest northward ITCZ shift is because the difference between the atmospheric net radiative balance in the Northern and Southern Hemispheres is largest (Table 6). The direction of the ITCZ shift in my COOKIE simulation set is also consistent with those of Voigt et al. (2021).

In all three of my simulation sets the Hadley cell strength is increased in the Southern Hemisphere and decreased in the Northern Hemisphere. However, none of these changes are statistically significant.

	φ_{ITCZ}	HC_{NH}	HC_{SH}
COOKIE	**0.5**	-1	9
Cirrus-COOKIE	0.0	-3	1
WB-Cirrus-COOKIE	0.3	-0	4

Table 5: Changes of mean ITCZ latitude and Hadley cell strength in the COOKIE, Cirrus-COOKIE and WB-Cirrus-COOKIE simulation sets. The change in the ITCZ latitude is given in units of °N. The ITCZ latitude φ_{ITCZ} is determined as the precipitation centroid between 20°N/S following Harrop et al. (2018). The Hadley cell strength HC is calculated as the maximum of the absolute value of the mass stream function. The units of HC are here 10^9 kg/s. The analysis script used in creating this table is an adaptation from the one used in Voigt et al. (2021). Statistically significant results according to a Student's t-test with a significance level of 5% are shown in bold.

	$\Delta R_{ATM,NH}$	$\Delta R_{ATM,SH}$	$\Delta R_{ATM,NH-SH}$
COOKIE	5.25	0.95	4.30
Cirrus-COOKIE	6.85	5.57	1.28
WB-Cirrus-COOKIE	10.84	9.20	1.64

Table 6: The atmospheric radiation flux balance, calculated according to Equation 11, in both hemispheres in the COOKIE, Cirrus-COOKIE and WB-Cirrus-COOKIE simulation sets. The units are given in W/m^2.

Evaluation of the hypotheses

The high-level clouds drive a northward ITCZ shift, which is stronger in the WB-Cirrus-COOKIE simulation set. This agrees with my initial hypothesis. On the other hand the hypothesized strengthening of the Hadley cell cannot be confirmed, as the Hadley cell strength only increases in the Southern Hemisphere, but there it is statistically not significant.

6. Conclusion

This thesis studies high-level clouds and their radiative impacts on the climate in climate model simulations. I investigate two main research questions.

Research question 1: What is the best way to study the cloud radiative effects and the cloud radiative heating of high-level clouds using climate model simulations?
I look at two different approaches to diagnose high-level clouds from model simulation data. The first method defines high-level clouds as all clouds at temperatures colder than a threshold of -35°C. This is the "cirrus diagnostic". The advantage of this method is that it is the easiest to implement. However, high-level clouds that have their true cloud base at temperatures warmer than -35°C are seen by this diagnostic as having a cloud base at the temperature threshold. Therefore, the use of the "cirrus diagnostic" causes a strong shortwave cooling and strong longwave heating at the chosen threshold, because more high-level cloud bases are located at this level, which is artificial (see e.g. Figure 20(c)). The second diagnostic, the "cirrus + warm base diagnostic", uses the same temperature threshold, but additionally includes cloud parts that extend to temperatures warmer than -35°C. In this way, the entire high-level cloud is considered. I recommend using this diagnostic over the "cirrus diagnostic", since it does not include the strong artificial heating at the temperature threshold level in the "cirrus diagnostic". The shortwave and longwave CRE of high-level clouds at the TOA and surface are larger when the "cirrus + warm base diagnostic" is used, because more clouds are considered compared to the "cirrus diagnostic".
Furthermore, I investigate two methods for calculating the cloud radiative effect of high-level clouds ($HCRE$) and the cloud radiative heating rate of high-level clouds ($\partial_t T|_{hlc}$), respectively. The first method calculates the cloud radiative effect and heating rate with respect to an all-sky atmosphere ($HCRE_{all-sky}$ and $\partial_t T|_{hlc,all-sky}$ respectively) and the second method with respect to a clear-sky atmosphere ($HCRE_{clear-sky}$ and $\partial_t T|_{hlc,clear-sky}$ respectively). The methods produce the same effects only in an atmospheric column where no clouds or only high-level clouds are present. At the TOA and at the surface using the $HCRE_{clear-sky}$ results in shortwave and longwave effects of greater magnitude than using the $HCRE_{all-sky}$, because non-high-level clouds partially mask the effects of the high-level clouds. For $\partial_t T|_{hlc,all-sky}$ and $\partial_t T|_{hlc,clear-sky}$ the net heating is similar when the "cirrus + warm base diagnostic" is used, while for the "cirrus diagnostic" $\partial_t T|_{hlc,clear-sky}$ is larger than $\partial_t T|_{hlc,all-sky}$. Furthermore, when using the "cirrus diagnostic" the artificial heating in $\partial_t T|_{hlc,all-sky}$ is located slightly lower in altitude than in $\partial_t T|_{hlc,clear-sky}$, since the artificial heating in $\partial_t T|_{hlc,all-sky}$ is mainly caused by the radiative interactions with non-high-level clouds, while in $\partial_t T|_{hlc,clear-sky}$ it is generated by the heating at the artificial cirrus cloud base. The two methods of computing the $HCRE$ and the cloud radiative heating of high-level clouds are equally valid, but provide a different perspective on high-level cloud radiative interactions. In general I recommend using $HCRE_{all-sky}$ and $\partial_t T|_{hlc,all-sky}$, since it does not ignore the radiative interactions of non-high-level clouds.

Research question 2: What is the cloud radiative impact of high-level clouds on the present-day atmospheric circulation and precipitation?
I have shown that the radiative interactions of high-level clouds heat the tropical upper troposphere, which increases specific humidity in the tropics. They also increase land surface and sea ice temperatures, especially over Antarctica. Surprisingly, the surface temperatures over the tropical land also increase when high-level clouds are radiatively active, even though high-level clouds have a cooling effect on the surface in the tropics according to their surface CRE. To explain this temperature in-

crease further investigation is needed.
High-level clouds strengthen the eddy-driven jet by heating the upper-troposphere. The total jet strengthening in the Northern Hemisphere is dominated by high-level clouds. In the Southern Hemisphere, they also contribute to a strengthening, but this is counteracted by an even stronger weakening effect of the non-high-level clouds. The eddy-driven jet shifts poleward in the Cirrus-COOKIE simulation set, while in the COOKIE and WB-Cirrus-COOKIE simulation sets the shifts are statistically not significant.
My results also demonstrate that the radiative heating of high-level clouds contributes to a decrease in tropical precipitation. The total cloud radiative impact on tropical precipitation is dominated by the high-level clouds. Furthermore, contrary to the expectations, high-level clouds do not have a statistically significant impact on the ITCZ shift and the Hadley cell strength.
Although the strength of the atmospheric radiative heating rates using the "cirrus diagnostic" and the "cirrus + warm base diagnostic" differ at the temperature threshold, the cloud radiative impacts of high-level clouds on the circulation and precipitation using the two different diagnostics differ mostly only in magnitude. The results of the WB-Cirrus-COOKIE simulation set are usually larger in magnitude, which is consistent with the fact that the shortwave and longwave CRE of high-level clouds at the TOA and surface are larger in magnitude when the "cirrus + warm base diagnostic" is used.

In summary, my results confirm that high-level clouds play a crucial role for the climate, as has been speculated by previous studies. High-level clouds dominate the cloud radiative impact on tropical mean precipitation and increase the strength of the eddy-driven jet. Furthermore, all high-level clouds at temperatures colder than -35°C contribute to a statistically significant poleward shift of the jet stream. In this thesis I also investigate the best way to study the radiative effects and radiative heating of high-level clouds using climate models. The two methods to calculate the cloud radiative effect and cloud radiative heating of high-level clouds equally valid. However, I recommend using the method that uses an all-sky atmosphere as a reference ($HCRE_{all-sky}$ and $\partial_t T|_{hlc,all-sky}$), except one studies the interactions of high-level clouds with radiation in a clear-sky atmosphere. Of the two approaches to diagnose high-level clouds that I explore in this thesis, my recommendation is to use the "cirrus + warm base diagnostic" because the use of the "cirrus diagnostic" leads a strong artificial heating at the temperature threshold.

7. Outlook

There are many possible ways, in which my work can be expanded. Therefore, I give here an outlook on what would be interesting to study.

In this thesis, two different methods of diagnosing high-level clouds have been investigated. Another possible high-level cloud diagnostic, not investigated here, is to consider only clouds colder than the temperature threshold and additionally exclude all high-level clouds that span over temperatures both warmer and colder than the temperature threshold. Those clouds could be referred to as "cold base cirrus clouds" and the diagnostic as the "cold base cirrus diagnostic", since all the cloud bases are located at temperatures colder than -35°C. Studying the cold base cirrus clouds is interesting, since they are purely ice clouds like the high-level clouds using the "cirrus diagnostic", but the cloud radiative heating at the temperature threshold should be weaker than in "cirrus diagnostic", because clouds that span over temperatures both warmer and colder than the temperature threshold are excluded. My expectation is that the cloud radiative impact of high-level clouds on the atmospheric circulation and precipitation should be weaker in this alternative high-level cloud diagnostic than in the other two high-level cloud diagnostics because fewer clouds are considered.

Since only one model is used in this thesis, the cloud radiative impact of high-level clouds on the atmospheric circulation and precipitation could be tested for robustness by using different climate models. Furthermore, it would also be interesting to look at the seasonal cloud radiative impacts of high-level clouds on the climate. I expect the impact to be different in the summer and winter months at the mid-latitudes because ice clouds, which I assume to be mostly high-level clouds, are observed more frequently in winter than in summer in this region (Hong and Liu, 2015).

Medeiros et al. (2021) showed that cloud radiative effects enhance tropical precipitation extremes across multiple climate models, but I have not analyzed the tropical precipitation extremes in this thesis. Therefore, it would be interesting to investigate whether high-level clouds dominate this cloud radiative impact.

Furthermore, the question of why the tropical land surface temperatures increase in the COOKIE, Cirrus-COOKIE and WB-Cirrus-COOKIE simulation sets remains unanswered in this thesis and therefore needs further investigation.

The main driver of many of the cloud radiative impacts on the circulation and precipitation seems to be specifically related to the high-level clouds in the tropics. To investigate whether the tropical high-level clouds do indeed dominate the overall high-level cloud response one could use a COOKIE-like approach, in which the "clouds on" simulation is compared to a simulation in which high-level clouds are only radiatively inactive only in a specific region, i.e., the tropics or the extratropics.

Since I have shown that the radiative interactions of high-level clouds have a considerable impact on the present-day atmosphere, it stands to reason that changes in high-level cloud contribute to the circulation changes under global warming, as has already been shown for the eddy-driven jet changes in Voigt and Shaw (2016). In a future study the impact of high-level cloud changes on the circulation

and precipitation changes could be studied with an adaptation of the cloud locking method, in which one prescribes the cloud changes from one climate state to another (Voigt et al., 2019). In order to "lock" a specific cloud type, the position of high-level clouds cannot be directly prescribed because the high-level clouds are expected to rise under global warming Li et al. (2019); Voigt et al. (2019), which would cause artificial cloud-free regions if the high-level clouds of the global warming scenario are prescribed to a present-day climate or a overlapping of clouds if the present-day high-level clouds are prescribed to a global warming scenario. One way around this would be to specify the radiative heating of the high-level clouds instead of the cloud position. Regarding the high-level diagnostic, I recommend, as mentioned in Chapter 6, the use of the "cirrus + warm base diagnostic" for the cloud locking of high-level clouds over the "cirrus diagnostic" to avoid strong artificial heating gradients inside the atmosphere.

A. Appendix

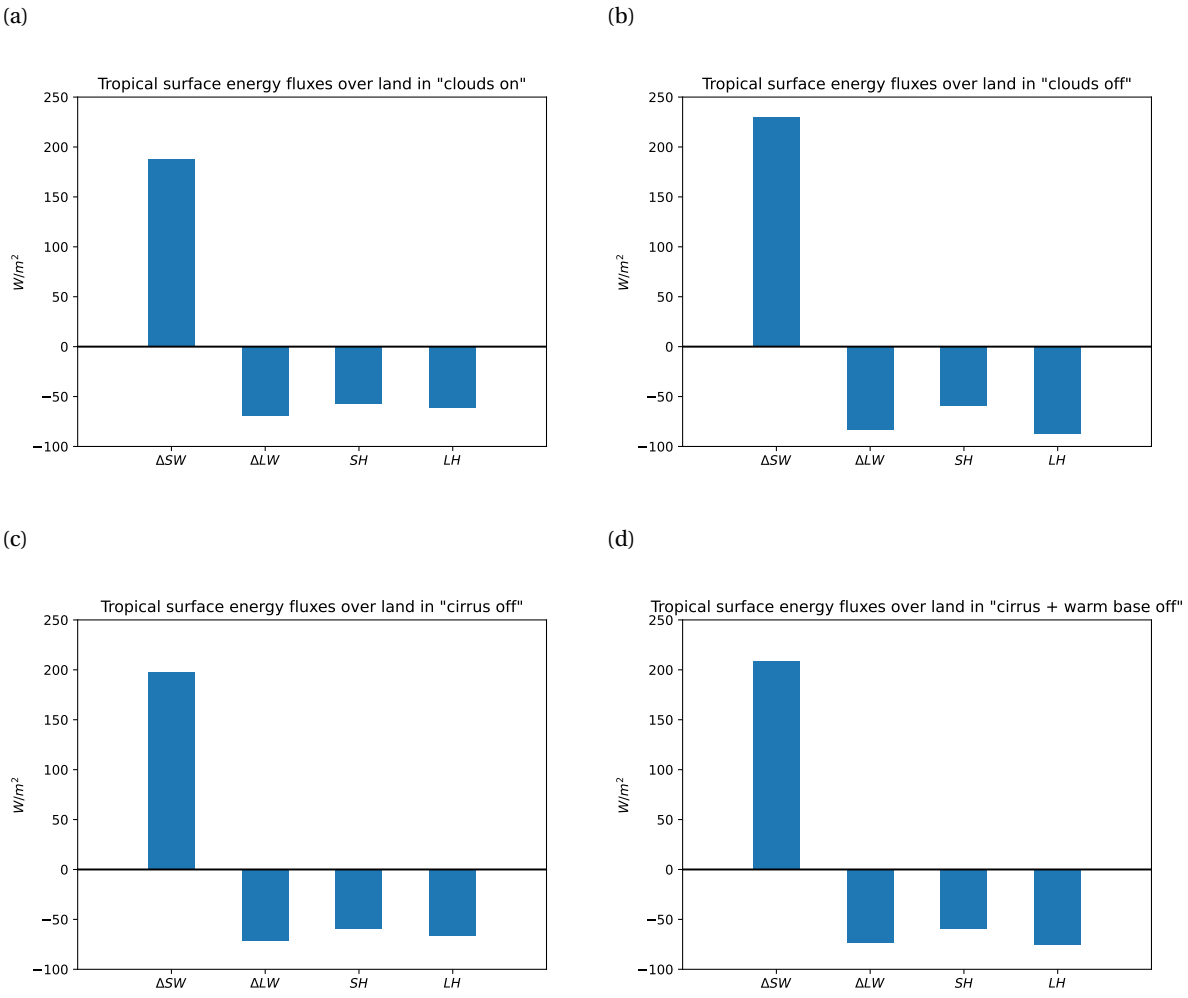

Figure A.1: Energy flux at the tropical land surface in the (a) "clouds on", (b) "clouds off", (c) "cirrus off" and (d) "cirrus + warm base off" simulations. ΔSW and ΔLW refer here to the difference between upwelling and downwelling shortwave/longwave radiative fluxes at the surface.

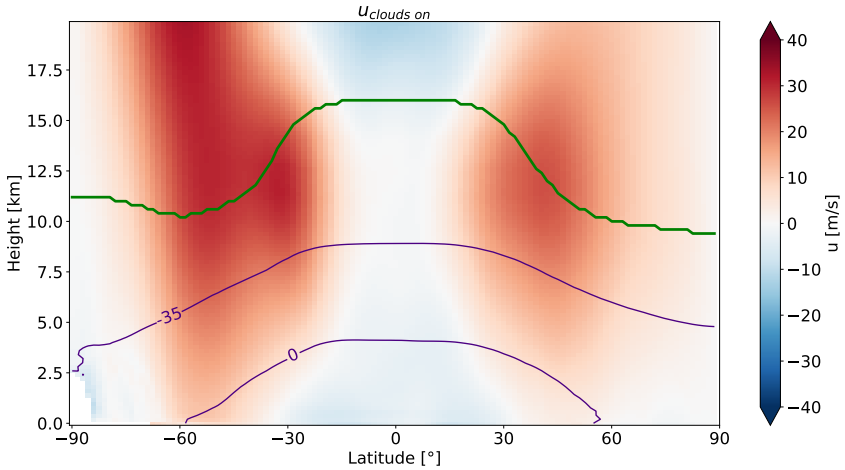

Figure A.2: Zonal winds in the "clouds on" simulation. Purple contour lines show the mean -35°C and 0°C isotherms. The green contour depicts the mean tropopause height, which is derived from the tropopause air pressure output of the simulation.

Bibliography

Albern, N., A. Voigt, S. A. Buehler, and V. Grützun (2018), Robust and Nonrobust Impacts of Atmospheric Cloud-Radiative Interactions on the Tropical Circulation and Its Response to Surface Warming. *Geophysical Research Letters* **45**(16), 8577–8585. , doi:https://doi.org/10.1029/2018GL079599.

Albern, N., A. Voigt, and J. G. Pinto (2019), Cloud-Radiative Impact on the Regional Responses of the Midlatitude Jet Streams and Storm Tracks to Global Warming. *Journal of Advances in Modeling Earth Systems* **11**(7), 1940–1958. , doi:https://doi.org/10.1029/2018MS001592.

Albern, N., A. Voigt, and J. G. Pinto (2021), Tropical cloud-radiative changes contribute to robust climate change-induced jet exit strengthening over Europe during boreal winter. *Environmental Research Letters* **16**(8), 084041. doi:10.1088/1748-9326/ac13f0.

Albern, N., A. Voigt, D. W. J. Thompson, and J. G. Pinto (2020), The Role of Tropical, Midlatitude, and Polar Cloud-Radiative Changes for the Midlatitude Circulation Response to Global Warming. *Journal of Climate* **33**(18), 7927 – 7943. doi:10.1175/JCLI-D-20-0073.1.

Barnes, E. A. and L. Polvani (2013), Response of the Midlatitude Jets, and of Their Variability, to Increased Greenhouse Gases in the CMIP5 Models. *Journal of Climate* **26**(18), 7117 – 7135. doi:10.1175/JCLI-D-12-00536.1.

Ceppi, P., F. Brient, M. D. Zelinka, and D. L. Hartmann (2017), Cloud feedback mechanisms and their representation in global climate models. *WIREs Climate Change* **8**(4), e465. , doi:https://doi.org/10.1002/wcc.465.

Dinh, T., B. Gasparini, and G. Bellon (2022), Clouds and radiatively induced circulations. In: *Cloud Physics and Dynamics: Showers and Shade from Earth's Atmosphere*. doi:10.1002/essoar.10512663.1.

Dixit, V., O. Geoffroy, and S. C. Sherwood (2018), Control of ITCZ Width by Low-Level Radiative Heating From Upper-Level Clouds in Aquaplanet Simulations. *Geophysical Research Letters* **45**(11), 5788–5797. , doi:https://doi.org/10.1029/2018GL078292.

Gasparini, B. and U. Lohmann (2016), Why cirrus cloud seeding cannot substantially cool the planet. *Journal of Geophysical Research: Atmospheres* **121**(9), 4877–4893. , doi:https://doi.org/10.1002/2015JD024666.

Gasparini, B., Z. McGraw, T. Storelvmo, and U. Lohmann (2020), To what extent can cirrus cloud seeding counteract global warming? *Environmental Research Letters* **15**(5), 054002.

Gasparini, B., A. Meyer, D. Neubauer, S. Münch, and U. Lohmann (2018), Cirrus Cloud Properties as Seen by the CALIPSO Satellite and ECHAM-HAM Global Climate Model. *Journal of Climate* **31**(5), 1983 – 2003. doi:https://doi.org/10.1175/JCLI-D-16-0608.1.

Gates, W. L. (1992), AN AMS CONTINUING SERIES: GLOBAL CHANGE–AMIP: The Atmospheric Model Intercomparison Project. *Bulletin of the American Meteorological Society* **73**(12), 1962 – 1970. doi:10.1175/1520-0477(1992)073<1962:ATAMIP>2.0.CO;2.

Gleckler, P. (2013), Atmospheric Model Intercomparison Project (AMIP).

Hantel, M. (2013), *Einführung Theoretische Meteorologie*. Springer-Verlag.

Hantel, M. and L. Haimberger (2016), *Grundkurs Klima*. Springer Berlin Heidelberg, Berlin, Heidelberg.

Harrop, B. E. and D. L. Hartmann (2016), The Role of Cloud Radiative Heating in Determining the Location of the ITCZ in Aquaplanet Simulations. *Journal of Climate* **29**(8), 2741 – 2763. doi:10.1175/JCLI-D-15-0521.1.

Harrop, B. E., J. Lu, F. Liu, O. A. Garuba, and L. R. Leung (2018), Sensitivity of the ITCZ Location to Ocean Forcing Via Q-Flux Green's Function Experiments. *Geophysical Research Letters* **45**(23), 13,116–13,123. , doi:https://doi.org/10.1029/2018GL080772.

Hong, Y. and G. Liu (2015), The Characteristics of Ice Cloud Properties Derived from CloudSat and CALIPSO Measurements. *Journal of Climate* **28**(9), 3880 – 3901. doi:https://doi.org/10.1175/JCLI-D-14-00666.1.

Hong, Y., G. Liu, and J.-L. F. Li (2016), Assessing the Radiative Effects of Global Ice Clouds Based on CloudSat and CALIPSO Measurements. *Journal of Climate* **29**(21), 7651 – 7674. doi:10.1175/JCLI-D-15-0799.1.

Huang, L., J. H. Jiang, Z. Wang, H. Su, M. Deng, and S. Massie (2015), Climatology of cloud water content associated with different cloud types observed by A-Train satellites. *Journal of Geophysical Research: Atmospheres* **120**(9), 4196–4212. , doi:https://doi.org/10.1002/2014JD022779.

Jungclaus, J. H., S. J. Lorenz, H. Schmidt, V. Brovkin, N. Brüggemann, F. Chegini, T. Crüger, P. De-Vrese, V. Gayler, M. A. Giorgetta, O. Gutjahr, H. Haak, S. Hagemann, M. Hanke, T. Ilyina, P. Korn, J. Kröger, L. Linardakis, C. Mehlmann, U. Mikolajewicz, W. A. Müller, J. E. M. S. Nabel, D. Notz, H. Pohlmann, D. A. Putrasahan, T. Raddatz, L. Ramme, R. Redler, C. H. Reick, T. Riddick, T. Sam, R. Schneck, R. Schnur, M. Schupfner, J.-S. von Storch, F. Wachsmann, K.-H. Wieners, F. Ziemen, B. Stevens, J. Marotzke, and M. Claussen (2022), The ICON Earth System Model Version 1.0. *Journal of Advances in Modeling Earth Systems* **14**(4), e2021MS002813, e2021MS002813 2021MS002813. , doi:https://doi.org/10.1029/2021MS002813.

Koop, T. and B. J. Murray (2016), A physically constrained classical description of the homogeneous nucleation of ice in water. *The Journal of Chemical Physics* **145**(21), 211915.

Li, Y., D. W. J. Thompson, and S. Bony (2015), The Influence of Atmospheric Cloud Radiative Effects on the Large-Scale Atmospheric Circulation. *Journal of Climate* **28**(18), 7263 – 7278. doi:10.1175/JCLI-D-14-00825.1.

Li, Y., D. W. J. Thompson, S. Bony, and T. M. Merlis (2019), Thermodynamic Control on the Poleward Shift of the Extratropical Jet in Climate Change Simulations: The Role of Rising High Clouds and Their Radiative Effects. *Journal of Climate* **32**(3), 917 – 934. doi:10.1175/JCLI-D-18-0417.1.

Lohmann, U. and E. Roeckner (1996), Design and performance of a new cloud microphysics scheme developed for the ECHAM general circulation model. *Climate Dynamics* **12**, 557–572.

Matus, A. V. and T. S. L'Ecuyer (2017), The role of cloud phase in Earth's radiation budget. *Journal of Geophysical Research: Atmospheres* **122**(5), 2559–2578. , doi:https://doi.org/10.1002/2016JD025951.

Mayer, B. (2018), Erwärmungs- und Abkühlungsraten – Wie wichtig ist der 3D-Strahlungstransport? *Promet* pp. 98–110.

Medeiros, B., A. C. Clement, J. J. Benedict, and B. Zhang (2021), Investigating the impact of cloud-radiative feedbacks on tropical precipitation extremes. *npj Climate and Atmospheric Science* **4**(1), 2397–3722. doi:https://doi.org/10.1038/s41612-021-00174-x.

Pincus, R. and B. Stevens (2013), Paths to accuracy for radiation parameterizations in atmospheric models. *Journal of Advances in Modeling Earth Systems* **5**(2), 225–233. , doi:https://doi.org/10.1002/jame.20027.

Schneider, T., T. Bischoff, and G. H. Haug (2014), Migrations and dynamics of the intertropical convergence zone. *Nature* **513**(7516), 45–53.

Siebesma, A. P., S. Bony, C. Jakob, and B. Stevens (2020), *Clouds and Climate: Climate Science's Greatest Challenge*. Cambridge University Press, Cambridge.

Stanfield, R. E., X. Dong, B. Xi, A. Kennedy, A. D. D. Genio, P. Minnis, and J. H. Jiang (2014), Assessment of NASA GISS CMIP5 and Post-CMIP5 Simulated Clouds and TOA Radiation Budgets Using Satellite Observations. Part I: Cloud Fraction and Properties. *Journal of Climate* **27**(11), 4189 – 4208. doi:10.1175/JCLI-D-13-00558.1.

Stevens, B., S. Bony, and M. Webb (2012), Clouds On-Off Klimate Intercomparison Experiment (COOKIE) .

Sundqvist, H., E. Berge, and J. E. Kristjánsson (1989), Condensation and Cloud Parameterization Studies with a Mesoscale Numerical Weather Prediction Model. *Monthly Weather Review* **117**(8), 1641 – 1657. doi:10.1175/1520-0493(1989)117<1641:CACPSW>2.0.CO;2.

Tiedtke, M. (1989), A comprehensive mass flux scheme for cumulus parameterization in large-scale models. *Monthly Weather Review* **117**(8), 1779–1800.

Voigt, A. and N. Albern (2019), No Cookie for Climate Change. *Geophysical Research Letters* **46**(24), 14751–14761. , doi:https://doi.org/10.1029/2019GL084987.

Voigt, A., N. Albern, P. Ceppi, K. Grise, Y. Li, and B. Medeiros (2021), Clouds, radiation, and atmospheric circulation in the present-day climate and under climate change. *WIREs Climate Change* **12**(2), e694. , doi:https://doi.org/10.1002/wcc.694.

Voigt, A., N. Albern, and G. Papavasileiou (2019), The Atmospheric Pathway of the Cloud-Radiative Impact on the Circulation Response to Global Warming: Important and Uncertain. *Journal of Climate* **32**(10), 3051–3067.

Voigt, A. and T. A. Shaw (2015), Circulation response to warming shaped by radiative changes of clouds and water vapour. *Nature Geoscience* **8**(2), 102 – 106. doi:https://doi.org/10.1038/ngeo2345.

Voigt, A. and T. A. Shaw (2016), Impact of Regional Atmospheric Cloud Radiative Changes on Shifts of the Extratropical Jet Stream in Response to Global Warming. *Journal of Climate* **29**(23), 8399 – 8421. doi:10.1175/JCLI-D-16-0140.1.

Watt-Meyer, O. and D. M. W. Frierson (2017), Local and Remote Impacts of Atmospheric Cloud Radiative Effects Onto the Eddy-Driven Jet. *Geophysical Research Letters* **44**(19), 10,036–10,044. , doi:https://doi.org/10.1002/2017GL074901.

List of Tables

1. Overview of all simulations used including their name, a short description, the simulated years and the output frequency. 14
2. Overview of the COOKIE, Cirrus-COOKIE and WB-Cirrus-COOKIE simulation sets, including the combination of simulations used, and a short description. 19
3. Jet position and jet strength changes in the COOKIE, Cirrus and WB-Cirrus-COOKIE simulation sets. 51
4. Changes in zonally averaged precipitation in the COOKIE, the Cirrus-COOKIE and the WB-Cirrus-COOKIE simulation set. 54
5. Changes of mean ITCZ latitude and Hadley cell strength in the COOKIE, the Cirrus-COOKIE and the WB-Cirrus-COOKIE simulation set. 55
6. The atmospheric net radiative balance ΔR_{ATM} in both hemispheres in the COOKIE, Cirrus-COOKIE and WB-Cirrus-COOKIE simulation sets. 55

List of Figures

1. The TOA CRE of liquid clouds, ice clouds, mixed-phase clouds, multi-layer (ML) clouds and all clouds. The Figure is taken from Matus and L'Ecuyer (2017). 6
2. The surface CRE of liquid clouds, ice clouds, mixed-phase clouds, multi-layer (ML) clouds and all clouds. The Figure is taken from Matus and L'Ecuyer (2017). 7
3. The ACRE of liquid clouds, ice clouds, mixed-phase clouds, multi-layer (ML) clouds and all clouds. The Figure is taken from Matus and L'Ecuyer (2017). 8
4. Cloud radiative impact on temperature and zonal wind derived using the COOKIE method. The Figure is taken from Li et al. (2015). 10
5. Depiction of the diagnostics used to separate high-level clouds from other clouds. . . . 17
6. A depiction of the cloud-radiation interactions in an atmosphere with radiatively active ACRE, and in an atmosphere with radiatively transparent high-level clouds according to the "cirrus diagnostic". 18
7. The simulated cloud fraction of liquid, mixed-phase, and ice clouds. 26
8. Zonal plot of the most dominant cloud type at a given location. 27
9. Vertical profiles of the cloud fraction of different cloud types averaged over the tropics, mid-latitudes, and high-latitudes. 28
10. Zonal plot of high-level clouds diagnosed by the "cirrus diagnostic", "cirrus + warm base diagnostic" and the difference between the two diagnostics. 29

11. Shortwave (sw), longwave (lw) and net *HCRE* at the TOA according to the "cirrus diagnostic". . . . 30

12. Shortwave (sw), longwave (lw) and net *HCRE* at the surface according to the "cirrus diagnostic". . . . 31

13. Shortwave (sw), longwave (lw) and net *HCRE* inside the atmosphere according to the "cirrus diagnostic". . . . 32

14. Shortwave (sw), longwave (lw) and net *HCRE* at the TOA according to the "cirrus + warm base diagnostic". . . . 33

15. Shortwave (sw), longwave (lw) and net *HCRE* at the surface according to the "cirrus + warm base diagnostic". . . . 34

16. Shortwave (sw), longwave (lw) and net *HCRE* inside the atmosphere according to the "cirrus + warm base diagnostic". . . . 35

17. Shortwave, longwave and net cloud radiative heating rates. . . . 36

18. Shortwave radiative heating rates with high-level clouds diagnosed using the "cirrus diagnostic". . . . 37

19. Longwave radiative heating rates with high-level clouds diagnosed using the "cirrus diagnostic". . . . 38

20. Net radiative heating rates with high-level clouds diagnosed using the "cirrus diagnostic". 40

21. Shortwave radiative heating rates with high-level clouds diagnosed using the "cirrus + warm base diagnostic". . . . 41

22. Longwave radiative heating rates with high-level clouds diagnosed using the "cirrus + warm base diagnostic". . . . 42

23. Net radiative heating rates with high-level clouds diagnosed using the "cirrus + warm base diagnostic". . . . 43

24. Zonal cross-section of the temperature impact in the COOKIE, Cirrus-COOKIE, and WB-Cirrus-COOKIE simulation sets. . . . 45

25. Land surface and sea ice temperature impact for the COOKIE, Cirrus-COOKIE and the WB-Cirrus-COOKIE simulation sets. . . . 47

26. Radiative energy flux changes at the tropical land surface diagnosed from the "clouds on", the "diagnose cirrus all-sky" and the "diagnose cirrus + warm base all-sky" simulations and the changes in energy flux at the tropical land surface from the COOKIE, Cirrus-COOKIE and the WB-Cirrus-COOKIE simulation sets. . . . 48

27. Zonal wind impact of the COOKIE, Cirrus-COOKIE and WB-Cirrus-COOKIE simulation sets. . . . 49

28. 700 hPa zonal wind differences in the COOKIE, Cirrus-COOKIE and WB-Cirrus-COOKIE simulation sets. . . . 50

29. 700 hPa zonal wind in the "clouds on", "clouds off", "cirrus off" and "cirrus + warm base off" simulations. . . . 51

30. Zonal cross-section of the relative impact on specific humidity in the COOKIE, Cirrus-COOKIE and the WB-Cirrus-COOKIE simulation set. 53

31. Zonal average precipitation difference in the COOKIE, Cirrus-COOKIE and WB-Cirrus-COOKIE simulation sets. 54

A.1. Energy flux at the tropical land surface in the "clouds on", "clouds off", "cirrus off" and "cirrus + warm base off" simulations. 60

A.2. Zonal winds in the "clouds on" simulation. 61